Alma Mater Studiorum – Università di Bologna

DOTTORATO DI RICERCA IN

CHIMICA

Ciclo XXIX

Settore Concorsuale di afferenza: 03/A2

Settore Scientifico Disciplinare: CHIMICA FISICA - CHIM/02

FUNCTIONAL MATERIALS FOR ELECTROCHEMILUMINESCENCE BIOSENSORS AND IMAGING

Presentata da: Elena Villani

Coordinatore Dottorato

Prof. Aldo Roda

Relatore

Prof. Francesco Paolucci

Correlatore

Dr. Giovanni Valenti

Esame finale anno 2017

"The future for ECL remains bright"

Allen J. Bard

ELECTROGENERATED CHEMILUMINESCENCE

Abstract

This doctoral thesis focuses on the investigation of innovative functional materials for the development of sensing applications, which use electrochemiluminescence (ECL) technology as transduction technique.

The demand for highly sensitive, selective and reliable sensors able to perform fast, economic and easy detection in clinical and analytical chemistry increases constantly. Among the electrochemical techniques, ECL is the most suitable transduction method for sensing applications. In fact, due to the electrochemical nature of the signal generation, extremely high range of sensitivity and very low detection limits can be reached. Moreover, the generation of the signal is achieved directly *in situ*, which enables spatial visualization and mapping of the signal distribution. This property of the ECL can be exploited for the imaging of small objects, such as micro-particles or cells, deposited directly on the surface of the electrode. In addition, efforts have been made to understand the complex interplay of the chemical and electrochemical reactions responsible of the signal generation at the electrode surface. The collected information might help towards the improvement of the technology at the basis of the ECL sensors, in order to obtain higher sensitivity and selectivity.

The functional materials studied in this thesis present different electrochemical characteristics and are expressly designed for sensor applications. In particular, the proper selection of the material and its optimization assure high performances of the device. For example, the combination of supramolecular chemistry with the ECL technology can be exploited for the development of a sensor for the early diagnosis of prostate cancer, or the excellent electrochemical properties of carbon-based materials can be used for the imaging of biological samples with high spatial resolution.

Key words: electrochemiluminescence; functional materials; sensors; imaging.

Table of contents

Acronyms

Au: Gold

BPO: Benzoyl Peroxide

CNTs: Carbon nanotubes

CTC: Circulating Tumor Cells

ECL: Electrogenerated Chemiluminescence or Electrochemiluminescence

EGFR: Epidermal Growth Factor Receptor

FTO: Fluorine-doped Tin Oxide

GC/GCE: Glassy Carbon Electrode

IJP-CNTs: Inkjet-printed carbon nanotubes

ITO: Indium-doped Tin Oxide

LOD: Limit of Detection

LOQ: Limit of Quantification

MMBs: Magnetic Microbeads

µPADs: Microfluidic Paper-based Analytical Devices

NPG: Nanoporous Gold

PCa: Prostate Cancer

PCA3: Prostate Cancer Antigen 3

POCT: Point-of-care Testing

PSA: Prostate Specific Antigen

Pt: Platinum

$[Ru(bpy)_3]^{2+}$: Tris(2,2'-bipyridyl)ruthenium(II) cation

SEECL: Surface Enhanced ECL

SPEs: Screen Printed Electrodes

Tiiii: Tetraphosphonate cavitand

Tiiii@MMBs: Tetraphosphonate cavitand with magnetic microbeads

TPrA: Tri-n-propylamine

Preface

Since the first observation of light generation during the electrochemical studies of hydrocarbons, Electrogenerated Chemiluminescence (ECL) has developed in the decades from a curious phenomenon to one of the most important leader technology in analytical and clinical chemistry. This has been possible thanks to the electrochemical method to generate the signal, which confers to the technique extremely high sensitivity. Furthermore, its determining success has been the development of ECL water systems that work optimally at neutral pH. Nevertheless, the mechanism of the ECL light generation is even now not completely clarified, even fundamental insights on the comprehension of the phenomenon has carried out mainly by Prof. Dr. Allen J. Bard.

The cornerstone of this PhD thesis is the investigation of new functional materials for their application in ECL. In chapter one, a comprehensive overview of the ECL technology is presented. The chapter will cover the timeline of the ECL development, from the first experiments on the electrochemistry of hydrocarbons, to the development of commercial instruments for clinical diagnostics. In chapter two, the development of a sensor for the detection of sarcosine in urine for the early diagnosis of prostate cancer is illustrated. This sensor works exploiting the synergic combination of the supramolecular chemistry for sarcosine recognition and capturing with ECL detection for its quantification. In chapter three, the investigation of different electrode materials for ECL generation is showed. The choice of the proper electrode material is one of the most important factor that affects the ECL signal behaviour, since the initial stimulus starts from the surface. In chapter four, two innovative approaches for the imaging and detection of cells using ECL is presented.

This work is the comprehensive experience that I have made on the ECL technology during my doctoral studies. I hope that it can be a valuable work of this fascinating technique.

Bologna, 31st of March 2017
Elena Villani

Chapter 1

Introduction to Electrogenerated Chemiluminescence

The purpose of the present chapter is to give to the reader a brief but comprehensive overview of the electrogenerated chemiluminescence technique, from the first observations of the phenomenon, to the most recent applications. The chapter deals with the fundamentals of the methodology, discussing the different mechanism pathways of light generation and the parameters that influence the signal behaviour. Moreover, a brief summary of the most recent applications will be presented. Finally, an overview of the most important clinical analyzers based on electrogenerated chemiluminescence technology will be also afford in these pages.

Key words: *electrochemiluminescence; electrochemistry; ruthenium-tris-bipyridine; tripropylamine; analytical chemistry.*

Cover picture: changing color leaves (maple), Matsushima, Miyagi Prefecture, Japan.

1.1 Overview

Electrogenerated Chemiluminescence, simply called *Electrochemiluminescence* or *ECL*, is the generation of light at the electrode surface[1]. Light generation is possible when highly exergonic electron transfer reaction between electrochemically generated species occurs, leading to an excited state formation that relaxes at lower energy level state through the emission of a photon. This principle is at the basis of the modern ECL technology widely used in clinical and analytical chemistry. The success of this technique is due, firstly, to the high level of sensitivity reached, possible because no light source is employed. Secondly, the high level of selectivity, reached manipulating the energetics of the chemical species involved in the process, avoids side reactions.

The first reports on ECL date back to the 1960s, when the electrochemical properties of aromatic hydrocarbons were studied. Since that period, ECL generation has been observed in many molecules including semiconductor nanoparticles, inorganic and organic systems. However, the major role of light emitters in ECL is represented from the coordination complexes of transition metals, where ruthenium tris-bipyridine complex is the most used chromophore, thanks to its remarkable chemical, electrochemical and photochemical properties.

1.2 $[Ru(bpy)_3]^{2+}$ as chromophore for ECL generation

The chromophore systems used in ECL can be classified in three different categories: 1) inorganic systems, mainly coordination complexes of transition metals; 2) organic systems, which include polycyclic aromatic hydrocarbons (PAHs); 3) nanostructured materials. The continuous research have produced a large variety of new dyes with suitable electrochemical properties ranging from organic systems[2], to metal complexes[3] and organometallic compounds[4].

The most used luminophore in ECL is ruthenium(II) tris(2,2'-bipyridine) - $[Ru(bpy)_3]^{2+}$ - which can be classified as inorganic system. The reasons for its widespread use is due, above all, to the excellent

combination between electrochemical and photochemical properties, but also for its water solubility and the relative high ECL efficiency at room temperature.

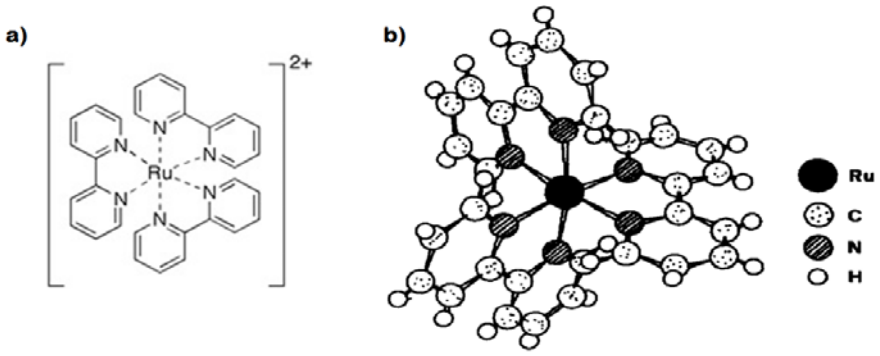

Figure 1.1: a), b) structure formulas of $[Ru(bpy)_3]^{2+}$ cation (counterion usually is Cl^- or PF_6^-). Image b) adapted with permission from ref. [5]. Copyright 1988 Elsevier Science Publishers B.V.

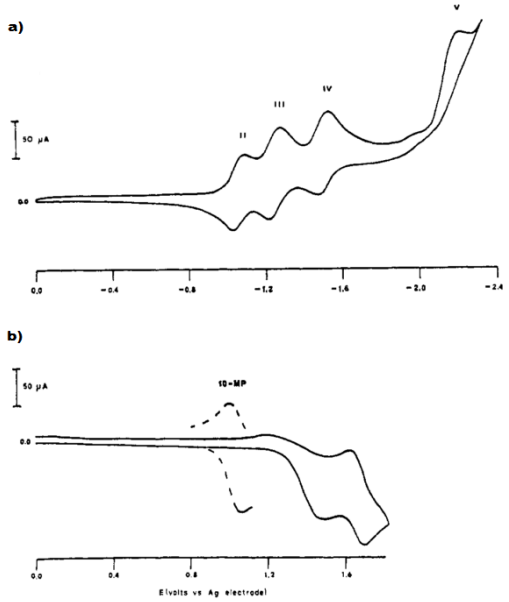

Figure 1.2: Cyclic voltammetry of $[Ru(bpy)_3]Cl_2$ in acetonitrile solution. Scan range: 0 -2.4 V (a) and 0 to +1.8 V (b). The irreversible oxidation at ~ 1.4 V can be attributed to oxidation of chloride ions. Reprinted with permission from ref. [6]. Copyright 1972 American Chemical Society.

$[Ru(bpy)_3]^{2+}$ is a yellow-orange coordination compound. Ru^{2+} is a d^6 system with electronic configuration $[Kr]4d^6$. The complex has an octahedral molecular geometry with D_3 simmetry, where the metal is surrounded by three bidentate bipyridine ligands[5] (figure 1.1).

$[Ru(bpy)_3]^{2+}$ cation shows one reversible oxidation and three reduction processes, all monoelectronic and reversible (figure 1.2). The three stepwise reductions involve the generation of +1, 0 and -1 charged species[6]. The fourth reduction (peak V in figure 1.2) occurs at potentials where 2,2'-bipyridine ligand itself reduces and probably arises from liberated free radical. The oxidation of $[Ru(bpy)_3]^{2+}$ to $[Ru(bpy)_3]^{3+}$ occurs at ~1.2 V and it represents the electrochemical step to obtain ECL generation:

$$[Ru(bpy)_3]^{2+} + [Ru(bpy)_3]^{3+} \rightarrow [Ru(bpy)_3]^{2+*} + [Ru(bpy)_3]^{2+}$$

$$[Ru(bpy)_3]^{2+*} \rightarrow [Ru(bpy)_3]^{2+} + hv \quad (\lambda_{emm} = 610 \text{ nm})$$

The electronic transition responsible of the emission is metal-to-ligand charge transfer (MLCT) transition from the ground state to the singlet charge transfer excited state. Rapid intersystem crossing occurs and the obtained maximum emission at 610 nm (2.04 eV) is phosphorescence[7].

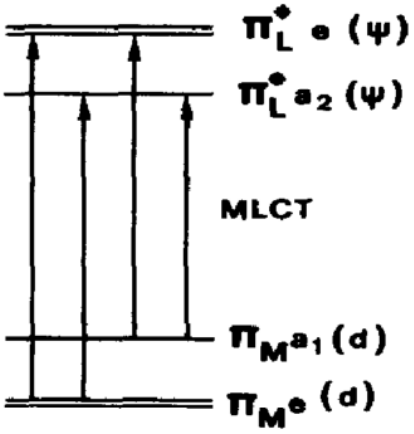

Figure 1.3: Representation of the MLCT transition in D_3 symmetry. Reprinted with permission from ref. [5]. Copyright 1988 Elsevier Science Publishers B.V.

1.3 Fundamentals of ECL: the mechanism of the signal generation

There are two predominant pathways to achieve ECL: the *annihilation pathway* and the *coreactant pathway*. In both cases, the generation of light is reached after an exergonic electron-transfer between intermediates electrochemically generated at the electrode surface. In the following sections, both mechanisms will be extensively discussed.

1.3.1 Annihilation pathway

The first works regarding the observation of light electrochemically generated after electrolysis of aromatic hydrocarbons were reported separately by Hercules and Visco in the mid-1960s[8],[9], although previous examination of the same phenomenon after electrolysis of luminol was reported at the end of the 1920s[10]. In the same period, ECL was also observed when the electrochemical properties of some aromatic hydrocarbons, such as 9,10-diphenylanthracene (DPA), were studied[11].

In the annihilation pathway, radical species electrochemically generated undergo an exergonic-electron transfer with the formation of an excited state as result. If R is a general chemical species, the annihilation mechanism can be represented as follows:

$R - e^- \rightarrow R^{\bullet +}$ (*oxidation at the electrode*) (eq. 1)

$R + e^- \rightarrow R^{\bullet -}$ (*reduction at the electrode*) (eq. 2)

$R^{\bullet -} + R^{\bullet +} \rightarrow R^* + R$ (*excited state formation*) (eq. 3)

$R^* \rightarrow R + h\nu$ (*light emission*) (eq. 4)

where $R^{\bullet +}$ and $R^{\bullet -}$ are the radical cation and radical anion respectively, generated at the electrode from the same chemical species after the application of alternate pulse potentials, and R^* is the excited state formed after annihilation reaction. Subsequently, the emission of a photon with energy $h\nu$ causes the relaxation of R^* to the

ground state R and, hence, the initial chemical species is regenerated at the end of the process.

The energy of the electron-transfer reaction (eq. 3) is responsible of the type of the excited state formed. If the energy involved is sufficient to populate the lowest singlet excited state (Es) the emitting state will be a singlet $^1R^*$; if the energy involved is sufficient to populate the lowest triplet excited state (Et), the emitting state will be a triplet $^3R^*$.

The energy requirement in eq. 3 is directly related to the enthalphy, which can be calculated from the redox potentials of the oxidation and reduction reactions (eq. 1 and 2 respectively) as defined in eq. 5:

$$-\Delta H_{ann} = E_p(R/R^{\bullet+}) - E_p(R/R^{\bullet-}) - 0.16 \qquad \text{(eq. 5)}$$

where $-\Delta H_{ann}$ (in eV) is the enthalpy for the annihilation reaction, E_p is the peak potential for the electrochemical oxidation and reduction processes (in V) and 0.16 is the entropy approximation term ($T\Delta S$ at 298 K, corresponding to 0.10 eV) with addition of 0.057 eV resulting from the difference between the reversible potential and the peak potential of the redox reactions (eq. 1 and 2).

It is possible to classify the annihilation process referring to the value of the enthalphy:

- if $-\Delta H_{ann} > Es$, the lowest singlet excited state can be directly generated. In this case, the system is called *"energy-sufficient system"* and the reaction is said to follow the *S-route*:

  $$R^{\bullet-} + R^{\bullet+} \rightarrow {}^1R^* + R$$
  (*excited singlet formation*) (eq. 3a)

- if $-\Delta H_{ann} < Es$ but $-\Delta H_{ann} > Et$, the lowest triplet excited state can be directly generated. In this case, the system is called *"energy-deficient system"* and the reaction is said to follow the *T-route*:

  $$R^{\bullet-} + R^{\bullet+} \rightarrow {}^3R^* + R$$
  (*excited triplet formation*) (eq. 3b)

  A particular case of the T-route is the *triplet-triplet annihilation* (*TTA*) when the triplet state $^3R^*$ is initially

formed, but it is rapidly converted to the singlet state $^1R^*$ after reaction with another triplet state $^3R^*$:

$$R^{\bullet-} + R^{\bullet+} \rightarrow {}^3R^* + R \qquad \text{(eq. 3b)}$$

$$^3R^* + {}^3R^* \rightarrow {}^1R^* + R \qquad \text{(eq. 3c)}$$

(*triplet-triplet annihilation*)

- if $-\Delta H_{ann} \sim Es$, the T-route can contribute to the formation of $^1R^*$ in addition to the S-route, leading to a mixed system called *ST-route*.
- In addition to singlet and triplet excited state formation, ion annihilation reactions can lead to the direct excimers (excited dimers) and exciplexes (excited complexes) formation, as depicted by eq. 6 and 7. These reactions are said to follow the *E-route*.

$$R^{\bullet-} + R^{\bullet+} \rightarrow R_2^* \qquad \text{(}\textit{excimer formation}\text{)} \qquad \text{(eq. 6)}$$

$$R^{\bullet-} + R'^{\bullet+} \rightarrow (RR')^* \qquad \text{(}\textit{exciplex formation}\text{)} \qquad \text{(eq. 7)}$$

$$^3R^* + {}^3R^* \rightarrow {}^1R_2^* \qquad \text{(TTA }\textit{excimer formation}\text{)} \qquad \text{(eq. 8)}$$

Excimer and exciplex can also be formed by TTA mechanism, as eq. 8 shows. The formation of these chemical species is possible when the participating molecules are able to align for a significant π-orbital overlapping; thus, this occurs mostly among planar polycyclic aromatic hydrocarbons (PAHs).

The main requirements necessary to obtain efficient annihilation ECL are: *i)* chemical precursors able to generate radicals sufficiently stable to generate the excited state; *ii)* good photoluminescence yield of the excited state; *iii)* electron-transfer sufficiently exergonic to populate the excited state.

ECL is also known for being the first experimental evidence of the existence of the Marcus inverted region[12]. Marcus revealed the kinetics of heterogeneous electron transfer as a function of the driving force. The rate constant augments with the driving force (Marcus normal region); at even higher driving force, the rate constant

decreases (Marcus inverted region). As Marcus demonstrated, the intersection of the potential energy surface of the reactants with that of the electronic ground-state products produces a large energetic barrier compared to that generated from the intersection of the same reactant energy surface with the one of an excited state. Therefore, in the Marcus inverted region, the formation rate of the ground-state products then becomes slow relative to the formation of the excited state[13].

1.3.2 Coreactant pathway

The first experiments regarding the ECL generation were performed in organic solvents, like CH_3CN or DMF. The use of water as solvent was limited until the beginning of the 1980s; in effect, the main disadvantage of using water is its narrow "potential window", that is the range of potentials available before its oxidation and reduction to oxygen and hydrogen, respectively. Therefore, the electrochemical behavior of water was not suitable for generation of the couple of radicals essential to achieve light generation. This problem was bypassed when the use of a "sacrificial" species was introduced as additional reactant[14],[15]. This species, called *coreactant*, is a chemical species that upon oxidation or reduction generates radicals sufficiently stable to react with the reduced or oxidized form of the chromophore: in other words, it possesses the energy requirements to generate the emitting excited state. The use of a coreactant is also convenient when one of the radical couple $R^{\bullet+}/R^{\bullet-}$ is not stable enough for ECL generation or even for some fluorescent compounds that present only a reversible electrochemical oxidation or reduction.

The essential characteristics for a chemical to act as a coreactant are solubility, stability and fast kinetics in order to avoid quenching effects. Obviously, the electrochemical properties are the most important aspect for a coreactant selection, since the species should be easily oxidized or reduced and gives rapid conversion to sufficiently stable radicals to react with the radicals generated from the luminophore. For this reason, the coreactant is not regenerated at the

end of the ECL process due to its consumption via electrochemical-chemical reactions.

There are mainly two different ECL coreactant mechanisms depending if the coreactant is oxidized or reduced: the *"oxidative-reduction"* mechanism when the coreactant is oxidized and the *"reductive-oxidation"* mechanism if the coreactant is reduced.

The use of oxalate ($C_2O_4^{2-}$) as coreactant is an example of the "oxidative-reduction" system and was the first coreactant studied by Bard at the end of the 1970s, before in CH_3CN solution with different chromophores[14] and then in water with $[Ru(bpy)_3]^{2+}$ as luminophore[15]. The mechanism of this system with $[Ru(bpy)_3]^{2+}$ is represented by eq. 9-15:

$$[Ru(bpy)_3]^{2+} - e^- \rightarrow [Ru(bpy)_3]^{3+} \quad \text{(eq. 9)}$$

$$[Ru(bpy)_3]^{3+} + C_2O_4^{2-} \rightarrow [Ru(bpy)_3]^{2+} + C_2O_4^{\bullet-} \quad \text{(eq. 10)}$$

$$C_2O_4^{\bullet-} \rightarrow CO_2^{\bullet-} + CO_2 \quad \text{(eq. 11)}$$

$$[Ru(bpy)_3]^{3+} + CO_2^{\bullet-} \rightarrow [Ru(bpy)_3]^{2+*} + CO_2 \quad \text{(eq. 12)}$$

$$[Ru(bpy)_3]^{2+} + CO_2^{\bullet-} \rightarrow [Ru(bpy)_3]^{+} + CO_2 \quad \text{(eq. 13)}$$

$$[Ru(bpy)_3]^{3+} + [Ru(bpy)_3]^{+} \rightarrow [Ru(bpy)_3]^{2+*} + [Ru(bpy)_3]^{2+} \quad \text{(eq. 14)}$$

$$[Ru(bpy)_3]^{2+*} \rightarrow [Ru(bpy)_3]^{2+} + hv \quad \text{(eq. 15)}$$

After oxidation of $[Ru(bpy)_3]^{2+}$ cation at the electrode surface (eq. 9), $[Ru(bpy)_3]^{3+}$ is able to oxidize oxalate in the diffusion layer close to the electrode surface in the oxalate radical anion $C_2O_4^{\bullet-}$ (eq. 10). This radical anion can break down to form the highly reducing radical anion $CO_2^{\bullet-}$ (eq. 11), which reacts with both oxidized and neutral forms of the chromophore leading to the formation of the emitting species and the reduced form $[Ru(bpy)_3]^{+}$ (eq. 12 and 13, respectively). The latter species can react with the oxidized form $[Ru(bpy)_3]^{3+}$ (eq. 14) to form the emitting excited state $[Ru(bpy)_3]^{2+*}$, which emits light with λ_{max} at 620 nm (eq. 15).

The first example of the "reductive-oxidation" ECL system reported in literature is represented by the use of peroxydisulfate (persulfate, $S_2O_8^{2-}$) as coreactant. The use of this chemical for ECL generation was

reported simultaneously by Bard and Balzani in 1982[16],[17], with different transition metals complexes. The representation of the electrochemical reactions involving $[Ru(bpy)_3]^{2+}$ and $S_2O_8^{2-}$ can be schematized by eq. 16-22:

$$S_2O_8^{2-} + e^- \rightarrow S_2O_8^{\bullet 3-} \quad \text{(eq. 16)}$$

$$[Ru(bpy)_3]^{2+} + e^- \rightarrow [Ru(bpy)_3]^{+} \quad \text{(eq. 17)}$$

$$[Ru(bpy)_3]^{+} + S_2O_8^{2-} \rightarrow [Ru(bpy)_3]^{2+} + S_2O_8^{\bullet 3-} \quad \text{(eq. 18)}$$

$$S_2O_8^{\bullet 3-} \rightarrow SO_4^{2-} + SO_4^{\bullet -} \quad \text{(eq. 19)}$$

$$[Ru(bpy)_3]^{+} + SO_4^{\bullet -} \rightarrow [Ru(bpy)_3]^{2+*} + SO_4^{2-} \quad \text{(eq. 20)}$$

$$[Ru(bpy)_3]^{2+} + SO_4^{\bullet -} \rightarrow [Ru(bpy)_3]^{3+} + SO_4^{2-} \quad \text{(eq. 21)}$$

$$[Ru(bpy)_3]^{+} + [Ru(bpy)_3]^{3+} \rightarrow [Ru(bpy)_3]^{2+*} + [Ru(bpy)_3]^{2+} \quad \text{(eq. 22)}$$

The reduction of persulfate radical $S_2O_8^{2-}$ (eq. 16) forms the strongly reducing sulfate radical anion $SO_4^{\bullet -}$ (eq. 19) which is responsible of the generation of the excited state (eq. 20-22). The sulfate anion is unreactive from the ECL point of view. The ECL intensity of this system is a function of persulfate concentration as reported in literature[16]. This result is due for both the role of persulfate as coreactant and as quencher of the $[Ru(bpy)_3]^{2+}$ excited state[18].

1.4 $[Ru(bpy)_3]^{2+}$/TPrA: the model ECL coreactant system

The $[Ru(bpy)_3]^{2+}$/TPrA system, where TPrA (Tri-n-propylamine) is a tertiary amine, is the model ECL coreactant system, since it shows the highest ECL efficiency. Since both chemicals are soluble in water solutions and the ECL intensity is maximum at neutral pH, this system is at the basis of commercial analyzers for immunoassays and DNA analysis[1], where the complex $[Ru(bpy)_3]^{2+}$ and its derivatives are used as label and TPrA as coreactant.

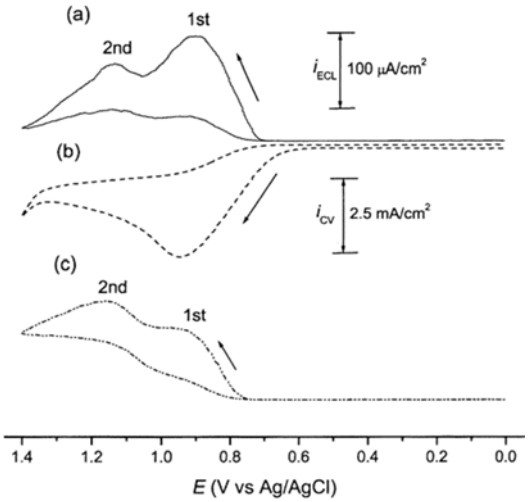

Figure 1.4: ECL (a) and cyclic voltammogram (b) of 1 nM $[Ru(bpy)_3]^{2+}$ in presence of 100 mM TPrA at glassy carbon electrode, scan rate 50 mV/s. (c) as (a) but with 1 μm $[Ru(bpy)_3]^{2+}$. The ECL intensity scale is given for (c) and should be multiplied by 100 for (a). Reprinted with permission from ref. [19]. Copyright 2002 American Chemical Society.

The use of TPrA as coreactant was firstly reported in the 1990s[20] and, although different authors investigated how the light is generated from these precursors, the mechanism of ECL generation is rather complicated and still unclear. Dr. Bard reported in 2002 four mechanistic proposals for the ECL signal generation from the $[Ru(bpy)_3]^{2+}$/TPrA precursors[19], which represent an example of "oxidative-reduction" coreactant system. Generally, the light generation as a function of the potential applied consists of two waves as reported in figure 1.4. The first ECL wave is in correspondence of the direct oxidation of TPrA at GC electrode, which has maximum at ~ 0.9V vs Ag/AgCl, while the second one occurs at 1.14V vs Ag/AgCl, in the potential region of the direct $[Ru(bpy)_3]^{2+}$ oxidation[21]. The two waves are associated with the emission of $[Ru(bpy)_3]^{2+}$ and usually merge when relatively high concentrations of the chromophore are used (~mM), but in the commercial systems where the concentration of $[Ru(bpy)_3]^{2+}$ label is very low (less than μM), the first wave is predominant.

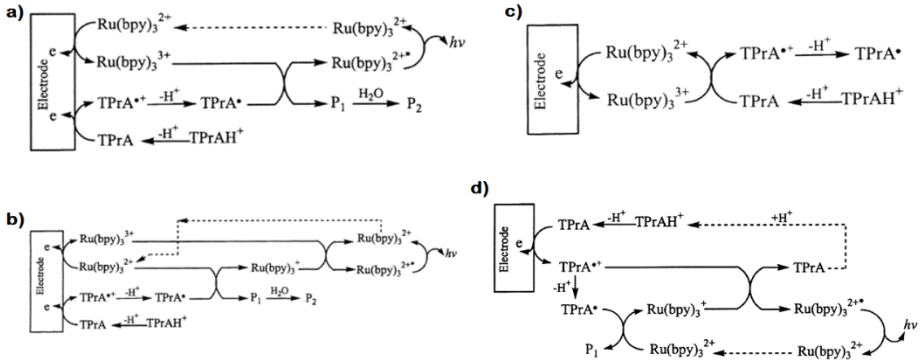

Figure 1.5: The four mechanism proposed by Bard. Reprinted with permission from ref. [19]. Copyright 2002 American Chemical Society.

To explain this behaviour, Dr. Bard proposed four different mechanisms (figure 1.5) that all contribute to the overall ECL signal generation, depending on the chromophore concentration and potential applied. All mechanisms predict that the oxidation of TPrA produces the oxidant species radical cation ($TPrA^{\bullet+}$) that upon deprotonation leads to the formation of the strong reductant species free radical ($TPrA^{\bullet}$) Both species are necessary to achieve ECL emission:

- TPrA and $[Ru(bpy)_3]^{2+}$ can be both oxidized at the electrode surface leading to the generation of the excited state through reaction with the strong reductant agent $TPrA^{\bullet}$ (scheme a, figure 1.5). This mechanism is usually referred as *"homogeneous coreactant ECL"*;
- $TPrA^{\bullet}$ can also reduce $[Ru(bpy)_3]^{2+}$ leading to the generation of light after annihilation reaction between the chromophore radicals (scheme b in figure 1.5);
- in scheme c, figure 1.5, is reported the so called "catalytic route", where the oxidation of the coreactant is achieved form the reaction whit the oxidized form of the chromophore. Generally, this mechanism prevails when high concentrations of $[Ru(bpy)_3]^{2+}$ are used;
- in scheme d, figure 1.5, only the oxidation of the coreactant generates the excited state formation. This mechanism

generally predominates when the diffusion of the chromophore towards the electrode surface is hampered and is usually referred as *"heterogeneous coreactant ECL"*. In fact, this mechanism is able to explain how the ECL signal is generated in the commercial analyzers (Origen Technology, now Roche). In an immunoassay, $[Ru(bpy)_3]^{2+}$-label species are immobilized on magnetic beads and successively attracted on to the electrode surface by magnetic forces: in this case, the diffusion of the chromophore is prevented and its oxidation would only occur by electron tunneling for those molecules close to the electrode surface (few nm). In this case, most of the labels on the beads surface would not contribute to the overall ECL signal. Nevertheless, the high sensitivity reached in these commercial analyzers has suggested that the majority of the labels on the beads can contribute to the signal and this can be justify considering the generation of radicals from TPrA oxidation. In particular, $TPrA^{\bullet+}$ cation radical might be sufficiently stable to diffuse in solution and generate the excited state, since its estimated lifetime in aqueous solution is ~ 0.2 ms[19].

Although there is no rule for the coreactant selection, amines are the most efficient ones, following the general trend: primary < secondary < tertiary amines, with tertiary amines producing the most intense ECL signal. In general, the amine should have a hydrogen atom connected to the α-carbon: only in this way, the cation radical species formed after oxidation can generate the strongly reducing free radical after deprotonation process. Moreover, the nature of substituents attached to nitrogen or α-carbon strongly influence the ECL intensity[22].

Nowadays, the coreactant selection is one of the most important challenges to improve ECL intensity and continuous efforts are destined towards the research of new and efficient coreactants[23]. Nevertheless, the complexity of the mechanism explains why the selection of new coreactants for $[Ru(bpy)_3]^{2+}$-labels is extremely difficult. In fact, the coreactant must form both oxidant (e.g. $TPrA^{\bullet+}$)

and reductant (e.g. TPrA$^{\bullet}$) with appropriate electrochemical properties and lifetimes.

1.5 Factors affecting the ECL efficiency

The ECL sensitivity of $[Ru(bpy)_3]^{2+}$/TPrA system is affected by several factors that influence the signal behaviour. Here, the most important causes are presented and briefly discussed.

pH. The ECL generation is strongly pH-dependent and the maximum signal is reached at pH 7.5[24]. The most credible reason to explain this dependency may be associated with the deprotonation reactions of the ammonium form (pKa=10.4) and the radical cation (schemes 1-6). In particular, it has been shown that at pH<5 the rate-determining step is the deprotonation of the ammonium species, whereas at pH>5 the deprotonation of the radical cation is the rate-determing step[25]. Moreover, TPrA solubility decreases increasing the pH and at pH>9 the electrochemically generated $Ru(bpy)_3^{3+}$ could react with hydroxide ions producing a significant ECL background (BG) signal.

Electrode material. The choice of the electrode material considerably influence the ECL generation. Carbon-based electrodes, like GC and CNTs, represent excellent material for ECL applications thanks to the favorable overpotential for TPrA oxidation, considered the rate-determining step for signal generation[26]. On the other hand, metallic electrodes, like Pt and Au, show weaker ECL emission compared to carbon-based materials, due to the formation of surface oxides that significantly reduce the direct oxidation of TPrA[21]. This point will be extensively illustrated in Chapter 3.

Oxygen. Oxygen dissolved in solution is considered, at the same time, a quencher of the excited state of $Ru(bpy)_3^{2+}$ [27] and the main responsible of the BG signal generation through the formation of singlet oxygen ($^1O_2$)[28]. The mechanism of its generation involves the reaction of oxygen with the radicals of TPrA formed after oxidation at the electrode. One of the strategies adopted to reduce its effect is the use of high TPrA concentrations, where the high generation of coreactant free radicals generated after oxidation could intercept and

reduce oxygen[29]. Moreover, several additives have been proposed for oxygen removal, like Melatonin[30] or Carotenoids[31].

Surfactants. The addition of surfactants in the solution mixture has proposed as a strategy for the ECL enhancement, since adsorption of surfactant molecules can increase the hydrophobicity of the electrode surface and reproducibility of the measurements[32],[33]. The increased hydrophobicity facilitates TPrA oxidation and ECL generation: this effect slight decrease increasing the surfactants chain length[34].

1.6 ECL vs CL: electrochemical or chemical pathway to form the excited state?

As ECL is a luminescent technique, also photoluminescence (PL) and chemiluminescence (CL) can be included in the same class. In CL, the formation of light is a product of chemical reaction after highly energetic electron-transfer between reactants. Although CL is used as diagnostic tool and it is the technology at the basis of several commercial systems, there are some limitations in the use of CL.

Firstly, in ECL the generation of light can be controlled with precise time and spatial resolution, thanks to the application of a potential at the electrode. In this way, it is possible to detect all the light generated improving the sensitivity. This behavior is not possible with CL, because the light is formed when the reactants are properly mixed, condition not subject to precise control. Secondly, the manipulation of the potential in ECL permits the manipulation of the energetics of the desired species, avoiding the generation of light from other molecules or impurities (side reactions). For this reason, ECL technique is more selective than CL. Thirdly, CL is a destructive technique since the species involved in the generation of light are chemically transformed or decomposed. Conversely, the emitting species in ECL is regenerated at the end of the process. Lastly, ECL does not require an external light source as PL requires, avoiding light scattering or luminescent impurities. Such conditions are ideal to work in biological environments because photobleaching is absent. Moreover, the background signal is extremely low leading to an increase of the signal to noise ratio (S/N) and hence sensitivity is extremely high. All these

conditions justify the success of the ECL technology, especially in clinical and medicinal chemistry.

1.7 ECL as analytical technique: a successful story

The importance of ECL as analytical technique is documented by the widespread applications developed in the last decades[35], ranging from food and environmental monitoring, clinical and medicinal chemistry. The majority of the applications are based on $Ru(bpy)_3^{2+}$/TPrA system, $Ru(bpy)_3^{2+}$ derivatives or other amines, which are mostly employed in the development of immunoassays. The state of the art of this technique is represented by the development of bench-top analytical analyzers commercialized all over the world.

1.7.1 ECL-based commercial systems: Roche Diagnostics and Meso Scale Discovery

The commercial ECL instruments are usually the combination of two distinct parts: the electrochemical device, where the electrochemical reaction for ECL generation takes place, and the optical device to detect the light. Light can be detect using a photomultiplier tube (PMT), a photodiode, or a charge coupled device (CCD). The latter one offers several advantages respect to the other detection devices, such as, high spatial resolution, multichannel detection possibility and immediate imaging manipulation.

The two most important ECL-based detection systems commercially available are from Roche and Meso Scale Discovery. Although both companies use ECL as detection technology for clinical diagnostics, the philosophy behind their products are completely different.

Roche is a global pioneer in pharmaceuticals and diagnostics and it is the leader in personalized healthcare, a strategy that aims to fit the right treatment to each patient in the best way possible. The Roche ECL technology is the Elecsys® technology, which combines ECL with paramagnetic beads for highly sensitive detection. The paramagnetic beads are streptavidin coated: the strong streptavidin-biotin bond, one

of the strongest non-covalent interaction known in nature, is used to affix the antigen/antibody complex directly to the beads surface. It is possible to obtain several immunoassay types using this approach, including competitive, sandwich and bridge assays. $Ru(bpy)_3^{2+}$ complex is used as luminescent label and TPrA is used as coreactant. The ECL detection is performed in several step. Firstly, during incubation, the binding step to form the immunocomplex occurs. Successively, sample and reagents are flow inside the electrochemical cell, a three-electrodes flow-through cell, where the application of magnetic forces ensure the capturing of the labeled paramagnetic beads on the working electrode. The aspiration of fresh solution containing TPrA provides the elimination of the unbound labels which might contribute to the overall luminescence for high sensitive measurements[36]. The constant efforts continuously spent by Roche to improve its technology is testified by the launch of its ultimate product on the market, the Cobas e 801 module[37], an immunochemistry analyzer designed for high performances, with a maximum capability of 300 tests/h.

Meso Scale Discovery (MSD) is a global leader in the development, manufacture and commercialization of innovative assays and instrument for the measurement of molecules in biological samples[38]. The approach is based on its own MULTI-ARRAY® technology, which combines ECL and arrays for precise quantitation of multiple analytes in a single sample requiring less time and effort than other assay platforms. The ECL-labels (SULFO-TAG™) conjugated to the detection antibodies are directly bound to the carbon-based electrode surface. MSD technology also uses $Ru(bpy)_3^{2+}$/TPrA as ECL generators. The electrical stimulation ensures ECL generation only from labels bound near the electrode surface enabling non-washed assays, for ultra-sensitive detection. The disposable MULTI-ARRAY and MULTI-SPOT plates are available in 96- and 384-well formats, with up to 10 spots per well, and allow simultaneously measurements of multiple analytes using very low sample volumes. The application of the electrical stimulation and detection of the ECL signal are ensured by MSD instruments (Sector S600, QuickPlex SQ 120) providing fast, simple assay processing, low sample volume and minimal consumption of reagents.

1.8 The aim of the thesis

In the last decades, ECL has become one of the most powerful analytical techniques, thanks to the electrochemical way to generate the signal. In fact, the absence of a light source renders this technique extremely sensitive and versatile for (bio)sensor applications. However, several factors, including the nature of the electrode material, strongly influence the ECL efficiency. Nowadays, the incessant research on this topic is directed towards the improvement of the signal generation. New strategies include selection of new coreactants, synthesis of new luminophores with high ECL quantum yield, design of new sensors for highly specific detection, just to mention a few. In particular, one of the most fascinating challenge is the study of new electrodic materials for ECL.

In the present doctoral thesis, the electrochemical investigation and study of different electrode materials for ECL-based biosensors are reported. In particular, it has been investigated how the signal generation is affected by the nature of the material, including in the present study metallic (platinum, gold and porous gold), carbon-based (carbon nanotubes -CNTs-, graphene) and transparent (indium tin oxide -ITO- with dyes functionalization, ink-jet printed CNTs layers) electrodes. Different electrochemical approaches have been used for this study, including chronoamperometry, cyclic voltammetry and impedence spectroscopy.

Successively, these materials have been employed for implementation and design of biosensors. In particular, two sensors for the early diagnosis of prostate cancer and for cell recognition have been developed. Moreover, the possibility to obtain transparent conductive electrodes is of great advantage for mechanistic studies. In particular, the imaging of small objects -beads or cells- deposited on the electrode is useful to analyze the signal generation in proximity of the electrodic surface. At this purpose, a microscope for ECL imaging has been optimized during this PhD.

Bibliography

[1]. A. J. Bard. *Electrogenerated Chemiluminescence.* Marcel Dekker, New York (2004).

[2]. Richter, M. M. *Chem. Rev.* **104,** 3003–3036 (2004).

[3]. Kapturkiewicz, A. *Anal. Bioanal. Chem.* **408,** 7013–7033 (2016).

[4]. A. Fiorani *et al.* in *Luminescence in Electrochemistry* pp 293–326 (2017).

[5]. Juris, A. *et al. Coord. Chem. Rev.* **84,** 85–277 (1988).

[6]. N. E. Tokel, A. J. Bard. *J. Am. Chem. Soc.* **94,** 2862–2863 (1972).

[7]. Lytle, F. E. and Hercules, D. M., *J. Am. Chem. Soc.* **587,** 253–257 (1968).

[8]. Hercules, D. M. *Science,* **145,** 808–809 (1964).

[9]. Chandross, E. A. and R. E. Visco, *J. Am. Chem. Soc.*, **86,** 5350–5351 (1964).

[10]. Harvey, N., *J. Phys. Chem.,* **33,** 1456-1459 (1929).

[11]. K. S. V. Santhanam, A. J. Bard. *J. Am. Chem. Soc.* **87,** 139–140 (1965).

[12]. Marcus, R. A. *Angew. Chem. Int. Ed. Engl.* **32,** 1111–1121 (1993).

[13]. Marcus, R. A. *J. Chem. Phys.* **43,** 2654–2657 (1965).

[14]. Chang, M. *et al. J. Am. Chem. Soc.* **99,** 5399–5403 (1977).

[15]. Rubinstein, I. and Bard, A. J. *J. Am. Chem. Soc.* **103,** 512–516 (1981).

[16]. White, H. S. and Bard, A. J. *J. Am. Chem. Soc.* **10,** 5399–5403 (1982).

[17]. Bolletta, F. Polypyridine Transition Metal Complexes as Light Emission Sensitizers in the Electrochemical Reduction of the Persulfate Ion. *Inorg. Chim. Acta* **62,** 207–213 (1982).

[18]. Bolletta, F. et al. *Inorg. Chim. Acta* **44,** L175–L176 (1980).

[19]. Miao, W., Choi, J. and Bard, A. J. *J. Am. Chem. Soc.* **124,** 14478–14485 (2002).

[20]. Leland, J. K. and Powell, M. J. *J. Electrochem. Soc.* **137,** 3127–3131 (1990).

[21]. Zu, Y. and Bard, A. J. *Anal. Chem.* **72,** 3223–3232 (2000).

[22]. Bruce, D., Mccall, J., Richter, M. M. *Analyst* **127,** 125–128 (2002).

[23]. Yuan, Y., Han, S., Hu, L., Parveen, S. and Xu, G. *Electrochim.*

Acta **82,** 484–492 (2012).
[24]. Knight, A. W. and Greenway, G. M. *Analyst* **121,** 101R–106R (1996).
[25]. Pastore, P., Badocco, D. and Zanon, F. *Electrochim. Acta* **51,** 5394–5401 (2006).
[26]. Valenti, G. *et al. Chem. Eur. J.* **21,** 12640–12645 (2015).
[27]. Timpson, C. J., Carter, C. C. and Olmsted, J. *J. Phys. Chem.* **93,** 4116–4120 (1989).
[28]. Kumar, S. S. and Bard, A. J. *Anal. Chem* **85,** 292–295 (2013).
[29]. Zheng, H. and Zu, Y. *J. Phys. Chem. B* **109,** 12049–12053 (2005).
[30]. Witt, M. D., Roughton, S., Isakson, T. J. and Richter, M. M. *J. Lumin.* **171,** 118–123 (2016).
[31]. Mascio, P. D. I., Raiser, S., Sies, H., Chemie, P. and Universitzt, D. *Arch. Biochem. Biophys.* **274,** 532–538 (1989).
[32]. Zu, Y. and Bard, A. J. *Anal. Chem.* **73,** 3960–3964 (2001).
[33]. Mccord, P. and Bard, A. J. *J. Electrocanal. Chem.* **318,** 91–99 (1991).
[34]. Factor, B. *et al. Anal. Chem.* **73,** 4621–4624 (2001).
[35]. Miao, W. *Chem Rev.* **108,** 2506–2553 (2008).
[36]. Imai, K. et al. *Hitachi Rev.* **57,** 1–7 (2008).
[37]. http://www.cobas.ch/de_CH/home/products_services/cobas-8000-modular-analyzer-series.html .
[38]. https://www.mesoscale.com/en/our_company .

Chapter 2

An electrochemiluminescent-supramolecular approach to sarcosine detection for the early diagnosis of prostate cancer

In the present chapter, the development of a sensor for the early diagnosis of prostate cancer is presented. Prostate cancer is the second worldwide most frequently diagnosed tumor. The early diagnosis is extremely important to improve the success of therapeutic treatments and to decrease mortality and intensive research is addressed towards this direction. The sensor proposed has been developed for the detection of sarcosine, a molecule recently pointed out as a marker for prostate cancer progression, which can be detected noninvasively in urine. The above-mentioned sensor is the synergic combination of a supramolecular approach for sarcosine recognition with the electrochemiluminescence technology for highly sensitive detection. In these pages, all the stages for the sensor design, development and optimization will be presented.

Key words: *prostate cancer; sarcosine; PCa marker; supramolecular receptor; sensor.*

Cover picture: famous people who died of prostate cancer.
First line from left: Frank Zappa, musician; François Mitterrand, politician. Second line from left: Charlton Heston, actor; Linus Pauling, chemist; Pablo Neruda, poet.

2.1 Prostate cancer: a global affair

According to the World Health Organization (WHO), the increasing incidence of cancer is the leading cause of death in developed countries and the second leading cause in developing countries[1]. In fact, more cancers occur in high-income countries than in low- and middle-income countries. In part, this is due to the different life expectation, because most cancers affect older adults. In addition, cancer tend to be diagnosed at later stages in many developing countries and, combined with reduced access to appropriate therapeutic treatments, it has and adverse effect on cancer survival. Another contributing factor is the irregular life style, where the developed countries are particularly affected: smoking, obesity, alcohol consumption, physical inactivity, unhealthy dietary intake are cancer-causing behaviors.

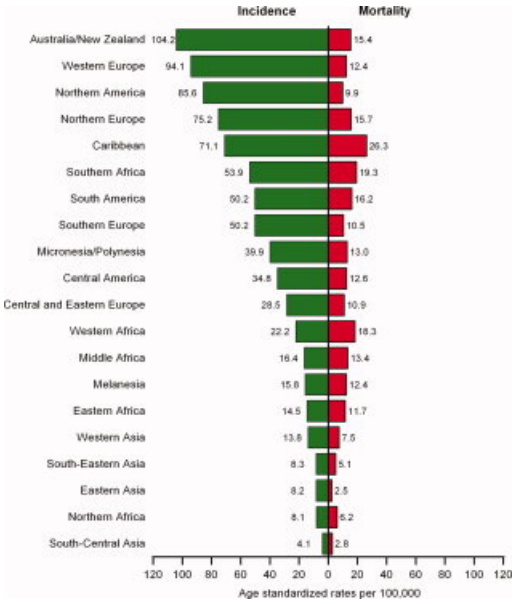

Figure 2.1: Estimated aged-standardized global incidence and mortality for prostate cancer in 2008 (source: Globocan 2008). Reprinted with permission from ref. [2]. Copyright 2011 American Cancer Society.

In this context, prostate cancer (PCa) is the second worldwide most frequently diagnosed tumour (14% of the total) and the sixth leading cause of cancer death in males[2]. Almost three-quarters of this cancer

cases are recorded in the developed countries, including Australia/New Zealand, Western and Northern Europe and Northern America[3] (figure 2.1). The high incidence recorded in these regions is mainly due to the widespread use of Prostate Specific Antigen (PSA) testing and subsequent biopsy to diagnose PCa. Relative high incidence is also present in several developing countries, including Caribbean, South America and sub-Saharan Africa, while South-Central Asia shows the lowest incidence rate. The death rates are almost similar between developed and developing countries, but the mortality is predominantly high in black populations, suggesting some genetic susceptibility[4],[5].

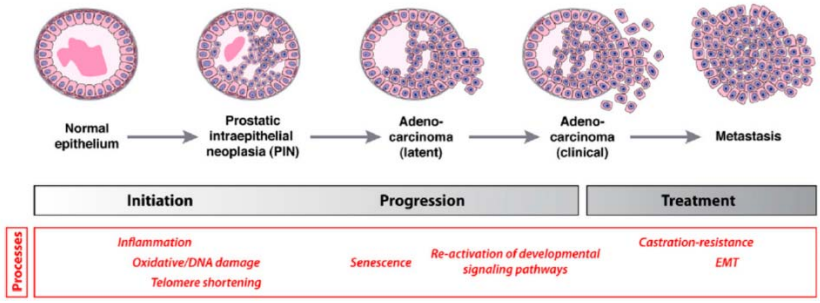

Figure 2.2: Prostate cancer evolution, including significant molecular processes at each stage. Adapted with permission from ref. [6]. Copyright 2010 Cold Spring Harbor Laboratory Press.

The most significant predisposing factor for prostate cancer incidence is the advanced age. However, the aging factor alone is not sufficient for the cancer development, since it varies remarkably among different populations. More likely, it is the result of a complex interplay of environmental, physiological and molecular events, where the advanced age exacerbates all these interactions. One of the major aging-associated factor for prostate carcinogenesis, suggested by different studies, is oxidative stress[7]. Oxidative stress results in the imbalance of reactive oxygen species (ROS), which can attack DNA directly or causing lipid peroxidation, with subsequent generation of a range of reactive products that can damage DNA[8]. Successively, prostate cancer progression is characterized by multiple and complex molecular events (figure 2.2) that include DNA mutations, protein

overexpression, abnormal disregulation of some signaling pathways and alteration of metabolic processes[6] (e.g. Warburg effect). Lastly, when prostate cancer metastasizes, it goes invariably to bones, causing characteristic osteoblastic lesions[9], although other common secondary target sites include lung, liver and pleura.

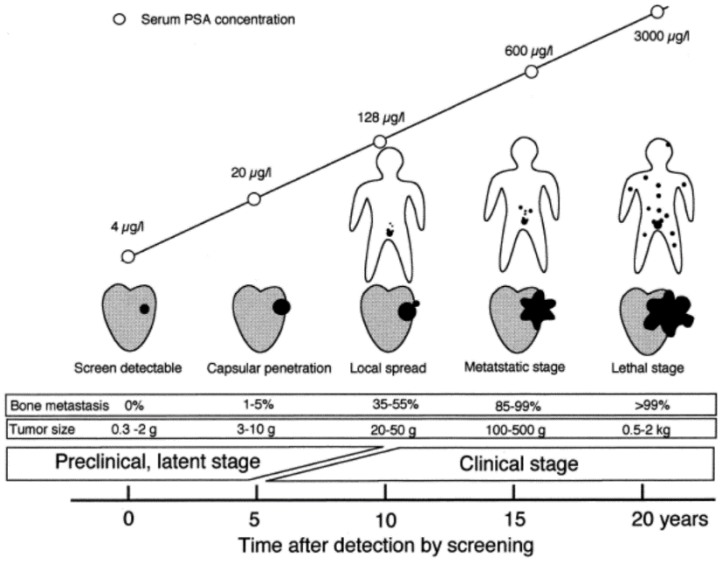

*Figure 2.3: Relationship between PSA concentration, cancer size and stage. Reprinted with permission from ref. [*10*]. Copyright 1999 Academic Press.*

The early diagnosis, when the tumor is organ-confined, drastically improves the success of therapeutic treatments and limits mortality. The PCa screening is carried out through PSA testing, an essay that has revolutionized the diagnosis of PCa, since it is now possible to detect this cancer at the earlier stages than before.

PSA, Prostate Specific Antigen, is a serine protease produced at high concentration in normal and malignant prostatic epithelium and it is mainly secreted into seminal fluid[10]. Although PSA is considered mainly prostate-specific, it is present in other extraprostatic tissues at extremely low concentrations. Only a minor amount of PSA leaks out into the circulating system from normal prostate, but this release is considerably increased when a prostate cancer is in progression. In fact, the concentration of PSA in serum is correlated with both the

volume of the cancer and the stage of the disease (figure 2.3). These reasons make PSA a sensitive biomarker for PCa, with a cut-off value of 4μg/L[11].

Nevertheless, one drawback of the PSA test is the lack in specificity, limited by the high frequency of false positive values; in fact, increased PSA serum levels have also observed in men with benign prostatic hyperplasia (BPH) or prostatitis. These results dramatically affect the test reliability. Moreover, the high risk of overdiagnosis may result in overtreatment with consequent long-term effects on the patient quality of life[12]. Thus, the early diagnosis needs to be augmented by the search of improved biomarkers for both more accurate diagnosis and selection of appropriate therapeutic treatments. The search has included gene expression profiling, serum proteomics, miRNA expression profiling and metabolomics. In particular, metabolomic profile studies represent a promising new approach in this direction, since they may allow to the development of noninvasive urine tests for cancer metabolities.

2.1.1 The role of sarcosine in the early diagnosis of prostate cancer

In the last decade, biomarkers discovery in urine samples has emerged as promising method for detecting and predicting aggressiveness of prostate cancer, since the degradation products of benign and malignant cells are secreted into urine. The development of noninvasive urine-based tests is a promising approach for large-scale screening programs, since present procedures are not totally satisfying. In fact, prostate tissue sampling by transrectal biopsy is invasive and it can not completely reflect the polyclonal nature of the tumour. In this direction, one urinary RNA marker, Prostate Cancer Antigen 3 (PCA3), has already passed the early phases of discovery and demonstrated clinical utility in multicenter studies[13].

However, the study of metabolomic profiles in urine is considered more promising whereas an important study has pointed out that sarcosine can be considered the key molecule that increases in metastatic PCa forms[14],[15]. In particular, the study reports that high levels of sarcosine in urine, an N-methyl derivative of the amino acid

glycine (figure 2.4), relate with the presence of the disease and its progression. Probably, sarcosine and its regulatory enzymes may play an intermediate role in tumour progression, modulating cell invasion and migration. Although the role of sarcosine as PCa biomarker is still debated[16], assessment of levels of sarcosine might help the development of a large scale PCa screening program, since the biomarker can be detect noninvasively in urine[17],[18].

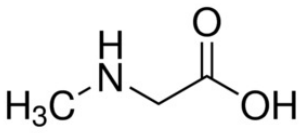

Figure 2.4: Chemical structure of sarcosine.

2.2 An ECL-supramolecular approach for sarcosine detection

The recent discovery of sarcosine as potential PCa biomarker and its noninvasive detection in urine have opened new interesting backdrops for the early diagnosis of prostate cancer. In particular, as alternative to the immunoassay molecular recognition, an ECL-supramolecular sensor for sarcosine detection may be proposed.

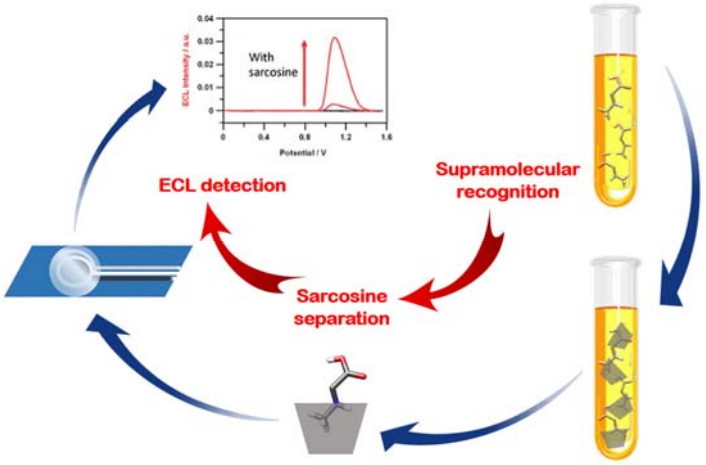

Figure 2.5: Schematic principle of the sensor developed in this thesis as synergic combination of supramolecular chemistry for sarcosine separation and ECL detection for its quantification.

Sensor technology is an efficient tool for the acquisition of information with real time accuracy. In more detail, a chemical sensor is a device where an amplified electrical signal is measured as a response of some chemical composition of the system in real time. The sensor development consists of two distinct parts: recognition and amplification. The recognition is supplied by a material capable of interacting with the desired analyte, whereas the amplification is provided by a transducer on which the material is coated. In the present case, the sensor developed is a synergic combination of ECL as transduction method, with supramolecular recognition offered by synthetic molecular receptors. This approach aims to discriminate sarcosine form other interferences present in urine with extremely high selectivity and sensitivity. High selectivity can be reached taking advantage of the ability of molecular receptors to bind specific target molecules. In this regard, chemists are nowadays able to synthetize molecular receptors that mimic the specific properties of biological ones and can control the host-guest interaction designing synthetic receptors according to the analyte to be detected. On the other hand, the high degree of sensitivity can be reached using ECL as detection method, thanks to the electrochemical way to generate the signal. Furthermore, the application of ECL in analytical science allows the development of sensors with good temporal and spatial resolution, robustness and versatility. In fact, ECL is nowadays the most used transduction methodology applied for the early PCa diagnosis for both research and commercial applications[19],[20]. For example, Roche already commercializes ECL instruments based on magnetic microbeads technology for PSA detection (Elecsys®[21]). Nonetheless, this instrumentation is considerably expensive for a wide spread use, although current technology is the most powerful available on the market. Hence, the sensor proposed has been developed to be inexpensive, portable and easy to use for more suitable and affordable field operation and point-of-care (POC) testing. Moreover, as already argued in Chapther1, amines are used as coreactant to achieve ECL signal generation. This is of primary importance for the development of the above-mentioned sensor, since sarcosine is an amine and it can be exploited as coreactant for ECL generation.

In the next sections, all the stages for the sensor development will be extensively illustrated.

2.3 Sensor development

The PCa sensor for sarcosine detection is the combination of two different approaches (figure 2.5):

- *supramolecular recognition:* tetraphosphonate cavitands highly selective towards sarcosine;
- *ECL detection*: magnetic microbeads technology for sarcosine separation and quantification in urine solution.

2.3.1 Tetraphosphonate cavitands: a supramolecular approach

The design of an optimal sensor should responses to precise characteristics. Firstly, responsiveness to detect the target analyte at very low concentrations. Secondly, selectivity to recognize primarily the target species in presence of interferents. Thirdly, sturdiness to withstand the widest operating conditions. Supramolecular chemistry can respond to these specific requests, thanks to the ability of synthetize molecular sensors with extremely high selectivity properties, and it has largely been used for specific recognition of analytes, ranging from small molecules to proteins[22],[23]. Supramolecular receptors of particular interest for the well-known selectivity properties are cavitands that are synthetic organic compounds provided with cavities of molecular dimensions. In particular, phosphonate cavitands[22], presenting one to four hydrogen (H) bonding acceptor P=O groups at the upper rim of the cavity, are of particular interest for the complexation of molecules able of H bonding. For this reason, to detect sarcosine, which is able of H bonding in its protonated form, a cavitand with four phosphate groups has been chosen. This tetraphosphonate cavitand has been provided by a collaboration with Prof. Enrico Dalcanale and his group at the University of Parma (Italy).

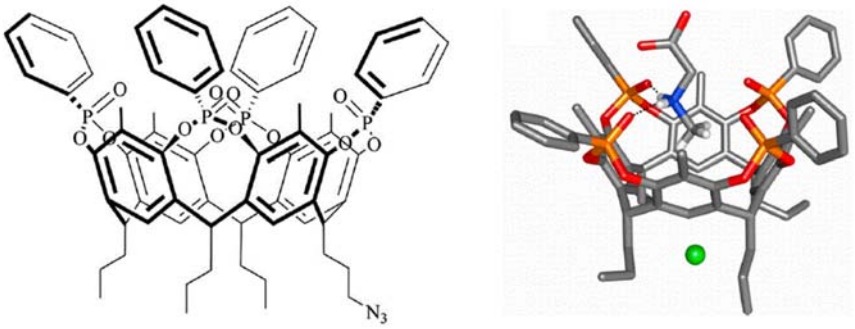

Figure 2.6: Chemical structure of the Tiiii cavitand receptor (left) and crystal structure of the complex Tiiii•sarcosine hydrochloride (right). Adapted with permission from ref. [24]. Copyright 2012 PNAS.

In the design of phosphate cavitands, the presence of P(V) stereocenters brings configurational properties into play, since the relative orientation of the P=O groups at the upper rim of the cavity (inward or outward with respect to the cavity) entails stereoisomeric properties to the cavitand. In the current nomenclature, the first capital letter gives the number of the bridging groups, while the second lower case letter indicates the in/out stereoisomer at each P(V) stereocenter. In particular, only the inward facing stereoisomers (i) with P=O groups facing towards the cavity are efficient receptors. In brackets R_1, R_2 and R_3 define the substituents at the lower rim, in the apical positions and on the P(V) stereocenters, respectively. Therefore, the tetraphosphonate cavitand used in this thesis has formula Tiiii[C_3H_7, CH_3, Ph], from now onward referred as Tiiii, and its chemical structure is reported in figure 2.6. In solution, Tiiii shows remarkable molecular recognition properties towards the N-methyl ammonium salts[25]. In fact, Tiiii is able to selectively recognize the protonated form of sarcosine in water anchoring the $^{+}NH_2CH_3$ group[24], with very high affinity constant (~$4x10^5$ M^{-1} in methanol[26]). The origin of this selectivity can be attributed to the interplay of three interaction modes: a) multiple ion-dipole interactions between the inward P=O groups of the Tiiii and the positively charged $^{+}NH_2CH_3$ group of sarcosine; b) H bonding involving the P=O groups of the cavitand; c) CH-π interactions between the methyl group of sarcosine

and the cavity of the receptor. The complexation activity of Tiiii towards sarcosine dictated by these three interaction modes result in a host-guest interaction.

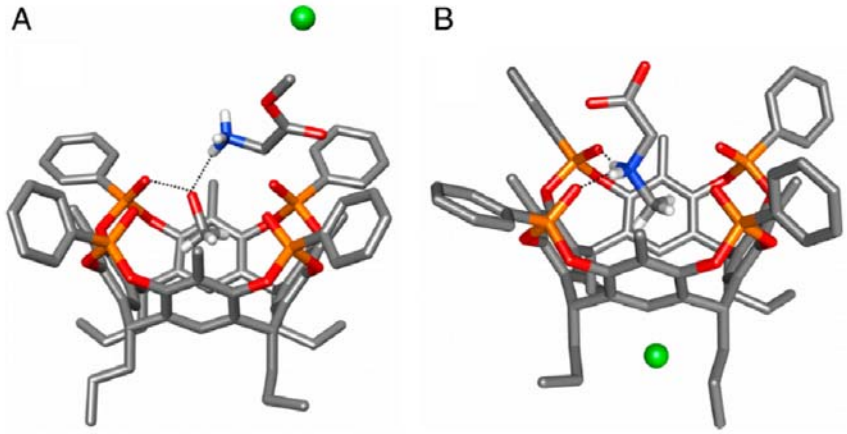

Figure 2.7: Crystal structure models of the complexes Tiiii•methanol•glycine methyl ester hydrochloride (A) and Tiiii•sarcosine hydrochloride (B). C = gray; O = red; P = orange; N = blue; Cl = green; H = white; H bonds = black dotted lines. The H atoms of the cavity and those not involved in the complexation activity have been omitted for clarity. Reprinted with permission from ref. [24]. Copyright 2012 PNAS.

The recognition of sarcosine in urine is the most challenging part for the sensor design and it is twofold. First, sensor operation in aqueous environment might be difficult due to the severe weakening of the H bonding interaction between host and guest. Second, urine is a complex matrix in which overwhelming amounts of potential interferents are presents, above all glycine that represents sarcosine precursor in biochemical pathway and one of the most abundant amino acid metabolite in urine. Nonetheless, the difference of binding modes between glycine and sarcosine are evident, as shown by crystal structure models obtained via slow evaporation of methanol/water solutions containing the host in presence of an excess of the guest[24] (figure 2.7). The complexation of glycine is mediated by a molecule of methanol which occupies the cavity of the host (figure 2.7 A), while for sarcosine the complexation activity is the result of the synergy of the three interaction modes described above (figure 2.7 B). The different complexation activity of Tiiii towards the two guests can be attributed

to the presence of the methyl group on the nitrogen in sarcosine. Its CH_3-π interaction with the cavity triggers the formation of two H bonds and cation-dipole interactions, which further stabilize the complex. The pivotal role of the N-methyl residue in stabilizing the complex formation has theoretically evaluated in 3.8 kcal mol^{-1} by Density Functional Theory (DFT) calculations[24]. Furthermore, NMR biphasic extraction experiments prove that water does not hamper the ability of Tiiii to bind sarcosine, while it completely shuts down glycine uptake[24]. This result can be explained recalling that water dramatically impairs H bonds formation, the only interaction present between Tiiii and glycine, while it does not affect the CH_3-π interaction in sarcosine. The final outcome is the preferential selectivity of Tiiii for sarcosine versus glycine in water.

For these reasons, the outstanding selectivity properties of Tiiii towards sarcosine can be exploited for the development of sensing device. In detail, since Tiiii recognizes only the protonated form of sarcosine, the idea is to modify the stability of Tiiii•sarcosine complex by tuning the pH, regulating both capture and release of the target molecule in urine solution.

2.3.2 Magnetic microbeads technology: ECL detection

To couple the capturing properties of the cavitand Tiiii with the ECL detection, commercial magnetic microbeads (MMBs) of 3.2 μm diameter have been functionalized at the surface with Tiiii (Tiiii@MMBs) through a click chemistry based protocol. The functionalization procedure, reported in appendix A.2, has been carried out in collaboration with the group of Prof. Luca Prodi at the University of Bologna. This step provides an efficient and robust linking between the MMBs surface and the supramolecular recognition moiety Tiiii.

The analytical protocol for sarcosine detection and quantification is schematized in figure 2.8 and it consists of three main steps[27] (appendix A.4 for experimental details):

1) *capturing:* at acidic pH, Tiiii@MMBs and sarcosine in the protonated form are incubated for recognition (figure 2.8, inset 1);

2) *separation and release:* maintaining constant the pH value, the application of a magnetic field attracts Tiiii@MMBs complexes, leading to separation of sarcosine hydrochloride from solution and other interferents. Successively, the replacement of fresh solution at basic pH leads to sarcosine deprotonation causing its release from Tiiii@MMBs complexes (figure 2.8, inset 2);
3) *detection:* at the supernatant containing sarcosine, $Ru(bpy)_3^{2+}$ chromophore is added. Finally, the solution is deposited on a disposable screen-printed electrode (carbon) and after application of the potential, sarcosine can be oxidized and the ECL signal can be recorded (figure 2.8, inset 3).

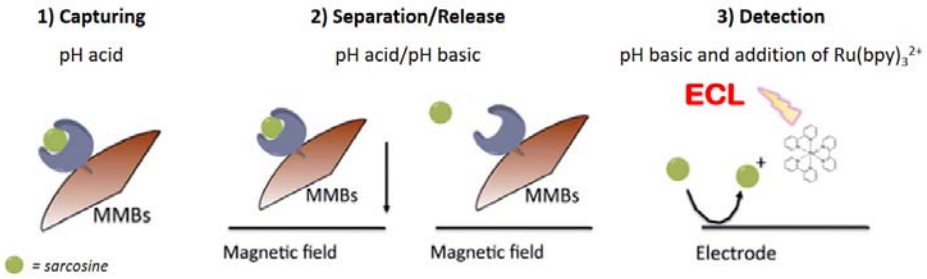

Figure 2.8: Schematic representation of the analytical protocol for sarcosine separation and quantification. Adapted with permission from ref. [27]. Copyright 2015 The Royal Society of Chemistry.

To obtain a quantitative sarcosine determination, the pivotal step is the exhaustive release of sarcosine from Tiiii@MMBs. In fact, Tiiii cavitand complexes sarcosine only when the biomarker is in its protonated form, since all three synergic interaction modes are activated. When the $^{+}NH_2CH_3$ group is deprotonated at basic pH ($^{+}NH_2CH_3$ converted in $^{+}NHCH_3$), the synergic combination of the three interaction modes is weakened and the Tiiii complexation activity is decreased, leading to sarcosine release in solution. For this reason, a precise control of pH is essential for the optimal operation of the sensor. Hence, it has been found that the optimal pH values for sarcosine capturing and release are 5 (pH << sarcosine pKa) and 12 (pH >> sarcosine pKa), respectively. As shown in figure 2.9 b, only when pH 12 is used sarcosine can act as coreactant for ECL

generation, since it is converted to the free base and released in solution by Tiiii@MMBs complex. In fact, its oxidation generates an increase of the ECL intensity when the $Ru(bpy)_3^{2+}$ is added (black signal compared with the red signal of $Ru(bpy)_3^{2+}$ alone, figure 2.9 b). If lower pH are used, for example at 9, sarcosine is not deprotonated and it can not be released by the cavitand: the ECL signal is mainly BG generated from the chromophore (comparison of black and red signals in figure 2.9 a).

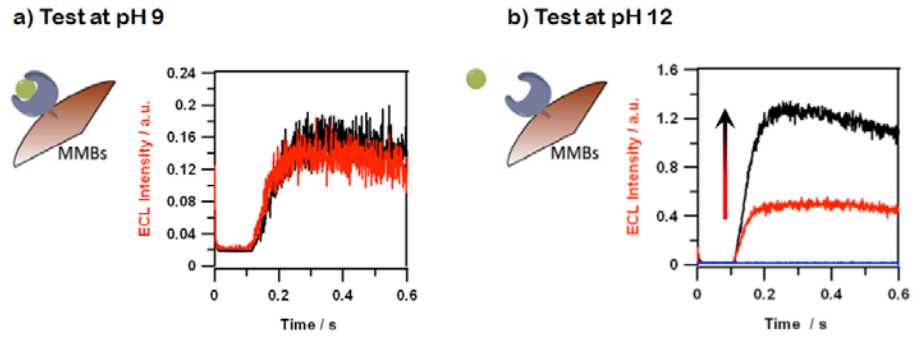

Figure 2.9: ECL/time transients of sarcosine 200 mM with 20 μM $Ru(bpy)_3^{2+}$ (black line), only 20 μM $Ru(bpy)_3^{2+}$ (red line) and only 200 mM sarcosine (blue line) at pH 9 (a) and at pH 12 (b) in phosphate buffer (PB) solution. PMT bias 750V. The potential program is switched between 0V (t_1 = 1 sec) and 1.4V (t_2 = 4 sec) vs Ag. Adapted with permission from ref. [27]. Copyright 2015 The Royal Society of Chemistry.

2.3.3 Sarcosine as coreactant for ECL generation

Considering the mechanistic proposals for the ECL coreactant pathway (chapter 1), the signal generation depends on both the chromophore and the coreactant concentrations. When the amines detection is the main analytical issue, a possible analytical approach is based on measuring the ECL intensity in presence of a constant concentration of luminophore. In this case, the light intensity depends exclusively on the amine concentration, which becomes the limiting factor for the signal generation. This approach has largely been used in literature for quantification of amino acids, peptides[28], nucleic acid[29], NAD[30] and it has also applied in portable devices for amine

detection[31]. For this reason, the choice of using ECL technique is justified not only for its high sensitivity, but also for the potential role of sarcosine to act as coreactant for light generation.

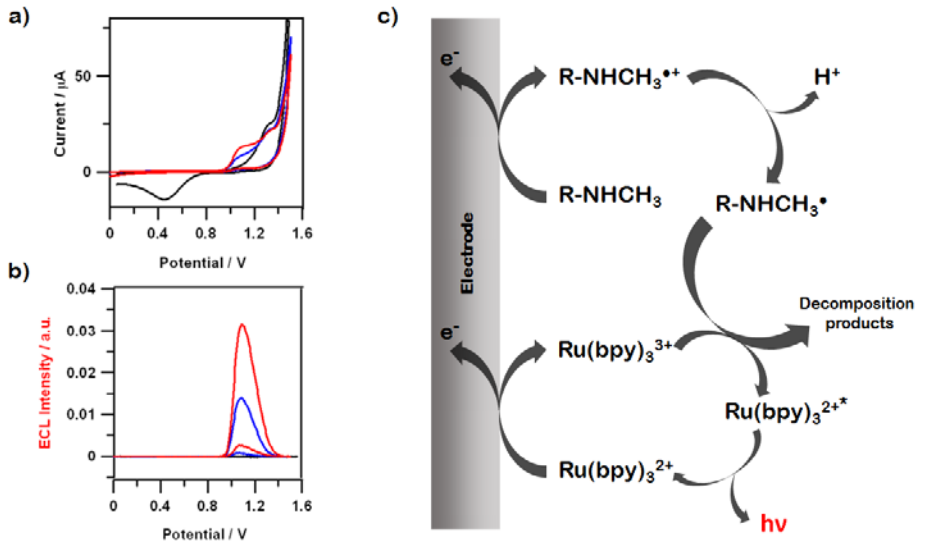

Figure 2.10: Cyclic voltammetry (a) and ECL (b) of 1 mM $Ru(bpy)_3^{2+}$ in PB solution without (black line), with 10 mM (blue line) and 20 mM (red line) of sarcosine. PMT bias 750 V. Schematic representation (c) of the ECL "oxidative-reduction" coreactant mechanism involving sarcosine as coreactant species with $Ru(bpy)_3^{2+}$ as luminophore.

Sarcosine is a secondary amine and it shows an irreversible oxidation peak at 1V (figure 2.10 a). Therefore, it likely possesses the energy requirements for generating the excited state of the chromophore. Its capability to act as coreactant for ECL generation has been tested according to the "oxidative-reduction" mechanism in PB solution with $Ru(bpy)_3^{2+}$ 1mM. As figure 2.10 b shows, ECL generation is obtained only when sarcosine is present (see black signal obtained in the absence of the amine), with a maximum intensity in correspondence of the full coreactant oxidation, and its intensity is a function of sarcosine concentration (see for comparison blue and red signals). This is also confirmed by the relative increase of the oxidation current at 1V after addition of increasing concentrations of sarcosine, as cyclic voltammetry shows (figure 2.10 a).

The ECL coreactant mechanism of sarcosine PCa biomarker is represented in figure 2.10 c. The oxidation reaction of sarcosine produces a cation radical species ($R\text{-}NHCH_3^{\bullet+}$) that immediately undergoes a deprotonation reaction leading to the formation of a highly stable radical species ($R\text{-}NHCH_3^{\bullet}$). The radical formed can react with both the oxidized form of the chromophore ($Ru(bpy)_3^{3+}$), generating the light emitting state, and the neutral form of the complex, causing its reduction ($Ru(bpy)_3^{2+}$ converted to $Ru(bpy)_3^{+}$, this meachanism has been omitted for clarity). The reduced form $Ru(bpy)_3^{+}$ can react with the oxidized form $Ru(bpy)_3^{3+}$ generating the emitting excited state $Ru(bpy)_3^{2+*}$. Both mechanisms are possible simultaneously and their contribution to the overall excited state formation depend on the concentration of the amine, since the concentration of the chromophore has maintained constant.

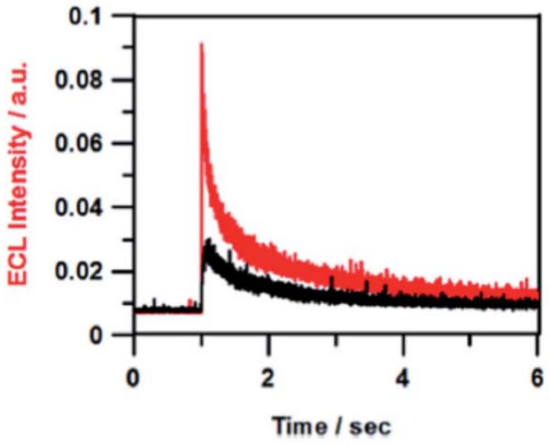

Figure 2.11: ECL/time transients for 10 mM sarcosine (black line) and 10 mM TPrA (red line) with 1mM $Ru(bpy)_3^{2+}$ in PB solution. PMT bias 750 V. Double step potential between 0V (t_1 = 1 sec) and 1.4V (t_2 = 5 sec). Reprinted with permission from ref. [27]. Copyright 2015 The Royal Society of Chemistry.

Finally, coreactant efficiency of sarcosine has been evaluated using TPrA as reference, since the latter one is the most efficient coreactant reported in literature. Unfortunately, the ECL generation efficiency for sarcosine is 30% less than TPrA (figure 2.11). This can be explained considering the different structures of the two amines: sarcosine is a

secondary amine, whereas TPrA is a tertiary amine. In fact, tertiary amines show higher ECL intensity than secondary amines, although this is not a rule for the choice of the coreactant. The different number of the alkyl substitutions on the nitrogen atom of the amine is responsible of the different stability of the radicals formed after the oxidation process. Consequently, the different stability influences the lifetime of the radicals and their diffusion, for a gradient of concentration, from the electrode surface, where they are generated, towards the bulk. In fact, for the nature of the ECL phenomenon, the light generation can be achieved only in the proximity of the electrodic surface.

2.4 Preliminary tests: detection of sarcosine in water

Preliminary tests of the sensor developed have been carried out through the detection of sarcosine in water using the three steps analytical protocol. The calibration curve in figure 2.12 reports the ECL intensity as a function of sarcosine concentrations, ranging from 50 to 3000 μM. The choice of this concentration range for preliminary investigations is motivated by the fact that the sarcosine urinary values for PCa early diagnosis are included in this range. In fact, these diagnostic values vary from μM-range for healthy patient to mM-range for PCa patient.

The data obtained have been analyzed considering the behaviour of the sensor as a typical ligand-receptor interaction, as represented by the following equation:

$$I_{ECL} = A[(B \cdot C_{sarcosine})/(1+B \cdot C_{sarcosine})] \qquad \text{(eq. 1)}$$

In equation 1, A is a constant proportional to the surface coverage of the cavitand on the microbeads surface and B is the affinity constant of the cavitand Tiiii for sarcosine hydrochloride in its protonated form. From the best fitting of the curve (figure 2.13), the value obtained for the affinity constant is $2x10^3$ M^{-1}, significantly lower than the value reported with ^{1}H-NMR spectroscopy. This discrepancy might be explained considering the reduced recognition properties of the Tiiii cavitand, probably affected by the working conditions, firstly the

functionalization on the microbeads surface. Secondly, application of magnetic forces or the necessary addition of the supporting electrolyte in the analytical solution or both might also have some negative influences on the Tiiii complexation activity. Nevertheless, the results displayed in figure 2.12 show, however, the great potential of the present approach for the quantitative determination of this important PCa biomarker, sine the sensor respond to sarcosine concentrations included in the diagnostic urinary values.

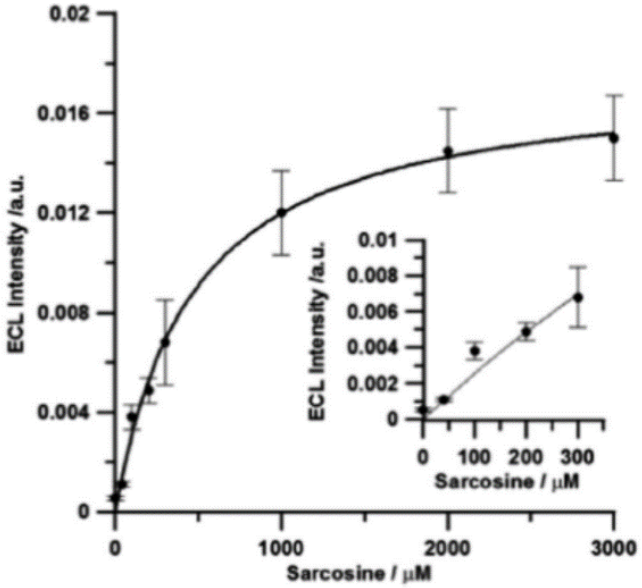

Figure 2.12: ECL signal as a function of sarcosine concentration (50, 100, 200, 300, 400, 1000, 2000, 3000 μM), obtained in PB solution, pH 12, with 20 μM $Ru(bpy)_3^{2+}$ after potential application (1.45V vs Ag). Tiiii@MMBs were incubated with sarcosine hydrochloride at pH 5 for 1 hour. Successively, Tiiii@MMBs-sarcosine hydrochloride were washed three times with 0.05% Tween 20 and PB pH 5. Inset, the linear part of the calibration curve. Error bars show standard deviations (n=3). Reprinted with permission from ref. [27]. Copyright 2015 The Royal Society of Chemistry.

The limits of detection (LOD) and quantification (LOQ) have finally determined and the values obtained are 30 μM and 50 μM for LOD and LOQ, respectively. These values are included in the diagnostic urinary window. Unfortunately, the LOD using ECL is higher than the LOD obtained using Liquid Chromatography coupled with Mass

Spectrometry (LC-MS) analysis, the standard technique used to reveal the presence of sarcosine. In fact, the LOD of the present ECL-based sensor corresponds to 2.7 μg mL^{-1}, whereas the LOD for LC-MS method is 1 ng mL^{-1}. However, this technique requires long times analysis and sarcosine derivatization[32], while in the present case, no chemical treatments of urine are necessary and the detection is fast.

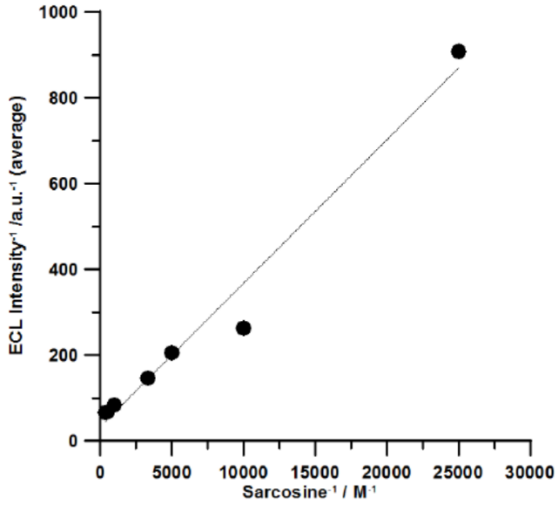

Figure 2.13: Linearization of the ECL intensity versus sarcosine concentrations (50, 100, 200, 300, 400, 1000, 2000, 3000 μM), obtained in PB solution, pH 12, with 20 μM $Ru(bpy)_3^{2+}$ after potential application (1.45V vs Ag). Tiiii@MMBs were incubated with sarcosine hydrochloride at pH 5 for 1 hour. Successively, Tiiii@MMBs-sarcosine hydrochloride were washed three times with 0.05% Tween 20 and PB pH 5. Reprinted with permission from ref. [27]. Copyright 2015 The Royal Society of Chemistry.

2.5 Sensor performances on real urine samples from patients with diagnosed PCa

In the latest stage of the sensor trial, the potential applicability of the proposed methodology in real samples has tested detecting sarcosine in three human urine samples, which have provided by the University Hospital of Verona (Italy), according to the rules of the local ethical committee and with the consent of the patients. The urine samples have been obtained by patients with diagnosed advanced

metastatic disease or advanced localized disease, confirmed by imaging technique and previously analyzed by commercial ELISA analysis for PSA test in serum. As negative control, urine sample derived from a healthy donor has used. The urine samples have been filtrated and centrifuged, without any chemical treatment or derivatization.

As reported in figure 2.14, the analysis of urine from patients with diagnosed PCa (case a and c) show significantly higher ECL signal than urine from healthy patient (case b). The concentrations of sarcosine evaluated with the present methodology are: a) 1.91 mM and c) 1.34 mM for metastatic PCa patients and b) 0.27 mM for the healthy subject[27]. The values obtained show an increase by one order of magnitude of sarcosine concentration for PCa patients. Importantly, it is noteworthy that this proposed ECL-based sensor responds to sarcosine concentrations encompassed in the diagnostic urinary values for PCa diagnosis. These promising results indicate both the potential role of sarcosine as biomarker for PCa and the applicability of the presented methodology in clinical assays to measure urinary levels of the amine.

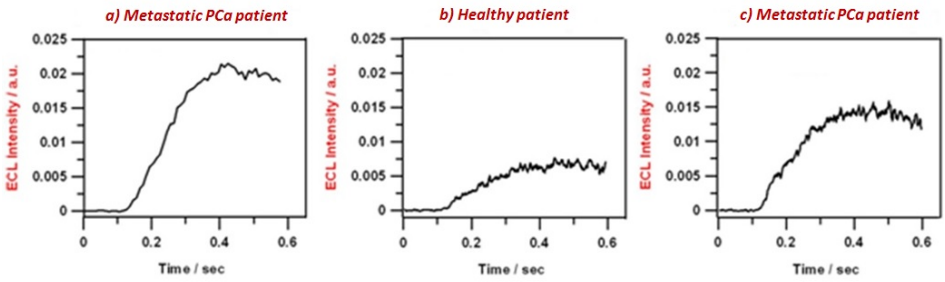

Figure 2.14: ECL intensity vs time applying 1.45V vs Ag, obtained in PB pH 12 solution with 10 μM $Ru(bpy)_3^{2+}$. a) and c) signals obtained from urine of metastatic PCa patients; c) signal obtained from urine of a healthy donor. All the urine samples were centrifuged with a molecular weight cut-off membrane of 3 kDa. MMMBs were previously functionalized with Tiiii cavitand; successively, Tiiii@MMBs were incubated for 1 hour with the urine samples adjusting the pH at 5 with PB. The resulting Tiiii@MMBs-sarcosine hydrochloride complexes were washed three times with 0.05% Tween 20 and PB pH 5. Adapted with permission from ref. [27]. Copyright 2015 The Royal Society of Chemistry.

2.6 Considerations

This ECL-based sensor is a valid proposal for the noninvasive detection of sarcosine in urine. The ECL magnetic microbeads technology, inspired by Roche technology, offers a strategic tool to separate sarcosine from a complex matrix such as urine. In fact, the synergic combination of the complexation activity of the Tiiii cavitand and the magnetic separation offered by magnetic microbeads guarantees the recognition of sarcosine between a large number of metabolites very similar to sarcosine for structure and molecular weight, first of all glycine, where sarcosine represents its methyl-derivative. This aspect is extremely important for the success of the proposed methodology. Furthermore, the sensor does not require particularly expensive instrumentation for the operation: a photomultiplier tube (PMT) to detect the light and a dark box to minimize the BG signal are sufficient. This aspect is of fundamental importance for a widespread use of the sensor, which can be used for point-of-care (POC) diagnosis, improving diagnostic solutions and healthcare of PCa patients. Finally, this ECL-based sensor is disposable, portable and easy to use.

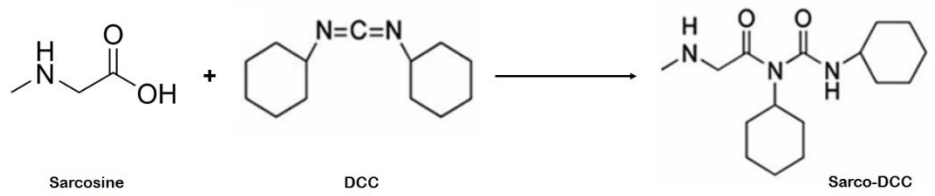

Figure 2.15: Derivatization scheme of sarcosine with DCC (N,N'-Dicyclohexylcarbodiimide) and its final chemical structure. Adapted with permission from ref. [32]. Copyright 2013 Wiley-VCH Verlag GmbH.

Nevertheless, the main drawback of the proposed methodology is the LOD. Unfortunately, the LOD using ECL technique is considerably higher that the LOD obtained with LC-MS technique, decreasing the sensitivity of the sensor. In fact, chromatography/mass spectrometry analysis are the most established methods for the recognition of large number of analytes in complex matrix. In particular, LC-MS can also discriminate the presence of sarcosine

between other two isomers, α-alanine and β-alanine, which have the same molecular weight and similar properties of sarcosine and they could interfere with its accurate detection. However, this technique requires long time analysis (optimal time analysis 12 hours) and implies sarcosine derivatization (figure 2.15) to improve its retention in stationary phases commonly used in chromatography and to facilitate its separation from other small polar molecules[32]. On the contrary, these treatments are completely avoided with the proposed sensor, which perform sarcosine detection directly on untreated urine samples, with fast response.

2.7 Conclusion

The present work demonstrates the development of a sensor for the early diagnosis of prostate cancer through the noninvasive detection of sarcosine in urine, since it has recently indicated as new biomarker for PCa. The approach proposed is the synergic combination of supramolecular chemistry for sarcosine separation and the ECL technology for its quantification. In details, the highly selective complexation properties of the tetraphosphonate cavitand Tiiii are combined with magnetic microbeads for sarcosine separation from a complex matrix, such as urine. In particular, Tiiii cavitand can discriminate sarcosine from glycine, the non-methylated form of sarcosine, thanks to the interplay of three interaction modes that work simultaneously for the complexation of the PCa biomarker. The final result is an inexpensive and disposable device, suitable for a widespread use and especially developed for POC diagnosis. Furthermore, since sarcosine is a secondary amine, its use as coreactant for ECL generation has been proved, although it shows lower efficiency compared with TPrA, the most efficient coreactant reported in literature. Finally, the potential applicability of the sensor presented here has been tested through quantification of sarcosine in real urine samples from patients with diagnosed metastatic level of PCa. Although the disadvantage of this approach is the high LOD compared with the LOD of the standard method LC-MS, no chemical treatments of urine or sarcosine derivatization are required, for a fast

and reliable detection. Hence, this promising approach can be used in future for POC diagnosis of the PCa at the early stage.

Appendix

A.1 Chemicals and Materials

Tris(2,2'-bipyridine)dichlororuthenium(II) ($[Ru(bpy)_3]Cl_2$), Tripropylamine (TPrA), phosphate buffer (PB at pH 5 or pH 12), propargylamine, bathophenanthrolinedisulfonic acid disodium salt were purchased from Sigma-Aldrich. Screen printed electrodes (SPEs) C110 were purchased from DropSens®. All the reagents were used without any additional purification.
Tiiii[N_3, CH_3, Ph] was synthesized according to reported procedures[33].

A.2 Magnetic microbeads functionalization - Tiiii@MMBs

Microbeads handling was achieved with magnetic separation and resuspending by vortexing.
200 µL of Carboxyl Magnetic Particles suspension (Sphero™ - CM-30-10, 2.5% w/v, 3.2 µm) was diluted in MES buffer (500 µL, 50 mM, pH 6.0, Triton X-100 0.01% w/v), and washed with the same buffer solution (4 x 500 µL). The microbeads were finally resuspended in MES buffer (160 µL), propargylamine (2 µL) was then added, followed by three separate additions of 40 µL of EDC•HCl in MES solution (50 mg mL^{-1}) performed over 3 h. The microbeads were then recovered and washed (4 x 500 µL, PBS 1x, pH 7.4), and 250 µL of the final 500 µL suspension was set aside as a control.
The remaining microbeads (250 µL) were recovered from the suspension and washed with TRIS buffer (2 x 1000 µL, 25 mM, pH 8.0, Triton X-100 0.01% w/v).
A TRIS buffer solution was then added (1400 µL), together with three small fragments of copper wire (~ 1 cm), a bathophenanthrolinedisulfonic acid disodium salt solution (120 µL, 6.2 mM, DMSO/water 1/1) and a Tiiii solution (150 µL, 12 mM, methanol/DMSO 3/1). This mixture was kept under gentle orbital stirring for 18 h. The magnetic microbeads were then recovered and washed with TRIS buffer (3 x 1000 µL) and PBS 1x buffer (2 x 500 µL), and stored at 4° C in 500 µL of PBS 1x buffer.

A.3 Electrochemistry and ECL measurements

The ECL measurements were carried out through deposition of 50 µL of the sample directly on the screen printed electrode surface (see the detection part for details). The ECL signal generated by performing the potential step program was measured with a photomultiplier tube (PMT, Hamamatsu R4220p) placed, at a constant distance, above the electrode and inside a dark box[34]. The PMT was supplied with a voltage in the range 550-750 V. The light/current/voltage curves were recorded by collecting the preamplified

PMT output signal (by ultralow-noise Acton research model 181) with the second input channel of the ADC module of the AUTOLAB instrument.

A.4 Sensor assembly and operation

Assembly of the sensor

Phosphate buffer (PB) solutions (total phosphate concentration 100 mM) at different pH (5 and 12) were prepared dissolving 12 g of NaH_2PO_4 in distilled water. Triton-X surfactant was added to the solution (0.01% w/v). The pH was adjusted adding NaOH solution until the required pH was reached. The pH variation during NaOH addition was controlled by a pH-meter. Sarcosine concentration was then measured by the analytical protocol reported in figure 2.8:

Capturing (figure 2.8, inset 1)

All samples were incubated at room temperature for one hour with PB (pH 5) under constant mixing.

Separation (figure 2.8, inset 2)

All samples were washed using PB (pH 5) to remove the unrecognized sarcosine molecules. Before washing, a magnet was applied for 5 minutes. Subsequently, the solution was removed and 200 µL of new PB (pH 5) solution were added. The magnet was removed and the samples were mixed to obtain homogeneous suspension. This procedure was repeated twice.

Release and detection (figure 2.8, inset 2 and 3)

Magnetic separation was applied for 5 minutes to remove the solution: 200 µL of PB (pH 12) with 20 µM of $Ru[(bpy)_3]Cl_2$ solution was then added and the microbeads were resuspended by vortexing. Disposable Carbon Screen Print Electrodes, SPEs (C 110 DropSens®[35]), were used as working electrodes. 50 µL of the sample were deposited onto the SPE electrode and ECL was measured throughout chronoamperometry technique (E_1 = 0V, t_1 = 1s ; E_2 = 1.4V, t_2 = 4s. PMT = 750V).

Urine treatment

The urine samples were collected in the University Hospital of Verona according to the rules of the local ethical committee. The urine samples were obtained with informed consent from all subjects.

Individual human urine samples (5 mL) were loaded onto 15 mL ultrafiltration filters with a molecular weight cut-off of 3000 Da and centrifuged at 8000 rpm at 15° C, finally adjusting the urine pH to 5.

Bibliography

[1]. WHO. The global burden of disease 2004. 1–148 (2004).

[2]. Jemal, A., Bray, F. and Ferlay, J. *CA Cancer J Clin* **61,** 69–90 (2011).

[3]. Ferlay, J. *et al. Int. J. Cancer* **127,** 2893–2917 (2010)

[4]. Bock, C. H. *et al. Hum. Genet.* **126,** 637–642 (2009)

[5]. Miller, D. C. *et al. Cancer Res.* **63,** 3486–3489 (2003)

[6]. Shen, M. and Abate-Shen, C. *Genes Dev.* 1967–2000 (2010)

[7]. Minelli, A., Bellezza, I., Conte, C. and Culig, Z. *BBA-Rev Cancer* **1795,** 83–91 (2009)

[8]. DeWeese, T. L., Hruszkewycz, A. M. and Marnett, L. J. *Urology* **57,** 137–140 (2001)

[9]. Logothetis, C. J. and Lin, S.-H. *Nat. Rev. Cancer* **5,** 21–8 (2005)

[10]. Stenman, U.-H., Leinonen, J., Zhang, W.-M. and Finne, P. *Semin. Cancer Biol.* **9,** 83–93 (1999)

[11]. Oesterling, J. E. *et al. JAMA-J. Am. Med. Assoc.* **270,** 860–864 (1993)

[12]. Klotz, L. *Curr. Opin. Endocrinol. Diabetes Obes.* **20,** 204–209 (2013)

[13]. Hessels, D. and Schalken, J. *Nat. Rev. Urol.* **6,** 255–261 (2009)

[14]. Sreekumar, A. *et al. Nature* **457,** 910–914 (2009)

[15]. Couzin, J. *Science,* **323,** 865 (2009)

[16]. Schalken, J. A. *Eur. Urol.* **58,** 19–20 (2010)

[17]. Abate-Shen, C. and Shen, M. M. *Nature* **457,** 799–800 (2009)

[18]. Khan, A. P. *et al. Neoplasia* **15,** 491–501 (2013)

[19]. Liu, Z., Qi, W. and Xu, G. *Chem. Soc. Rev.* **44,** 3117–3142 (2015)

[20]. Rampazzo, E. *et al. Coord. Chem. Rev.* **256,** 1664–1681 (2012)

[21]. Elecsys Technology (accessed March 2017): http://www.cobas.com/home/product/clinical-and-immunochemistry-testing/technology-elecsys-ecl.html

[22]. Pinalli, R. and Dalcanale, E. *Accounts Chem. Res.* **46,** 399–411 (2013)

[23]. Shu, Q., Adam, C., Sojic, N. and Schmittel, M. *Analyst* **138,** 4500–4504 (2013)

[24]. Biavardi, E. *et al. P. Natl. Acad. Sci. USA* **109,** 2263–2268 (2012)

[25]. Yebeutchou, R. M. and Dalcanale, E. *J. Am. Chem. Soc.* **131,** 2452–2453 (2009)

[26]. Dionisio, M. *et al. J. Am. Chem. Soc.* **134,** 2392–2398 (2012)
[27]. Valenti, G. *et al. Faraday Discuss.* **185,** 1–11 (2015)
[28]. Hendrickson, H. P., Anderson, P., Wang, X., Pittman, Z. and D. R. Bobbitt, *Microchem. J.* **65,** 189–195 (2000)
[29]. Wei, H., Du, Y., Kang, J. and Wang, E. *Electrochem. Commun.* **9,** 1474–1479 (2007)
[30]. Martin, A. F. and Nieman, T. A. *Anal. Chim. Acta* **281,** 475–481 (1993)
[31]. Delaney, J. L., Hogan, C. F., Tian, J. and Shen, W. *Anal. Chem.* **83,** 1300–1306 (2011)
[32]. Chen, J., Zhang, J., Zhang, W. and Chen, Z. *J. Sep. Sci* **37,** 14–19 (2014)
[33]. Dionisio, M. *et al. J. Am. Chem. Soc.* **134,** 6540–6543 (2012)
[34]. Valenti, G. *et al. Chem. Commun.* **48,** 4187-4189 (2012)
[35]. Dropsens Screen-printed electrodes (accessed March 2017): http://www.dropsens.com/en/screen_printed_electrodes_pag.html.

Chapter 3

Investigation of different electrode materials for Electrochemiluminescence

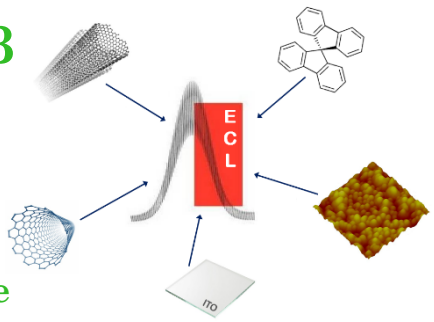

Electrochemiluminescence is a phenomenon that occurs in the proximity of the electrode surface, since the radicals involved in the formation of the light-emitting excited states are generated after an electrochemical stimulus. The choice of the electrode material is crucial for the light generation, since it influences the kinetic of the heterogeneous electron transfer reaction. For this reason, the deep understanding of the whole ECL system of the relative target application under development is of fundamental importance for the proper choice of the electrode material. In the present chapter, different electrode materials have studied for different ECL applications, ranging from porous gold electrodes for ECL enhancement, through transparent electrodes that combine ECL with microscopy techniques, to carbon-based electrodes, which present fast kinetics for coreactant oxidation. Their electrochemical behaviour and their ECL efficiencies have been investigated mainly with $[Ru(bpy)_3]^{2+}$/TPrA coreactant system in "oxidative-reduction" mechanism, but other coreactants have been tested, such as peroxydisulfate and benzoyl peroxide in "reductive-oxidation" mechanism. A comprehensive and exhaustive electrochemical study of the above-written materials will be presented in the next pages.

Key words: *electrode materials; gold; nanoporous gold; carbon-based materials; spirobifluorene; transparent electrodes; carbon nanotubes; peroxydisulfate.*

3.1 The role of the electrode material for ECL generation

Nowadays, coreactant-based ECL is one of the most sensitive analytical technique commercially available and it has largely applied in different research fields, mainly for biosensing applications[1]. The success of the ECL technique is due not only for the electrochemical way to generate the signal, but also for the continuous and incessant efforts spent for the optimization of all the parameters involved in light generation. These efforts include the selection of the best coreactant[2], the design of new chromophores[3],[4],[5], addition of additives to improve the light intensity and, of primary importance, the choice of the proper electrodic material.

The choice of the electrode material is the most crucial point that affect the technique sensitivity, because the chemical and physical state of the electrode surface and its electrochemical behaviour have dramatic effect on the ECL generation. In fact, the coreactant heterogeneous electron transfer reaction is one of the key parameter for the optimization of the signal-to-noise ratio and it strictly depends on the material employed. In particular, the electrode surface state has direct effect on the heterogeneous electron transfer kinetic of the coreactant oxidation reaction, which forms the radicals involved in the ECL mechanism. In detail, the surface state either can reduce the kinetics leading to a decrease in the ECL efficiency (as shown by metallic electrodes) or increase the kinetics increasing the ECL efficiency (as shown by carbon-based electrode materials).

3.1.1 Electrochemical behaviour of metallic and carbon-based electrodes

3.1.2 Metallic electrodes: platinum and gold

Platinum (Pt) and gold (Au) electrodes are even now widely used electrode materials in electrochemistry, especially for the fast kinetics of electron transfer reactions. These materials have also used for the investigation of ECL annihilation reactions in organic solvents and for the electrochemical investigation of new ECL luminophores. Furthermore, gold electrode was used in the first Origen ECL analyzer commercialized from 1994 by IGEN International[6], now Roche.

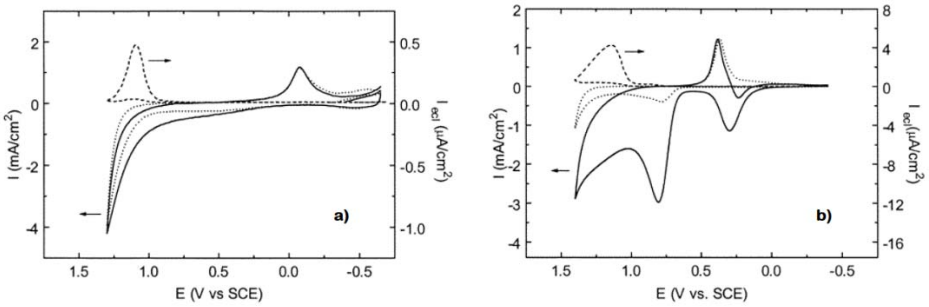

Figure 3.1: Cyclic voltammogram and ECL curve at Pt (a) and Au electrodes (b) in 0.15 M PB solutions (pH 7.5) containing 100 mM TPrA and 1 μM $[Ru(bpy)_3]^{2+}$. The dotted line represent the signals obtained in the absence of both TPrA and $[Ru(bpy)_3]^{2+}$. Potential scan rate, 0.1 V/s. Reprinted with permission from ref. [7]. Copyright 2000 American Chemical Society.

Despite the large use of these metallic electrodes in electrochemistry, their applicability for ECL generation is not appropriate. Aqueous ECL systems need high potentials to generate ECL emission and the use of Pt electrodes is not convenient. First of all, in the potential range from 0.8 to 1.2 V, where the oxidation of both coreactant and chromophore (generally TPrA and $[Ru(bpy)_3]^{2+}$) is achieved, Pt is susceptible of chemical modification of the surface state that dramatically affects the ECL efficiency. In fact, in aqueous solution, Pt tends to be oxidized causing the formation of oxide layers on its surface. This surface state modification, which confers an increased hydrophilic character to Pt, is considered responsible of the decrease of the heterogeneous electron transfer reaction of TPrA[7]. This phenomenon is called electrode *passivation*. Consequently, the ECL generation and the technique sensitivity are severely weakened. To avoid oxide generation, or at least decrease its negative effect on the TPrA heterogeneous electron transfer, several strategies have been proposed. These strategies include the addition of halide ions to the ECL measuring solution[8] or the adsorption of surfactants, both ionic[9] and non-ionic[10],[11], on the electrode surface before performing ECL measurements. In both cases, the addition of these additives competes with oxide generation and significantly postpone the electrode passivation, making the surface more hydrophobic; hence,

higher amount of TPrA can be readily oxidized, increasing the ECL efficiency. Nevertheless, Pt shows 100 times lower ECL intensity compared with Glassy Carbon electrode (GCE) at the same experimental conditions[12]. In addition, Pt is highly reactive towards the oxidation of water and proton reduction with consequent strong bubbles generation at the electrode surface. Lastly, adsorption of chemical intermediates, for example coreactant by-products, on metallic electrode surface might cause the "poisoning" of the electrode surface[13], decreasing the catalytic effect towards the oxidation of TPrA.

Gold-based materials show the similar behaviour of Pt, where the main drawback is the surface oxide formation in aqueous solutions[14],[15],[16], with negative consequences on ECL generation. Respect to Pt, Au electrodes show 10 times higher ECL emission for $[Ru(bpy)_3]^{2+}$/TPrA system at the same experimental conditions[7],[12]. This difference in the ECL efficiency is mainly due to the different reactivity for the oxide growth on the gold surface. In fact, the oxide growth on Au is approximately 400 mV more positive than Pt (see figure 3.1): the delayed passivation for Au improve TPrA oxidation respect to Pt. The strategies adopted to minimize the Au electrode passivation include the adsorption of surfactants or alkanethiols[8], or the modification of the surface with self-assembled monolayers (SAMs). In both cases, the surface becomes more hydrophobic, promoting TPrA oxidation. Another strategy can be realized with addition of halide ions in the measuring solution that activates the surface by anodic dissolution of gold[7].

3.1.3 Carbon-based electrodes: from GCE to CNTs

Carbon-based electrodes are promising materials for ECL generation thanks to the fast kinetics of the coreactant heterogeneous electron transfer reaction. For example, the Multiarray Technology of MSD uses carbon-based material both as a platform for the essay linking and as electrode for ECL initiation[17].

One of the most used carbon-based material is Glassy Carbon Electrode (GCE), which combines fast kinetics of coreactant oxidation with high overpotentials for water oxidation that minimize bubbles

generation at the electrode surface. Nevertheless, the surface properties of GCE might change during the oxidation potential step. For example, it has been reported that anodical pretreatment of GCE facilitates TPrA oxidation, but simultaneously ECL generation is greatly suppressed[18]. This opposite effect is attributed to the rapid deprotonation of $TPrA^{\bullet+}$ cation radicals by the increased adsorption of oxygen-derived species formed on the GCE surface during pretreatment. Due to this increased reactivity of $TPrA^{\bullet+}$ cation radicals, the intermediate products $TPrA^{\bullet}$ free radicals would be more subject of oxidative consumption at the electrode surface leading to the generation of degradation products (figure 3.2 B) and consequently, to a suppression of the ECL emission[18]. However, the ECL intensity generated at GCE is 10 times and 100 times more efficient than Au and Pt electrodes respectively[7].

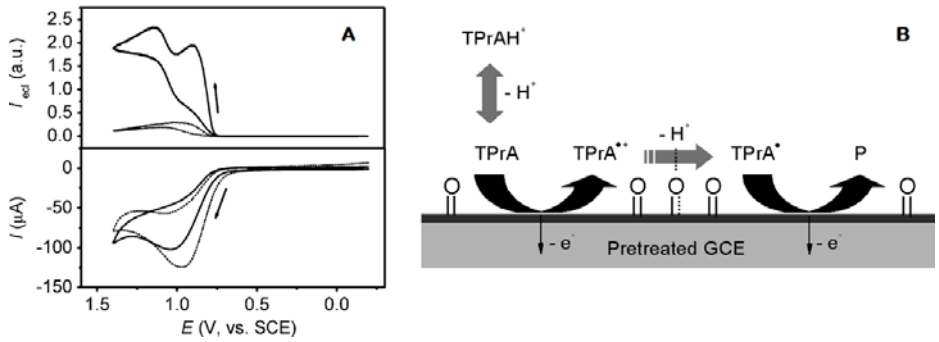

Figure 3.2: A) cyclic voltammogram and ECL curves of 10 mM TPrA and 1 μM $[Ru(bpy)_3]^{2+}$ in 0.15 M PBS (pH 7.5) solution at freshly polished GCE (solid line) and pretreated GCE in the potential range from -0.2V to +1.8V for 10 cycles (dashed line). Scan rate 0.1 V/s. B) Oxidation of TPrA at an electrochemically pretreated GCE. Adapted with permission from ref. [18]. Copyright 2008 American Chemical Society.

In addition to GCE, several research works has appeared recently using carbon nanotubes (CNT) as carbon-based electrode materials for ECL. Their use is mainly reserved for biosensing applications, for instance, for the detection of dopamine[19], palytoxin[20] and cancer biomarker proteins[21]. Their pivotal role for ECL generation is essentially due to their ability to transfer electrons efficiently. For example, the TPrA oxidation process at CNT electrode is 30 times

higher than commercial indium-doped tin oxide (ITO) electrode, with estimated heterogeneous electron transfer constant (k_{het}) of $2.6x10^{-2}$ cm/s (respect to ITO, k_{het} of $8x10^{-4}$ cm/s)[22]. As a consequence of this efficient kinetic behaviour, the ECL emission is more efficiently generated at CNT electrodes, showing 10 times higher emission intensity than ITO electrodes (figure 3.3), which usually exhibit sluggish kinetics for electrochemical reactions involved in the ECL generation[20]. Furthermore, CNT possess excellent characteristics including low electrical resistance, high active surface area, chemical stability and electrocatalytic properties in several electrochemical reactions. They also perfectly combine high transmittance with high conductivity.

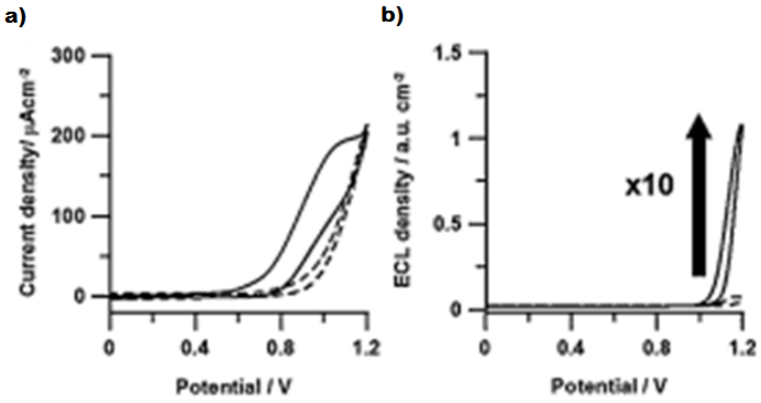

Figure 3.3: a) cyclic voltammogram and b) ECL signal for 10 μM $[Ru(bpy)_3]^{2+}$ and 80 mM TPrA in PB solution 0.1 M for CNT-based electrode (solid line) and for ITO electrode (dashed line). Scan rate 0.1 V/s, PMT bias 750V. All potentials are reported vs Ag/AgCl (3 M). Reprinted with permission from ref. [22]. Copyright 2015 Wiley-VCH Verlag GmbH.

In recent years, graphene-based electrodes have been proposed as new and innovative material for ECL generation[23],[24],[25]. Graphene is a two-dimensional (2D) crystal, composed of monolayers of sp^2 carbon atoms arranged to form a honeycombed network with six-membered rings[26],[27]. Its tremendous interest in ECL has emerged for its unique properties, such as the high surface-to-volume ratio, the high electron transfer rate and the outstanding thermal stability[24]. Nevertheless,

one of the main disadvantage of the carbon-based materials is the quality of the carbon structures. In fact, sp^3 carbon or edges are intrinsic defects of the carbon structures, which might cause generation of unspecific signal, increasing the BG signal during analysis. However, their application as electrodes for ECL generation is promising, especially for the development of transparent and efficient ECL devices for sensor applications[22].

3.1.4 Other examples of materials

In literature, numerous research papers regarding the study of electrode materials for ECL can be find and an exhaustive review has recently published on this topic[28]. There are different examples of materials expressly studied for ECL applications and, although their dissertation fall outside the aim of this chapter, a brief overview of the most important ones is given.

For example, transparent electrodes have paved the way for the possibility of combine ECL with microscopy techniques, performing imaging of small objects on the electrode surface, such as microbeads[29], fingerprints[30],[31] or cells[32]. The advantage of this imaging technique is the easy visualization of processes limited on the surface proximity, avoiding refraction of thicker layers of solution that can decrease image resolution. This approach is particularly helpful for the imaging of biological samples, where the autofluorescence might significantly contribute to the signal-to-noise ratio. Generally, transparent electrodes for ECL applications might be divided in two main groups: glass/metal oxides, such as ITO and fluorine-doped tin oxide (FTO), and carbon-based electrodes.

Microfluidic Paper-based Analytical Devices (μPADs) represent a class of materials that can be coupled with ECL detection. These systems combine conventional microfluidic devices with the simple use of diagnostic strip tests and represent a new class of POC diagnostic devices that are affordable, sensitive, user-friendly and specifically designed for the use in developing countries[33], where people frequently can not afford expensive tests and basic infrastructures are often not available. These POC devices are made of patterned paper prepared by photolithographic processes. In fact, paper is low cost

material, commercially available and provided with advantageous characteristics including thickness, lightweight and flexibility. Paper is also easily disposable after incineration, ensuring safety after use. μPADs are easy to use since they require only small amounts of sample volume to perform the analysis and do not need external supporting equipment or power supply, because the fluid movement is controlled mainly by capillarity and evaporation. Recently, μPADs have been applied in the design of different ECL sensing systems[34] and an example of μPADs combined with SPEs for the design of a device for amine detection using ECL has recently been demonstrated[35].

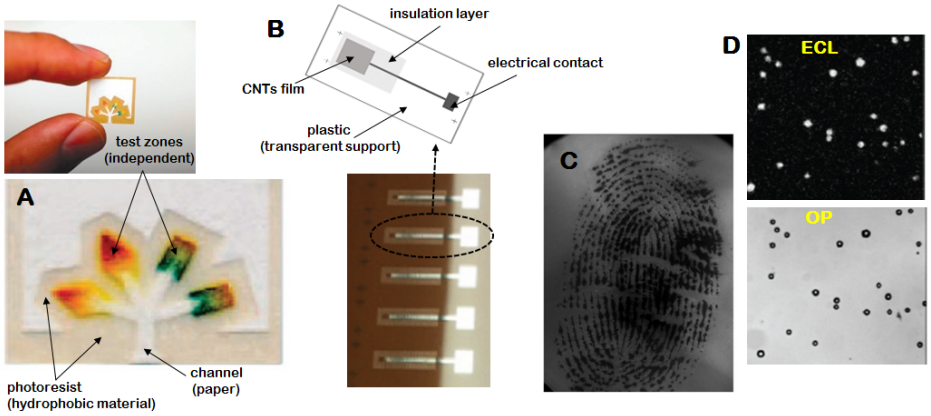

Figure 3.4: A) Example of μPADs fabricated by photolithography for the detection of glucose and protein (adapted with permission from ref. [33]. Copyright 2010 American Chemical Society). B) Photograph of one batch of inkjet-printed CNT electrodes (IJP-CNT) (bottom) and schematic representation of the electrode structure (top) (adapted from ref. [36]. Copyright 2014 Elsevier). C) ECL image of a sebaceous fingerprint deposited on ITO electrode (adapted from ref. [30]. Copyright 2012 Wiley-VCH Verlag GmbH). D) ECL (top) and transmitted light (bottom) images of $[Ru(bpy)_3]^{2+}$-conjugated polystyrene microbeads using biotin-streptavidin interaction deposited on FTO electrode (adapted from ref. [29]. Copyright 2009 American Chemical Society).

Among the extremely large diversity of electrodes composition used in ECL, boron-doped diamond (BDD) is considered one of the most efficient electrode material in electrochemistry[37]. BDD is a large band-gap semiconductor and it possesses optical transparency in the visible and infrared regions of the spectrum. Importantly, BDD possesses wide potential window compared with conventional electrode materials[38], which permits electrochemical studies at high

oxidation or reduction potentials. Although BDD presents these advantageous characteristics, only few examples of its use for ECL generation can be found in literature[39],[40].

3.2 Aim of the study: selection of the proper electrode material for the desired ECL application

The choice of the proper electrode material is essential for the successful development of the desired ECL application. In fact, the deep knowledge of the application characteristics, the whole ECL system intended to use and the working conditions of the final application, permit to choice the most suitable electrode material. For instance, materials that present fast kinetics are ideal for (bio)sensor applications, otherwise transparent electrodes are suitable for morphological studies of small objects using ECL as transduction method. Importantly, the characteristics of the material strongly influence the heterogeneous electron transfer kinetic of the coreactant oxidation, since this step is vital for the ECL generation.

In this context, different electrode materials for different purposes have been extensively investigated in this PhD research work. Firstly, gold electrodes with different porosities, obtained by etching procedure, have studied for surface-enhanced ECL (SEECL). This effect, achievable using noble metals, results in an increase of the ECL efficiency: these materials might find application in sensor field. Secondly, two different kinds of transparent electrodes have been investigated mainly to perform imaging studies. On one hand, ITO offers the advantage of surface functionalization and it is used to link spirobifluorene-based chromophores: this material can be proposed as transparent patterned surface for sensor development and morphological studies. On the other hand, suspensions of CNT can be printed on transparent polymeric supports to obtain electrodes with good conductivity, fast electron transfer kinetics and, extremely important, transparency. The final goal is the use of these kind of electrodes to perform morphological studies of biological sample (cells for instance) using ECL as transduction method and generally coupled with photoluminescence technique. The great advantage to combine ECL with transparency electrodes is the possibility to achieve

extremely high sensitivity, since biological sample usually show photobleaching or autofluorescence.

In the next sections, an accurate and complete electrochemical investigation of these materials will be presented.

3.3 Porous gold electrodes for surface enhanced ECL

The ECL emission of $[Ru(bpy)_3]^{2+}$ alone is rather weak in solution. As already mentioned, multiple ways have explored to enhance its ECL intensity (chapter 1). For instance, there has been a little attention on a strategy proposed called *surface-enhanced ECL*. The first work on this topic was reported by Lakowicz and coworkers in 2004[41]. In this paper, they consider the interaction of the excited state of $[Ru(bpy)_3]^{2+}$ with surface plasmons on gold electrodes. The excited states of the fluorophore, miming the action of the incident light, generate a resonance interaction with electron oscillations of the gold metal. They refer to this phenomenon as *surface plasmon-coupled emission (SPCE)*. When the excited state of $[Ru(bpy)_3]^{2+}$ is obtained via ECL through the coreactant pathway, the phenomenon is said *surface plasmon-coupled ECL (SPCECL)*[41]. The result is an enhancement of the ECL signal intensity. Hereafter, the same kind of research has carried out by another group, which propose the application of SPCECL for environmental monitoring[42] and cancer diagnosis[43],[44]. Based on these applications, they have developed a new branch of surface enhanced spectroscopy called *surface enhanced ECL (SEECL)*[45].

Ergo, in this doctoral research, gold-based electrodes with different porosity have investigated to evaluate the presence of SEECL phenomenon. The final goal is to verify whether the gold materials might present remarkable ECL enhancement thanks to this plasmonic effect. In this case, gold-based materials might be proposed as a platform for the development of sensors with highly sensitive detection limits. The gold-based electrodes studied in this PhD work have provided by Dr. Sandro Cattarin and his group at the Istituto per l' Energetica e le Interfasi (ICMATE CNR) of Padua, Italy.

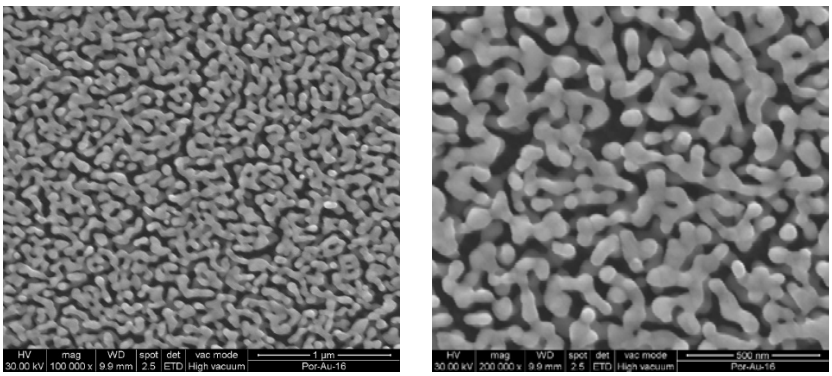

Figure 3.5: SEM images showing the morphology of NPG layer of 200 nm thickness, obtained by prolonged etching process of the $Ag_{75}Au_{25}$ alloy. It is noteworthy the formation of a regular, crack-free surface.

The porous gold electrodes have obtained by etching process of $Ag_{75}Au_{25}$ alloy deposited with different thickness (120 and 200 nm) on Silicon wafers (see appendix A.1.2 for experimental procedure). The composition of the alloy has been selected on the basis of literature reports in order to get a robust sponge of porous gold. The etching process confers roughness to the surface leading to the formation of well-defined and crack-free porous surface (see figure 3.5): this kind of material is indicated as nanoporous gold (NPG) electrode. The adopted slow etching procedure in relatively diluted (48%) HNO_3 solution provides good quality NPG films, homogeneous and crack-free over large surface, with a coarsened ligaments/pores structure. On the contrary, fast etching procedure in concentrated (65-70%) HNO_3 solution produces a number of microscale voids and cracks, presumably due to rapid volume shrinkage, that would produce NPG layer with irregular surface. Typical ligament and pore sizes have evaluated from image analysis in the range 35-70 nm and 40-85 nm, respectively.

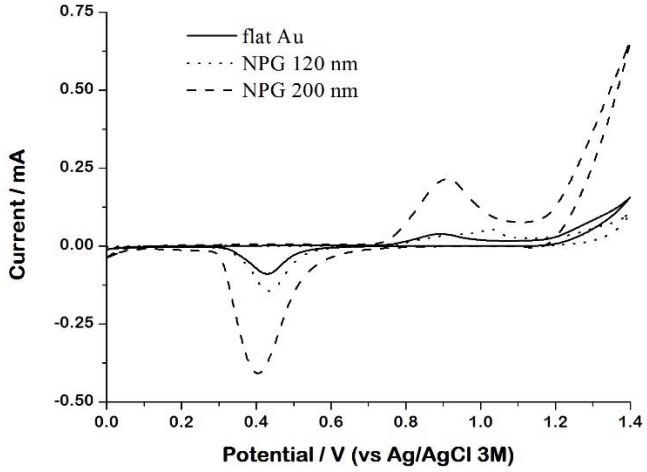

Figure 3.6: Cyclic voltammetry of flat gold (solid line), NPG 120 nm thickness (dotted line) and NPG 200 nm thickness (dashed line) in PB 0.2 M, pH = 6.8. Scan rate: 0.1 V/s.

The effect of the different surface morphology has been preliminary investigated in phosphate buffer (PB) solution (figure 3.6). Flat gold electrode obtained by deposition of Au layer on Silicon wafer without any etching treatment has used as reference. As reported in literature, at ~ 0.75 V (vs Ag/AgCl 3 M) the growth of surface oxide begin[7] and its reduction is evident in the backward scan at ~ 0.6 V for all the three different electrodes. The current related to the oxide growth increase of 252% for NPG 200 nm and of 32% for NPG 120 nm respect to flat gold. Furthermore, according to the data reported in literature, the anodic charge for a monolayer of surface oxide formation on Au electrode correspond to 400 μC/real cm^2 [16]. Hence, it is possible to evaluate the area of the different materials: 0.032 cm^2 for flat gold, 0.047 cm^2 for NPG 120 nm and 0.167 cm^2 for NPG 200 nm. The increased electroactive surface area is attributed to the effect of the etching process.

3.3.1 ECL measurements using TPrA as coreactant

The ECL intensity of the gold-based electrodes has been evaluated using the system $[Ru(bpy)_3]^{2+}$/TPrA and performing the coreactant strategy to obtain the excited state (see appendix A.1.4 for experimental details). Chronoamperometry technique has used for the investigations, switching the potential between 0 V to 1.4 V (vs Ag/AgCl 3 M). The preparation step at 0 V has been chosen in order to avoid any surface modification, since no electrochemical process are pointed out for all the different materials. The ECL emission has recorded at 1.4 V in the potential region where the oxidation of both chromophore and coreactant is achieved, according to the *homogeneous* ECL mechanism proposed by Bard[46] and discussed in chapter 1.

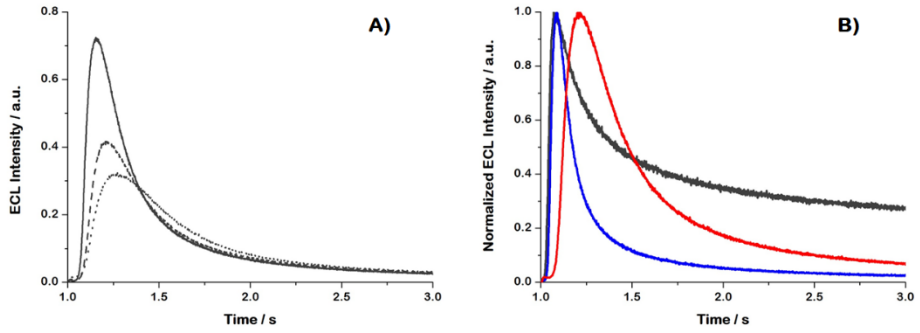

Figure 3.7: A) ECL/time transients for NPG 200 nm thickness, electrode stability: first cycle (solid line), second cycle (dashed line) and third cycle (dotted line). B) Normalized ECL/time transients for flat gold (black line), NPG 120 nm thickness (blue line) and NPG 200 nm thickness (red line). All ECL measurements were performed in phosphate buffer (PB) solution 0.2 M, pH = 6.8, with 10 μM $[Ru(bpy)_3]^{2+}$ and 30 mM TPrA. PMT bias 750 V. Potential step (chronoamperometry) vs Ag/AgCl 3 M: E_1 = 0 V at t_1 = 1s ; E_2 = 1.4 V at t_2 = 4s.

Unexpectedly, the gold-based electrodes show unpredictable behaviour. Primarily, the materials show instable responses in the measuring conditions, as repeated ECL cycles show progressive decrease of the signal intensity for the NPG 200 nm (see figure 3.7 A). This trend is the same for the three different electrode morphologies and it might be a symptom of the surface modification occurring during

the application of the potential: indeed, metallic electrodes are particularly susceptible of oxide generation. Secondly, the ECL intensity does not increase increasing the surface area of the material, as expected. In particular, the higher ECL intensity has recorded only for flat gold, which theoretically possesses the lowest active surface area between the samples analyzed. Importantly, flat gold also shows the slowest signal decay. This parameter is extremely important and it has to take into account when an electrode material is chosen for sensor applications. In fact, if the signal decay is slow, more sensitive the measurement will be. On the contrary, NPG electrodes show faster signal decay than flat gold, beyond lower ECL intensities. Furthermore, NPG 200 nm presents signal delay, since the ECL emission is not reached immediately upon potential application. It is hypothesized that all these aspects are indicating factors of surface modification occurring when the potential is applied, rather than mechanistic effects in the excited state formation. However, in order to prove the above-mentioned hypothesis, surface analysis has performed with Atomic Force Microscopy (AFM) technique.

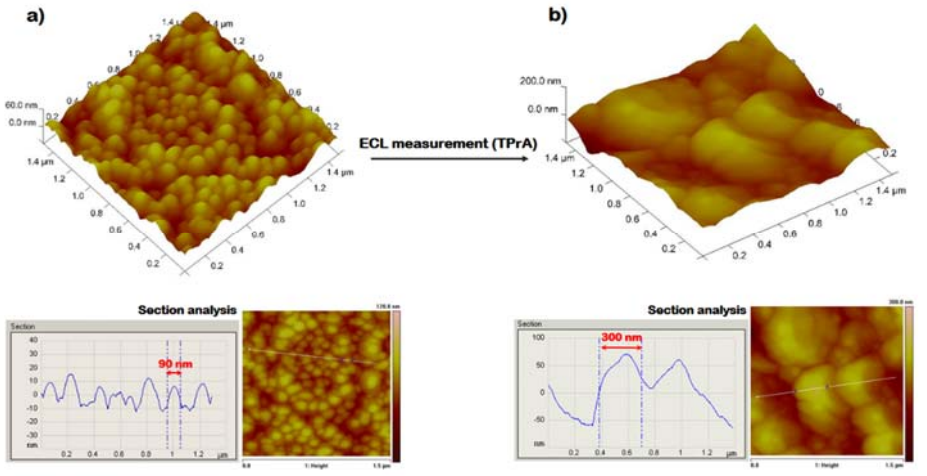

Figure 3.8: AFM images 1.5 x 1.5 μm² of a) pristine NPG 200 nm thickness and b) NPG 200 nm thickness after ECL measurement carried out in PB solution at pH = 6.8 containing 30 mM TPrA, potential applied 1.4 V (vs Ag/AgCl 3 M) for 4 seconds. Bottom graphs: AFM section analysis (right side) and morphology profile diagrams - height vs distance- (left side) along the white line on the AFM image, starting from the white circle.

Surprisingly, morphological investigations have revealed that the surface porosity drastically changes after ECL measurements, when the material is in contact with TPrA and the potential is applied. In particular, the pores dimension for pristine NPG 200 nm changes from 80-100 nm range to 300-320 nm range after ECL measurement. This remarkable surface modification is considered responsible of the instable responses obtained with these gold-based electrodes. To explain this behaviour, it is hypothesized that the amine in solution might react with the metallic surface of the gold electrodes. In fact, it has been demonstrated that amine chemisorption on metallic surface could provoke surface dissolution, leading to organometallic complex formation[13]. In particular, when a metal oxide is exposed to very basic environments (such as the case of amine solution), the metal oxides and hydroxides disassociate causing the exposition of the underlying metallic ions. The amine groups, which are Lewis bases, can easily react with the metallic ions, which are Lewis acids, leading to metal-amine complexation through an acid-base reaction. According to the previous results obtained and to the chemistry of the system under investigation, these gold-based materials are considered unsuitable for ECL generation with $[Ru(bpy)_3]^{2+}$/TPrA system in the "oxidative-reduction" coreactant strategy.

3.3.2 ECL measurements using peroxydisulfate as coreactant

In order to verify the stability of the gold-based electrodes in different conditions, ECL emission has evaluated in "reductive-oxidation" coreactant mechanism, using peroxidisulfate, $S_2O_8^{2-}$, as coreactant. At the beginning of the 1980s, Bard[47] and Bolletta[48] investigated separately the mechanism of peroxydisulfate with coordination compounds, such as $[Ru(bpy)_3]^{2+}$. As depicted in figure 3.9 b, the ECL emission is produced by the reaction of electrogenerated $[Ru(bpy)_3]^{+}$ with the strongly oxidizing intermediate, $SO4^{\bullet-}$, generated during the reduction of $S_2O_8^{2-}$. The preliminary experiments with gold-based materials have successfully performed. The gold electrodes have demonstrated stability in the measuring conditions, achieving ECL emission with "reductive-oxidation" pathway in water solution. In

particular, as represented in figure 3.9 a, the ECL intensity considerably increases of 2.42 times for NPG 200 nm respect to flat gold. It is noteworthy that the reduction of $[Ru(bpy)_3]^{2+}$ to $[Ru(bpy)_3]^{+}$ can be seen on the NPG 200 nm. The reduction peak at -0.6 V on flat gold is attributed to oxygen reduction. The same peak is evident also on the NPG 200 nm, but shifted at less negative potential of about 300 mV.

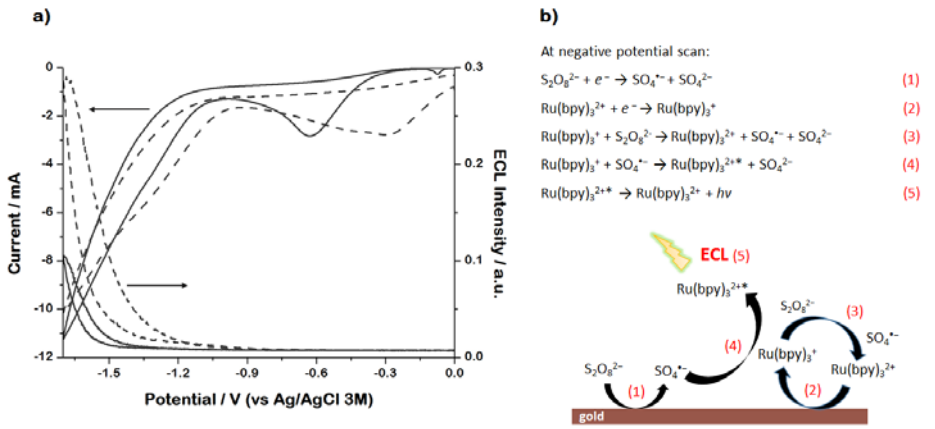

Figure 3.9: a) Current and ECL intensity profiles as a function of potential applied for flat gold (solid line) and NPG 200 nm of thickness (dashed line). The measurements were performed in phosphate buffer (PB) solution 0.2 M, pH = 6.8, with 10 µM $[Ru(bpy)_3]^{2+}$ and 50 mM $S_2O_8^{2-}$. PMT bias 750 V. b) Schematic representation of the "reductive-oxidation" coreactant ECL mechanism involving $S_2O_8^{2-}$ as coreactant and $[Ru(bpy)_3]^{2+}$ as emitting species.

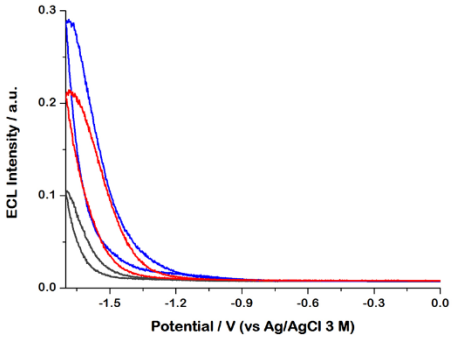

Figure 3.10: ECL intensity profiles as a function of potential applied for flat gold (black line), NPG 120 nm (red line) and NPG 200 nm of thickness (blue line). The measurements were performed in phosphate buffer (PB) solution 0.2 M, pH = 6.8, with 10 µM $[Ru(bpy)_3]^{2+}$ and 50 mM $S_2O_8^{2-}$. PMT bias 750 V.

The effect of the different porosity on the ECL emission has also tested in these conditions. As reported in figure 3.10, the ECL signal intensity increases increasing the porosity of the material. Generally, the enhancement of the porosity leads to an increase of the active surface area available for the electrochemical generation of the radicals involved in light generation. From the experimental results, it has been conclude that the effect of the ECL enhancement is not attributable to the SEECL effect, but to the increase of the electroactive surface area of the gold materials.

3.4 Patterned ITO with spirobifluorene dye

In the past years, spirobifluorene-based molecules have been applied in different technological fields due to their chemical versatility[49]. In particular, it was demonstrated that spirobifluorene molecule bearing two triphenylamine groups in position 2 and 7 produces blue emission with higher quantum yield than the standard 9,10-diphenylanthracene[50]. Although many organic molecules have been investigated in solution, studies about the ECL properties in solid state of this kind of compounds are still limited. In order to investigate the ECL properties on solid state, a transparent surface of ITO electrode has been covalently functionalized with a monolayer of spirobifluorene-based molecule. The particular way to obtain the emitting excited state in ECL renders the technique suitable for the visualization of emitting species in the proximity of the electrode surface. For example, spatially resolved ECL was used to observe the concentration distribution of the radicals involved in the light generation[51].

The functionalized ITO surfaces studied in this thesis have been obtained in collaboration with the Istituto di Scienze e Tecnologie Molecolari (ISTM) in Milan, Italy, and prepared as reported in appendix A.2.2. ITO surface has been covalently functionalized whit spirobifluorene molecule through alkyl linkers with different length. As shown by cyclic voltammetry measurements (figure 3.11), the presence of the spirobifluorene on the surface is highlighted by an increase of the ECL signal that is absent when only the alkyl chain is linked to the surface. The effect of the linker length has also been

tested, since the distance dye-surface plays a fundamental role in the electrochemical properties. In fact, the ECL signal is detectable only at short distance dye-surface, while with longer linker no signal has been observed (figure 3.11 b). According to this preliminary results, it has been demonstrated that spirobifluorene-based molecules can be reasonable employed as dyes for solid state ECL applications.

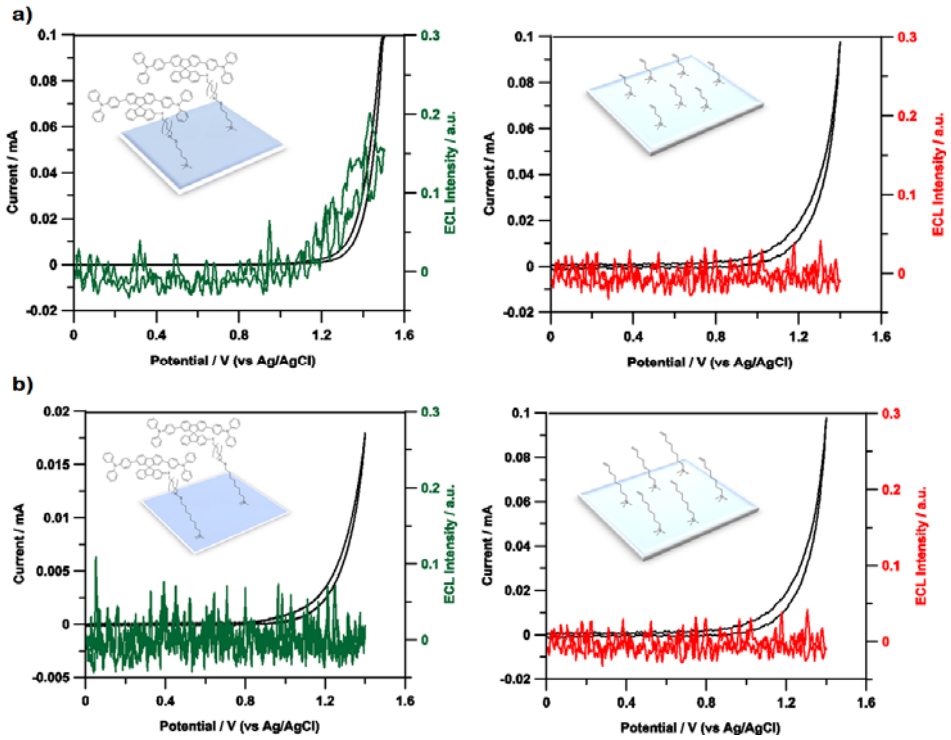

Figure 3.11: Cyclic voltammetry and ECL intensity of functionalized ITO-spirobifluorene surface with short distance linker (a) and with long distance linker (b). Measurements performed in phosphate buffer solution 0.2 M, pH=6.8, in presence of 200 mM TPrA. Scan rate: 0.1 V/s. Potentials reported vs Ag/AgCl 3M.

In order to perform visualization of the functionalized surface using ECL, spirobifluorene dyes have directly patterned on activated ITO substrates in ordered lines of 25 x 15 μm. The patterned dye lines can be visualized in photoluminescence (figure 3.12 a), after directly excitation of the dye. However, the visualization of the ECL emission using TPrA as coreactant has not been achieved.

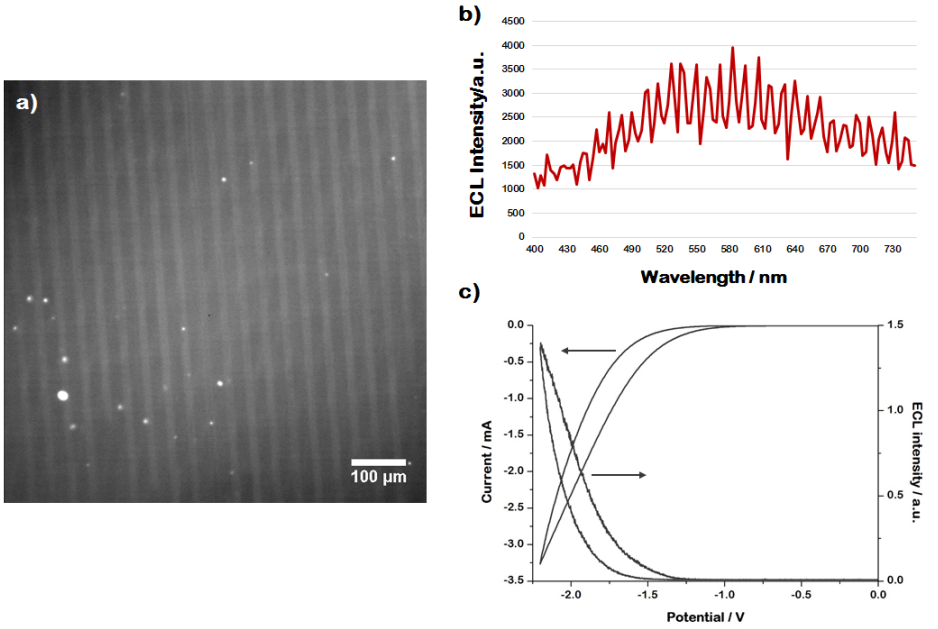

Figure 3.12: a) Photoluminescence image of spirobifluorene dyes patterned on ITO surface, lines 25 x 15 µm (acquisition time 150 ms, CCD mode, gain 3, 10x obj, filter excitation 330-380 nm, emission > 400 nm); b) ECL emission spectra of the patterned spirobifluorene on ITO surface in ACN with 7 mM BPO and 40 mM TBAH; c) Current and ECL intensity profiles in ACN with 7 mM BPO and 40 mM TBAH. PMT bias 750 V, amplification range 0.0 µA/V.

Further investigations have been performed using bezoyl peroxide (BPO) as coreactant. The ECL profile of the patterned surface has been obtained performing cyclic voltammetry (figure 3.12 c) and the ECL emission spectra has been recorded in the same experimental conditions (figure 3.12 b). Unfortunately, several trials to visualize the patterned surface using BPO have also failed. This inconvenient has definitely hampered further studies of solid state ECL.

3.5 CNT-based materials as transparent electrodes for ECL imaging

As already mentioned, CNT-based electrodes are ideal materials for ECL applications thanks to the favorable potential for TPrA oxidation and for the minimized surface modifications occurring during potential application. Recently, the development of transparent electrodes composed of CNT layers has been reported in literature[22]. The possibility of combining CNT characteristics with transparency paves the way for the development of materials that can be used for ECL imaging studies. This breakthrough for the ECL application in analytical science will be discussed in chapter 4.

In this context, with the aim to perform imaging studies of beads or cells layed down on the electrode surface, transparent CNT-based electrodes have been specifically developed for this purpose. In particular, these materials have been prepared by inkjet printing (IJP) technology, in collaboration with the group of Prof. Hubert Girault at the École Polytechnique Fédérale de Lausanne (EPFL).

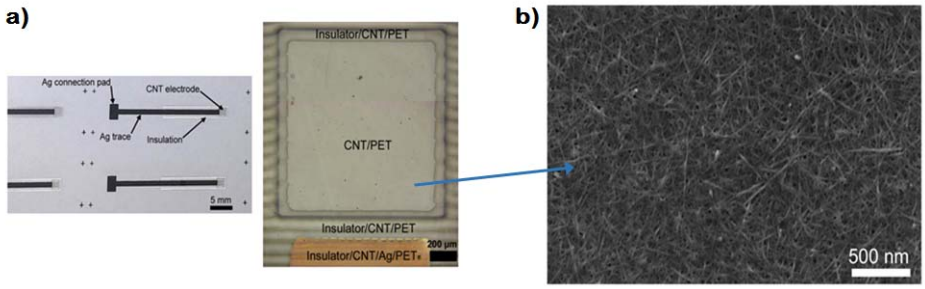

Figure 3.13: a) Optical images of the transparent electrodes and their manufacture; b) Scanning Electron Microscopy (SEM) image of the CNT electrode surface.

The transparent electrodes studied in this thesis have obtained by inkjet printing[36] of CNT-based ink on flexible and transparent polymeric sheets made of polyethylene terephthalate (PET). The active electrode material is composed of a commercial dispersion of double wall carbon nanotubes (DWCTs), suitable for the fabrication of stand-alone CNT electrodes with high electrical conductivity and electrochemical activity, thanks to the percolation of the randomly

spread CNT networks (see SEM image in figure 3.13 b). For the electrical connection, a silver layer is used. Finally, an insulating layer to precisely define the active electrode area completes the CNT electrode. The IJP fabrication process permits to obtain electrodes with highly reproducible electrode surface on a large scale. Moreover, the electrode results highly transparent with low transmission (>90% in the range 500-700 nm).

3.5.1 Preliminary investigations of the CNT electrodes

A first evaluation of the electrochemical behaviour of the CNT electrodes has been tested by cyclic voltammetry (CV) in water solution containing Ferrocenemethanol (FcMeOH) as redox active species. In particular, CV study at different scan rates has been performed (figure 3.14 a). A peak waved shape, typical for the electrochemical processes limited by semi-infinite linear diffusion, has measured in all cases for the oxidation of FcMeOH and the reduction of the electrochemically generated $FcMeOH^+$ with a formal potential $E^0 = 0.329$ V vs Ag/AgCl 3 M. The anodic peak currents I_{pa} are a linear function of the square root of the scan rate ($v^{1/2}$) for all cases, corroborating that the electrochemical process is controlled by semi-infinite linear diffusion.

Preliminary ECL investigations on the CNT electrodes have performed in "oxidative-reduction" coreactant strategy, using $[Ru(bpy)_3]^{2+}$ as emitting species and TPrA as coreactant. As depicted in figure 3.14 c, ECL emission starts at around 0.9 V, which corresponds to TPrA oxidation ($E^0 = 0.88$ V vs Ag/AgCl) and it reaches its maximum at around 1.2 V (red line in figure 3.14 c). This behaviour suggests that ECL emission is triggered only by the direct oxidation of TPrA, as Bard proposed[46]. Importantly, the fast kinetics for TPrA oxidation typical of CNT materials is reflected by the high ECL signal recorded compared with the ECL signal generation recorded at ITO electrode, currently the most used transparent electrode for ECL analysis of cells (see for comparison red and black signals in figure 3.14 c). In fact, CNT electrodes show one order of magnitude higher ECL signal compared to ITO.

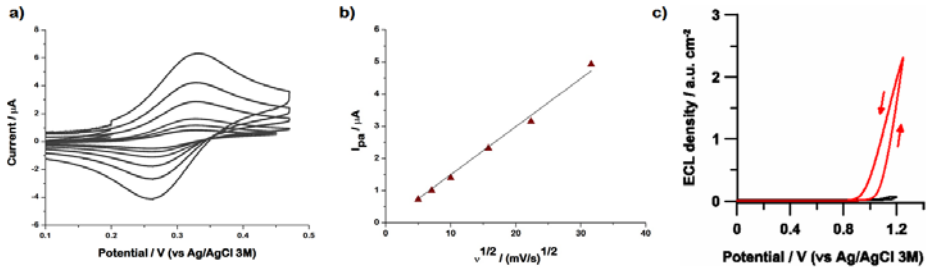

Figure 3.14: a) CVs at different scan rates of the CNT electrode in 1 mM FcMeOH and 0.1 M $LiClO_4$. Scan rate: 25, 50, 100, 250, 500 and 1000 mV/s. b) Anodic peaks current (i_{pa}) vs $v^{1/2}$. R^2: 0.997. c) ECL intensity normalized by electrode surface area vs potential applied for 20 μM $[Ru(bpy)_3]^{2+}$ with 60 mM TPrA in phosphate buffer (PB) 0.2 M for the CNT-based electrode (red line) and ITO (black line). Scan rate: 0.1 V/s. PMT bias 750 V. Amplification 00.0 μA.

In conclusion, the outstanding properties of CNT materials towards TPrA oxidation and the possibility to produce electrode materials provided with transparency paves the way to the development of biocompatible and disposable sensors for the analysis of cells and ultrasensitive imaging techniques. This point will be treated in more detail in Chapter 4.

Appendix

A.1 Porous gold electrodes

A.1.1 Chemicals and materials

Tri-n-propylamine (TPrA), Ammonium peroxydisulfate ($(NH_4)_2S_2O_8$) and Tris(2,2'-bipyridyl)dichlororuthenium(II) hexahydrate ($[Ru(bpy)_3]Cl_2*6H_2O$) were from Sigma-Aldrich and used without any further purification. PB 0.2 M, pH 6.8 was obtained mixing 0.2 M of sodium phosphate monobasic dihydrate ($NaH_2PO_4*2H_2O$) and 0.2 M of sodium phosphate dibasic (Na_2HPO_4), both from Sigma-Aldrich and used as received.

A.1.2 Electrodes preparation and deposition of alloy films

Silicon-based (Si) substrates were used for electrodes preparation. Si (100) wafer was thoroughly degreased in boiling acetone and dried with nitrogen flux. Ti layer of 5 nm (adhesion promoter) and Au layer of about 100 nm thickness were subsequently deposited in high vacuum ($1x10^{-6}$ mbar) by means of electron beam evaporation at the deposition rate of 0.1 nm/s. The coated Si wafer was then cut into rectangular pieces with typical dimensions of 12 x 36 mm and washed again in boiling acetone.
The porosity was obtained through the deposition of $Ag_{75}Au_{25}$ alloy (at.%) in a DC turbo sputter coater (Emitech K575X, Emitech Ltd., Ashford, Kent, UK), using a silver/gold alloy sputtering target $Ag_{62.3}/Au_{37.7}$ (wt.%), GoodFellow. The sputtering was performed at room temperature under Ar gas flow at pressure of $7x10^{-3}$ mbar and a DC sputtering current of 20 mA.
The Au-Ag alloy films were immersed for 7 hours (room temperature 23-25 °C) in 48% HNO_3 solution, obtained diluting 70% Sigma-Aldrich solution (ACS reagent). After etching process, the samples were rinsed for 1 hour in 0.1 M $HClO_4$, then for 2 hours in deionized water (resistivity $\rho > 15$ MΩ cm), dried with nitrogen flux and stored. SEM images were recorded with a FEI Quanta 200 FEG ESEM instrument, equipped with a field emission gun, operating at an accelerating voltage variable in the range of 20-30 kV.

A.1.3 Morphological investigation of the electrode surface

Morphological investigations of the electrode surface were carried out by Atomic Force Microscopy (AFM) analysis using a Digital NanoScope 3D Multimode microscope (Veeco, USA) equipped with phosphorus n-doped silicon probes (spring constant 20-80 N/m; resonance frequency 250-300 kHz; nominal tip radius < 10 nm) operated in tapping mode.

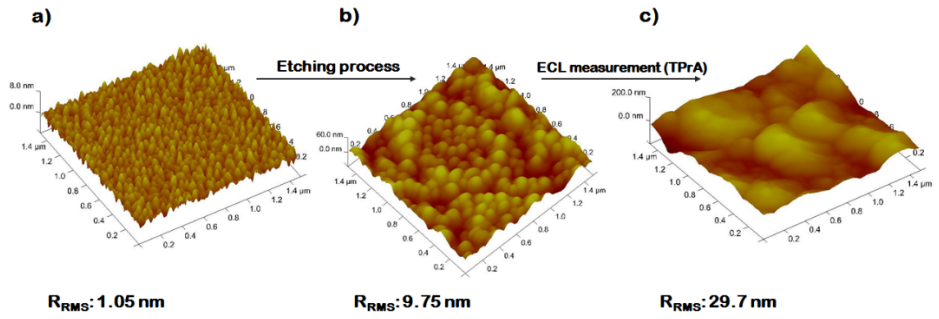

Figure 3.15: AFM images 1.5 x 1.5 µm² of a) pristine flat gold, b) pristine NPG 200 nm of thickness obtained after etching process and c) NPG 200 nm of thickness after ECL measurement using 10 µM $Ru[(bpy)_3]^{2+}$ with 30 mM TPrA in PB solution 0.2 M, pH = 6.8. Roughness root mean squared (R_{RMS}) values were evaluated by morphology analysis for every step of electrode investigation.

A.1.4 ECL measurements

All ECL measurements were conducted in a conventional three electrodes arrangement in a poly(methyl methacrylate) (PMMA) cell with flat Au or NPG as working electrode, Pt spiral as counter electrode and a homemade Ag/AgCl (3 M) as reference electrode (figure 3.14) with PGSTAT302 (AUTOLAB Instrument). The $[Ru(bpy)_3]^{2+}$/TPrA ECL measurements were carried out in phosphate buffer (PB) solution 0.2 M (pH 6.8) with TPrA 30 mM and $[Ru(bpy)_3]Cl_2$ 10 µM. The $[Ru(bpy)_3]^{2+}/S_2O_8^{2-}$ ECL measurements were carried out in phosphate buffer (PB) solution 0.2 M (pH 6.8) with $(NH_4)_2S_2O_8$ 50 mM and $[Ru(bpy)_3]Cl_2$ 10 µM. The ECL signal generated by performing the potential step program was measured with a photomultiplier tube (PMT, Hamamatsu R4220p) placed at a constant distance above the cell and inside a dark box. A voltage of 750 V was supplied to the PMT. The light/current/voltage curves were recorded by collecting the preamplified PMT output signal (by an ultralow-noise Acton research model 181) with the second input channel of the ADC module of the AUTOLAB instrument. Stabilization of the gold surface was carried out before each measurement by electrochemical cleaning, performing 10 voltammetric cycles between 0.4 and 1.4 V in PB solution (pH 6.8) with scan rate 0.1 V/s.

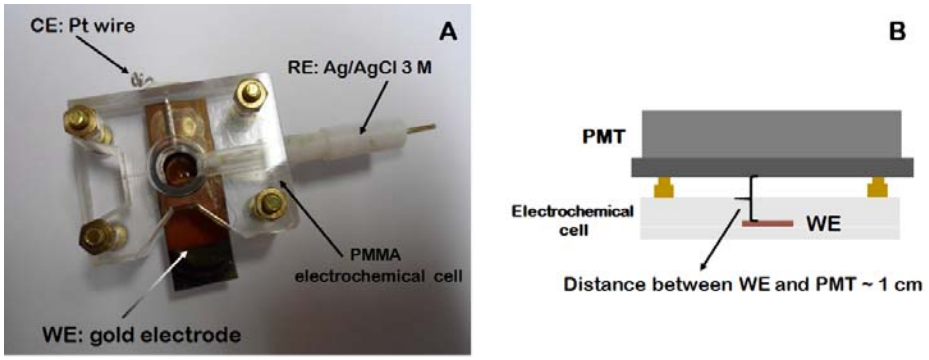

Figure 3.16: A) Electrochemical cell and B) experimental set up for ECL measurements with gold electrodes. This electrochemical set up ensured constant distance between the PMT and the electrochemical cell. It is located inside a dark box.

A.2 ITO patterned with spirobifluorene dye

A.2.1 Chemicals and materials

Tri-n-propylamine (TPrA), Benzoyl peroxide (BPO), Tetrabutylammonium hexafluorophosphate (TBAH) and Methyl cyanide (ACN) were from Sigma-Aldrich and used without any further purification. PB 0.2 M, pH 6.8 was obtained mixing 0.2 M of sodium phosphate monobasic dihydrate ($NaH_2PO_4*2H_2O$) and 0.2 M of sodium phosphate dibasic (Na_2HPO_4), both from Sigma-Aldrich and used as received. ITO was purchased from Kuramoto Seisakusho Co. Ltd. (Tokyo, Japan).

A.2.2 Spirobifluorene functionalization on ITO substrates

The glass-coated ITO substrates were prepared as follows. Substrates were first washed by sonication in ultrasonic bath with different solvents (pentane, acetone and dichloromethane) for 5 minutes each, followed by two washes with Milli-Q water in ultrasonic bath for 2 minutes each. After carefully drying with Ar stream, the substrates were activated with oxidizing mixture H_2O:NH_4OH:H_2O_2 (5:1:1) at 70°C for 1 hour and then dried carefully with Ar stream.

The substrates were then used to grow the monolayer: a) by deeping them in a solution of spirobifluorene dye in toluene (0.5 mM) under Ar at 40°C for 3 hours, then washed extensively with toluene, dichloromethane, ethanol,

water to give homogeneous monolayer; b) by Micromolding in Capillaries (MIMIC) technique to obtain structured film.
For b), polydimethylsiloxane (PDMS) stamps were prepared by casting PDMS (Sylgard 184A and Sylgard 184B (10:1)) on the silicon wafer model, followed by thermal curing at 80°C for 24 hours. A solution of spirobifluorene dye in dimethylformamide (DMF) (0.1 M) was prepared. During the printing, the stamp (lines 25x15 μm; 50x30 μm; 100x50 μm) was put onto the substrates; then 2 μL were dropped around the stamp edge observing the diffusion of the solution for capillarity. The substrate was heated at 40°C for 20 minutes; the stamp was removed and the substrate washed with dichloromethane in ultrasonic bath for 5 minutes, then rinsed extensively with dichloromethane and ethanol.

A.2.3 ECL measurements and imaging

ECL measurements were carried out with PGSTAT302 (AUTOLAB Instrument) in a three electrodes arrangement using functionalized ITO as working electrode, a Pt wire as counter electrode and Ag as quasi reference electrode. The ECL measurements with TPrA as coreactant were conducted in phosphate buffer (PB) solution 0.2 M, pH=6.8, in presence of 200 mM TPrA. The ECL measurements with BPO as coreactant were conducted in dry conditions (ACN) with TBAH 40 mM as supporting electrolyte and 7 mM BPO. Oxygen was removed from the solution by Ar purging. The ECL signal generated by performing the potential step program was measured with a photomultiplier tube (PMT, Hamamatsu R4220p) placed at a constant distance above the cell and inside a dark box. A voltage of 750 V was supplied to the PMT. The light/current/voltage curves were recorded by collecting the preamplified PMT output signal (by an ultralow-noise Acton research model 181) with the second input channel of the ADC module of the AUTOLAB instrument.
The ECL/optical/photoluminescence imaging was performed in a PTFE (Teflon) homemade electrochemical cell. An epifluorescence microscope from Nikon (Chiyoda, Tokyo, Japan) equipped with ultrasensitive Electron-Multiplying CCD camera (EM-CCD 9100-13 from Hamamatsu, Hamamatsu Japan) was used with a resolution of 512 pixel x 512 pixel with a size of 16 x 16 μm. The microscope was enclosed in a homemade dark box to avoid interferences from external light. It was equipped with a motorized microscope stage (Corvus, Marzhauser, Wetzlar, Germany) for sample positioning and with long distance objectives from Nikon (10x/0.30 DL17, 5mm, 20x/0.40 DL13mm). The system was connected to the AUTOLAB potentiostat to provide the needed potential for the ECL reaction.

A.3 CNT-based electrodes

A.3.1 Chemicals and materials

Ferrocenemethanol (FcMeOH), Tri-n-propylamine (TPrA) and Tris(2,2'-bipyridyl)dichlororuthenium(II) hexahydrate ($[Ru(bpy)_3]Cl_2*6H_2O$) were from Sigma-Aldrich and used without any further purification. PB 0.2 M, pH 6.8, was obtained mixing 0.2 M of sodium phosphate monobasic dihydrate ($NaH_2PO_4*2H_2O$) and 0.2 M of sodium phosphate dibasic (Na_2HPO_4), both from Sigma-Aldrich and used as received. ITO was purchased from Kuramoto Seisakusho Co. Ltd. (Tokyo, Japan). Carbon nanotube ink CNTRENE 3024 A3-R (Brewer Science), Ag ink Silverjet DGP-40LT-15C (w/w 35%, Sigma-Aldrich) and dielectric ink EMD6201 (Sun Chemical) were used for inkjet printing as received. Polyethylene terephthalate sheets (PET, 125 μm thick) were obtained from Goodfellow as substrates for inkjet printing.

A.3.2 Inkjet printing of CNT electrodes

CNT electrodes were fabricated by using an X-Serie CeraPrinter (Ceradrop, France) equipped with three parallel printheads, i.e., two Q-Class Sapphire printheads with 256 nozzles (QS-256; Dimatix Fujifilm) and one disposable DMC-11610 cartridge (Dimatix Fujifilm). An integrated UV LED FireEdge FE300 (380-420 nm; Phoseon Technology) allows simultaneous printing and UV photopolymerization of the dielectric ink using the Dimatix cartridge with three active nozzles. The post-processing station of the printer contains a PulseForge 1300 photonic curing system (Novacentrix, USA) for the rapid in-line curing of the Ag and CNT patterns as printed with a QS-256 with 80 pL nominal droplet volume and a Dimatix cartridge, respectively.
Firstly, Ag patterns for the electrical connections and as conductive traces were printed and cured on PET. Secondly, a CNT pattern was printed that only slightly overlapped with the Ag pattern for the electrical connection in order to form a stand-alone CNT electrode on PET. After photonic curing of the CNT, the UV curable insulator was printed to define the active CNT working electrode area and to cover the Ag trace. The CNT electrodes could directly be used.

A.3.3 Electrochemistry and ECL measurements

CV measurements were carried out with PGSTAT302 (AUTOLAB Instrument) in a three electrodes arrangement using the CNT electrode as working electrode, a Pt wire as counter electrode and Ag/AgCl 3 M as homemade reference electrode. No pretreatment of the CNT electrodes was

performed. Storage in air for several weeks did not change the electrochemical response of the CNT electrodes.

The ECL experiments were conducted in a conventional three electrodes arrangement as described above, in phosphate buffer (PB) solution 0.2 M (pH 6.8) with TPrA 60 mM and $[Ru(bpy)_3]Cl_2$ 20 μM. The ECL signal generated by performing the potential step program was measured with a photomultiplier tube (PMT, Hamamatsu R4220p) placed at a constant distance above the cell and inside a dark box. A voltage in the range 750-800 V was supplied to the PMT. The light/current/voltage curves were recorded by collecting the preamplified PMT output signal (by an ultralow-noise Acton research model 181) with the second input channel of the ADC module of the AUTOLAB instrument.

Bibliography

[1]. Miao, W. *Chem Rev.* **108,** 2506–2553 (2008).

[2]. Yuan, Y., Han, S., Hu, L., Parveen, S. and Xu, G. *Electrochim. Acta* **82,** 484–492 (2012).

[3]. A. Fiorani, G. Valenti, E. Villani, Marcaccio. M., E. Rampazzo, L. Prodi and F. Paolucci in *Luminescence in Electrochemistry* pp 293–326 (2017).

[4]. Kapturkiewicz, A. *Anal. Bioanal. Chem.* **408,** 7013–7033 (2016).

[5]. Richter, M. M. *Chem. Rev.* **104,** 3003–3036 (2004).

[6]. Leland, J. K. and Powell, M. J. *J. Electrochem. Soc.* **137,** 3127–3131 (1990).

[7]. Zu, Y. and Bard, A. J. *Anal. Chem.* **72,** 3223–3232 (2000).

[8]. Zu, Y. and Bard, *Anal. Chem.* **73,** 3960–3964 (2001).

[9]. Xu, G., Pang, H.-L., Xu, B., Dong, S. and Wong, K.-Y. *Analyst* **130,** 541–544 (2005).

[10]. Workman, S. and Richter, M. M. *Anal. Chem.* **72,** 5556–5561 (2000).

[11]. Factor, B. *et al. Anal. Chem.* **73,** 4621–4624 (2001).

[12]. Kitte, S. A. *et al. Anal. Bioanal. Chem.* **408,** 7059–7065 (2016).

[13]. Aufray, M. and Roche, A. A. *Appl. Surf. Sci.* **254,** 1936–1941 (2008).

[14]. Nishida, S., Harima, Y. and Yamashita, K. *Inorg. Chem.* **28,** 4073–4077 (1989).

[15]. Angerstein-Kozlowska, H., Conway, B. E., Hamelin, A. and Stoicoviciu, L. *J. Electroanal. Chem.* **228,** 429–453 (1987).

[16]. Conway, B. E., Barnett, B., Angerstein-Kozlowska, H. and Tilak, B. V. *J. Chem. Phys.* **93,** 8361–8373 (1990).

[17]. https://www.mesoscale.com/en/our_company.

[18]. Chen, Z. and Zu, Y. *J. Phys. Chem. C* **112,** 16663–16667 (2008).

[19]. Wu, B. *et al. Sens. Actuators B* **195,** 22–27 (2014).

[20]. Zamolo, V. A. *et al. ACS Nano* **6,** 7989–7997 (2012).

[21]. Sardesai, N. P., Barron, J. C. and Rusling, J. F. *Anal. Chem.* **83,** 6698–6703 (2011).

[22]. Valenti, G. *et al. Chem. Eur. J.* **21,** 12640–12645 (2015).

[23]. Li, F., Yu, Y., Li, Q., Zhou, M. and Cui, H. *Anal. Chem.* **86,** 1608–1613 (2014).

[24]. Su, Y. and Lv, Y. *RSC Adv.* **4,** 29324 (2014).

[25]. Deng, S., Lei, J., Huang, Y., Cheng, Y. and Ju, H. *Anal. Chem.* **85,** 5390–5396 (2013).
[26]. Avouris, P. *Nano Lett.* **10,** 4285–4294 (2010).
[27]. Meyer, J. C. *et al. Nature* **446,** 60–63 (2007).
[28]. Valenti, G., Fiorani, A., Li, H., Sojic, N. and Paolucci, F. *ChemElectroChem* **3,** 1990–1997 (2016).
[29]. Dolci, L. S., Zanarini, S., Della Ciana, L., Paolucci, F. and Roda, *Anal. Chem.* **81,** 6234–6241 (2009).
[30]. Xu, L., Li, Y., Wu, S., Liu, X. and Su, B. *Angew. Chem. Int. Ed.* **51,** 8068–8072 (2012).
[31]. Xu, L., Zhou, Z., Zhang, C., He, Y. and Su, B. *Chem. Commun.* **50,** 9097–9100 (2014).
[32]. Zhou, J. *et al. Anal. Chem.* **87,** 8138–8143 (2015).
[33]. Martinez, A. W., Phillips, S. T., Whitesides, G. M. and Carrilho, E. *Anal. Chem.* **82,** 3–10 (2010).
[34]. Ge, L., Yu, J., Ge, S. and Yan, M. *Anal. Bioanal. Chem.* **406,** 5613–5630 (2014).
[35]. Delaney, J. L., Hogan, C. F., Tian, J. and Shen, W. *Anal. Chem.* **83,** 1300–1306 (2011).
[36]. Lesch, A. *et al. J. Electroanal. Chem.* **717–718,** 61–68 (2014).
[37]. A. Fujishima, Y. Einaga, T. N. Rao and D. A. Tryk *Diamond Electrochemistry First Edition.* (Elsevier Science, 2005).
[38]. A. Fujishima, Y. Einaga, T. N. Rao and D. A. Tryk in *Diamond Electrochemistry First Edition* pp 28–30 (Elsevier Science, 2005).
[39]. Irkham *et al. J. Am. Chem. Soc.* **138,** 15636–15641 (2016).
[40]. K.Honda, M.Yoshimura, Tata N. Rao, and A. Fujishima *J Phys Chem B* **107,** 1653–1663 (2003).
[41]. Zhang, J., Gryczynski, Z. and Lakowicz, J. R. *Chem. Phys. Lett.* **393,** 483–487 (2004).
[42]. Wang, D. *et al. Electrochim. Acta Acta* **150,** 123–128 (2014).
[43]. Wang, D., Li, Y., Lin, Z., Qiu, B. and Guo, L. *Anal. Chem.* **87,** 5966–5972 (2015).
[44]. Yang, R. *et al. Electroanalysis* **28,** 1783–1786 (2016).
[45]. Wang, D. *et al. Sci. Rep.* **5,** 1–7 (2015).
[46]. Miao, W., Choi, J. and Bard, A. J. *J. Am. Chem. Soc.* **124,** 14478–14485 (2002).
[47]. White, H. S. and Bard, A. J. *J. Am. Chem. Soc.* **10,** 5399–5403

(1982).
[48]. Bolletta, F. et al. *Inorg. Chim. Acta* **62,** 207–213 (1982).
[49]. Saragi, T. P. I., Spehr, T., Siebert, A., Fuhrmann-Lieker, T. and Salbeck, J. *Chem. Rev.* **107,** 1011–1065 (2007).
[50]. Polo, F., Rizzo, F., Veiga-Gutierrez, M., De Cola, L. and Quici, S. *J. Am. Chem. Soc.* **134,** 15402–15409 (2012).
[51]. Amatore, C. *et al. ChemPhysChem* **7,** 1322–1327 (2006).

Chapter 4

Electrochemiluminescence and imaging of cells

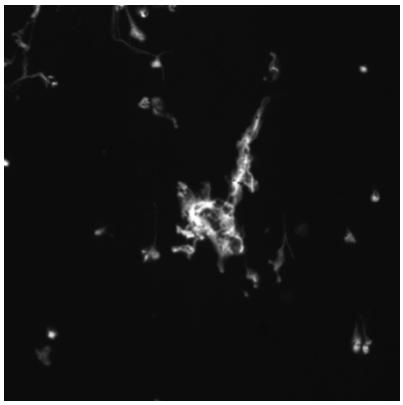

The development of the ECL coreactant water systems has paved the way to the application of this electrochemical technique to the biological field. This has been possible for the electrochemical nature of the ECL methodology that renders the technique extremely sensitive. Since the light generation is achieved directly in situ, one of the latest innovation of the ECL is its use as transduction method for the imaging and study of cell morphology. This new application is at the beginning.
In this chapter, the imaging study of normal epithelial cells using ECL is presented. The aim is to visualize and study the morphological aspect of the cells, combining the information obtained from photoluminescence and ECL technologies. In particular, the use of ECL is largely convenient respect to photoluminescence, since drawbacks such as photobleaching and sample auto-fluorescence are avoided. Detailed information on this innovative topic will be provided.

Key words: *ECL imaging; MCF10A cells; EGFR; carbon nanotubes; photoluminescence.*

Cover picture: fluorescence image of a damaged epithelial cell after treatment with a fluorescent dye.

4.1 The study of cells using ECL

The great success of the ECL as analytical technique has strengthened in the decades, since a wide variety of applications and commercial instruments have been developed after its appearance in the scientific community[1]. As already mentioned in chapter 1, ECL technique presents several advantages respect to the other analytical methods, which include high sensitivity and selectivity, low background signal and working condition in water environments at neutral pH.

In this chapter, the study of cells using ECL as transduction technique is presented. Normal epithelial cells, cultured directly on the surface of the electrode and labeled with $[Ru(bpy)_3]^{2+}$ complex as ECL probe, have been visualized with a microscope using ECL. This approach permits not only the investigation of the cell morphology, but it is also a valuable tool to perform mechanistic studies to understand the complex generation of the light signal. Furthermore, a protocol for the direct detection of cells has also developed. The cells recognition has performed taking advantage of magnetic carbon nanotubes expressly functionalized with an antibody specific for the selective capturing of the cells. The ECL detection of cells has performed using magnetic forces to obtain cells separation from other interferences present in the measuring solution.

4.2 ECL imaging: background

The first report regarding the combination of spatial visualization with ECL was reported in 2006 by Prof. C. Amatore and coworkers[2]. They reported the observation of concentration profiles of species generated at the electrode surface with micrometric resolution for the first time. Starting from that work, increasing attention has been reserved to the application of ECL for imaging studies. For instance, this innovative approach has been used in the areas of metabolic toxicity screening[3],[4], colorimetric devices[5], microfluidic high-throughput analysis[6] and biosensor arrays[7],[8]. Moreover, remarkable attention has deserved the visualization of single objects[9],[10],[11], nanoparticles (NPs)[12],[13] and discrete events at the electrode surface[14].

The success of the ECL as imaging technique is mainly due to the superior way of visualizing electrochemical processes on the surface, since the light-emitting species is formed directly *in situ*. At the same time, the tight dependence of the distance between the emitting species and the electrode surface represents one limitation of this technology. For instance, the ECL generation from microbeads, which are exploited in numerous immunoassays, has highlighted this dependence. In this case, the chromophore is distributed homogeneously on the surface of the bead, but only the chromophores present in the proximity of the surface (few μm) can actively participate in the light generation. In fact, since the diffusion of the chromophore towards the electrode is blocked, the excitation can be provided only by the radicals of the coreactant generated at the electrode after its oxidation (in the case of TPrA, $TPrA^{\bullet+}$ cation radical and $TPrA^{\bullet}$ free radical). This mechanism, where only the coreactant is oxidized, is defined *heterogeneous ECL mechanism* (more details can be found in chapter 1).

In this context, simulation studies are a powerful tool to understand the role of the multiple factors, such as diffusion and radical lifetimes, taking part in the signal generation. For example, simulation studies were applied to the comprehension and optimization of the ECL generated from silica NPs[15],[16].

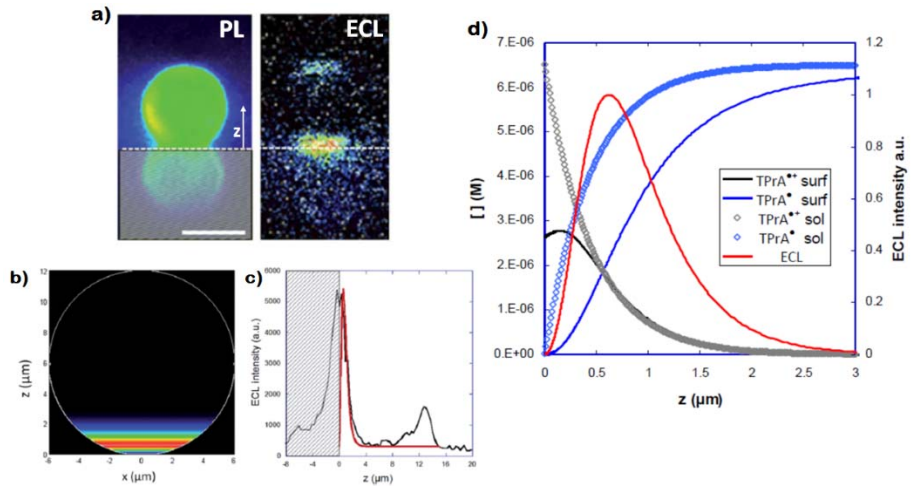

Figure 4.1: a) Lateral-view images of 12 µm polystyrene bead labelled with $[Ru(bpy)_3]^{2+}$ complex: photoluminescence image (left) and ECL image (right) obtained in 200 mM TPrA solution, pH = 7.4. The dashed line indicates the position of the electrode surface (z=0) and the hatched zone is the reflection on the electrode surface; scale bar: 10 µm. b) Lateral-view of the simulated distribution of the $[Ru(bpy)_3]^{2+*}$ excited state at the surface of a 12 µm bead. c) Comparison of the experimental (black line) and simulated (red line) ECL intensity profiles at the level of the single bead (the hatched zone represents the reflection of the ECL light on the electrode surface). d) Concentration profiles of $TPrA^{\bullet+}$ (black curve), $TPrA^{\bullet}$ (blue curve) and the resulting ECL intensity (red curve) with the $[Ru(bpy)_3]^{2+}$ complex immobilized on the bead surface. Images adapted from ref. [17] with permission. Copyright 2014 The Royal Society of Chemistry.

The mechanism of the reaction of $[Ru(bpy)_3]^{2+}$ complex with different coreactants has been investigated recently through the mapping of the ECL signal generation at the level of a single bead[17]. Micrometric non-conductive beads labeled with $[Ru(bpy)_3]^{2+}$ complex have used as a model to simulate the ECL generation on a single bead surface, considering the lifetimes of the radicals and their diffusion from the electrode surface. The mapping of the signal generation using TPrA as coreactant has demonstrated the generation of the excited state of the $[Ru(bpy)_3]^{2+}$ chromophore at micrometric distance from the electrode (~3 µm, see figure 4.1 b and c) for reaction with TPrA diffusing radicals. Correlated imaging studies on the single bead have permitted to visualize the ECL formation mainly at the bottom of the bead and in close proximity of the electrode surface (figure 4.1 a, ECL

image). On the contrary, all the chromophores present on the bead surface take part in the emission when they are stimulated whit an external light source, such as in fluorescence (see figure 4.1 a, PL image). Simulated concentration profiles of the TPrA radicals species (figure 4.1 d), where the deprotonation rate constant of the $TPrA^{\bullet+}$ cation radical represents one of the limiting factors, have demonstrated that the maximum ECL intensity occurs in the micrometric region where the concentration of both $TPrA^{\bullet+}$ cation radical and $TPrA^{\bullet}$ free radical are the highest. Hence, only the chromophores constricted in that region next to the surface will participate in the ECL generation.

In this specific case, all these aspects have to take into account also for the imaging of cells. In fact, cells, which have dimensions ranging from few μm in bacteria to several tens of μm in human beings, can be considered as beads deposited on the electrode surface. Consequently, the dimension of the investigated cell is an important parameter to consider and analyze for the signal detection.

4.3 ECL imaging: some examples reported in literature

One of the first example of the ECL imaging reported in literature concerns the visualization of latent fingermarks through the immunodetection of secretions in human perspiration[18] (figure 4.2 a). In particular, ECL imaging was combined with enzyme immunoassay for the highly sensitive detection of protein/polypeptide residues in fingermarks, providing both an effective method for fingermark detection and identification of an individual. The detection and ECL imaging of fingermarks using the $[Ru(bpy)_3]^{2+}$ / TPrA system was reported previously by the same authors[11].

The use of ECL for the imaging of cells was reported recently for the measurement of active membrane cholesterol at single living cell[19]. The strategy reported was to record in one image the luminescence generated from luminol and hydrogen peroxide upon potential application, enabling the simultaneous analysis of hydrogen peroxide produced at the surface of multiple cells (figure 4.2 b).

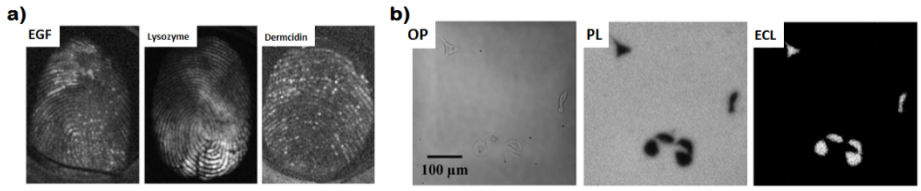

*Figure 4.2: a) ECL images of eccrine fingermarks treated for the detection of EGF (left), lysozyme (center) and dermcidin (right). Images adapted with permission from ref. [*18*]. Copyright 2014 The Royal Society of Chemistry. b) Images of Hela cells on ITO electrode: optical (OP, left), luminescent (PL, center) and ECL (right). Images adapted with permission from ref. [*19*]. Copyright 2015 American Chemical Society.*

The peculiarities of the ECL method permit this kind of approach. In fact, respect to photoluminescence technique, in ECL both photobleaching and sample auto-fluorescence are absent. Photobleaching is the photochemical degradation of the chromophore structure occurring after irradiation at energetic wavelengths, which causes the decrease of its emission quantum yield. This inconvenient is avoided in ECL, since the chromophore is excited via electrochemical pathway. Auto-fluorescence is the light emission of the surrounding biological environment usually recorded in photoluminescence, which cause a considerable and not negligible background signal. To avoid this inconvenient, the use of proper cut-off systems and filters permits to restrict the emission wavelength of few nm in correspondence of the maximum emission wavelength of the chromophore.

4.4 Aim of the study: ECL imaging at single cell level

The aim of this research is to visualize, for the first time, a single cell adhered on the electrode surface using ECL imaging technique.

To perform this goal, a transparent electrode composed of CNTs material has been chosen as suitable surface for cell culture. Moreover, carbon-based electrodes present high conductivity and fast kinetics for the coreactant oxidation reaction that result in considerable higher ECL signal compared with other commercial transparent electrodes, such as ITO. The electrochemical properties of these electrodes, obtained in collaboration with the École Polytechnique Fédérale de

Lausanne (EPFL), have already presented in chapter 3. The cells used for this study are normal mammary epithelial cells, called MCF10A, and they have been cultured in the laboratory of Dr. Stefania Rapino at the Dept. of Chemistry "G. Ciamician", University of Bologna.

MCF10A cells have cultured directly on the CNTs electrode surface. Successively, a $[Ru(bpy)_3]^{2+}$-labelled antibody, specific for a membrane protein, is used to attach the chromophore on the cell surface, enabling ECL emission when TPrA coreactant is present and the potential is applied. This architect, depicted in figure 4.3, represents an innovative approach to cell imaging, thanks to the combination of the ECL technology with the excellent properties of CNTs materials.

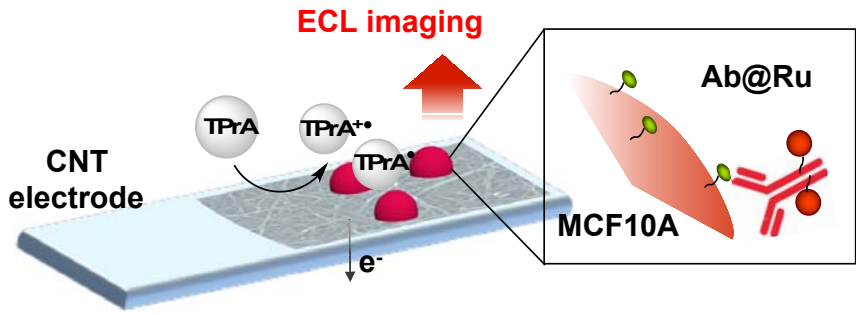

Figure 4.3: Schematic representation of the ECL imaging from adherent cells.

4.5 The model system: ECL imaging of beads

In order to perform imaging study of cells adhered on the electrode surface, magnetic microbeads of different dimensions have been used as model system to simulate the ECL signal generated from cells. The ECL of microbeads labeled with $[Ru(bpy)_3]^{2+}$ complex was already investigated in presence of TPrA as coreactant[20]. In particular, the ECL emission profile of a single bead was evaluated (see figure 4.4). The ECL emission of the bead deposited on CNTs electrode was particularly more intense respect to that one recorded on ITO electrode. As demonstrated in this study, this remarkable difference is due to the fast kinetics of electron transfer reaction for the coreactant oxidation shown by CNTs materials.

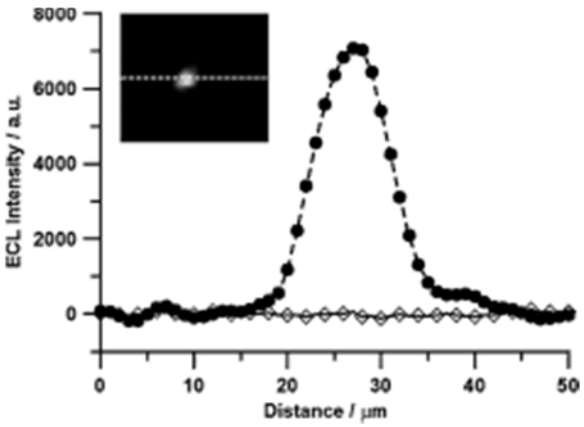

Figure 4.4: ECL intensity profile of a single microbead labelled with $[Ru(bpy)_3]^{2+}$ complex for CNTs (●) and ITO (◊) electrodes in phosphate buffer solution 0.1 M and 80 mM TPrA; potential applied: 1.2 V (vs Ag/AgCl 3M) for 7 seconds; 20x obj. Reprinted with permission from ref. [20]. Copyright 2015 Wiley-VCH Verlag GmbH & Co.

In the work reported in this thesis, it has been used CNTs electrode as a platform for beads deposition and for signal generation. In particular, this CNTs electrode combines excellent electrochemical properties with transparency (chapter 3). In fact, transparency is an important property of the material for the visualization of cells or biological samples, since it enables the visualization of the object in transmitted light.

The micro-particles used in this work as a model system are commercial magnetic beads with diameter of 1 and 2.8 μm. These beads are composed of polystyrene particles and coated with streptavidin. The presence of a dispersion of Fe_3O_4 inside the polystyrene particle confers magnetic properties to the beads. The procedure of beads labeling with $[Ru(bpy)_3]^{2+}$-biotin complex (reported in appendix A.1.4) has carried out exploiting the strong covalent interaction between streptavidin and biotin.

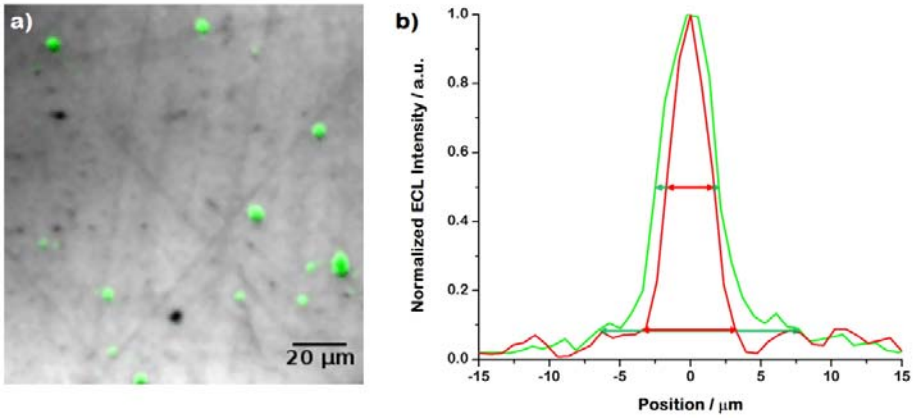

Figure 4.5: a) ECL image of 1 and 2.8 µm beads labelled with $[Ru(bpy)_3]^{2+}$ complex deposited on the electrode surface, in presence of 200 mM TPrA in phosphate buffer solution 0.2 M (pH 6.8). Potential applied: 1.4 V (vs Ag/AgCl 3 M) for 10 seconds; 20x obj. b) Normalized ECL intensity profile of a single bead of dimension 1 µm (red line) and 3 µm (green line). The experimental conditions are the same reported in a).

The ECL image of the beads and their intensity profiles are reported in figure 4.5. The beads can be distinguished from their different dimensions (figure 4.5 a), since the 2.8 µm beads show more intense ECL signal compared to 1 µm beads. The study of their normalized ECL intensity profiles help to understand the origin of this difference (figure 4.5 b). As mentioned previously, the chromophore is fixed on the bead surface and its diffusion is prevented. Only the coreactant can be oxidized and the radicals formed are free to diffuse in solution. Consequently, only the chromophores constricted in the electrode surface area accessible to the radicals will take part in the signal generation. In the case of 2.8 µm beads, larger surface is accessible to the coreactant radicals and, hence, a larger number of chromophores can be excited respect to 1 µm beads. In fact, the difference of the peaks amplitude between the beads are 1.5 µm at half intensity and 6 µm at the basis of the signal (highlighted by colored arrows in figure 4.5 b).

The beads model system simulates perfectly the situation encounter in the case of cells. The use of carbon-based material assures a constant efflux of $TPrA^{\bullet+}$ cation radical and $TPrA^{\bullet}$ free radical, both necessary for signal generation, thanks to the fast kinetics of

coreactant oxidation. Nevertheless, the dimension of the object investigated has to take into account, since the signal generation is localized only in the close proximity of the electrode surface.

4.6 ECL imaging at single cell level

The cells selected for imaging studies are MCF10A cells, normal epithelial mammary cells. MCF10A cells present, over-expressed, the *Epidermal Growth Factor Receptor (EGFR)*, a transmembrane protein that is a specific receptor for the *Epidermal Growth Factor (EGF)* of extracellular protein ligands. EGFR is a protein also over-expressed in cells of several tumors[21]: for this reason, the study of MCF10A cells represents a case of real biological and clinical interest.

MCF10A cells have cultivated directly on the transparent CNTs surface. Cetuximab monoclonal antibody, labelled with $[Ru(bpy)_3]^{2+}$ chromophore (Ab@Ru in figure 4.3), has been used for the efficient and selective targeting of EGFR[22],[23] on the MCF10A cells surface. The resulting adherent labelled cells have analyzed in a conventional three electrodes arrangement in presence of 200 mM TPrA in 0.2 M phosphate buffer solution, pH=6.8 (experimental details reported in appendix A.1.5-A.1.6).

The effective conjugation of the Ab@Ru has been tested analyzing the emission behavior from a single cell. In figure 4.6 b, a typical fluorescence image recorded upon an excitation from 330 to 380 nm has reported. Intense and uniform photoluminescence has recorded from all the cells, as a proof of the homogeneous EGFR recognition realized by Ab@Ru on the cell membrane. This step has been necessary also to adjust the focus of the objective on the cell surface. Successively, the excitation light source has switched off and a positive potential has applied during image acquisition. In figure 4.6 c, the ECL mapping of EGFR on a single cell has reported. Thanks to the excellent electrochemical properties of the CNTs material, expressly designed for this purpose, the ECL signal intensity results very intense with high spatial resolution. Furthermore, the electrochemical nature of the ECL technique, used to generate the excited state of the luminophore without an external light source, permits to obtain

images without scattering of the excitation light and, even more important, without auto-fluorescence typical of biological samples.

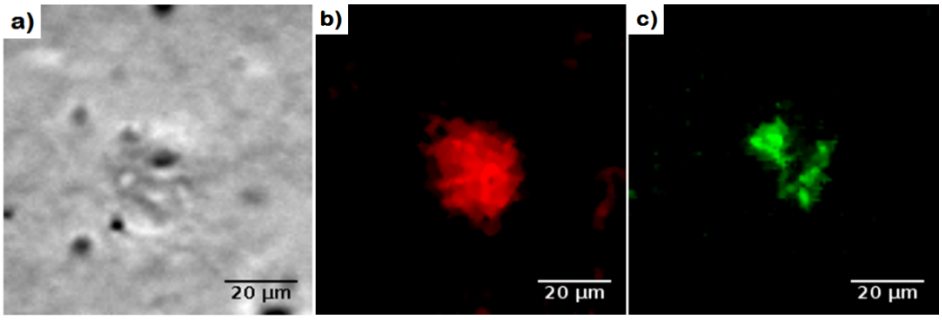

Figure 4.6: Optical (a), photoluminescence (b) and ECL images (c) of a single MCF10A cell, labelled with Ab@Ru and adhered on the CNTs electrode, in phosphate buffer solution 0.2 M (pH=6.8) in presence of 200 mM TPrA. PL (b): acquisition time: 800 msec (CCD mode, gain 3, 20x obj, filter excitation: 330-380 nm, emission > 400 nm). ECL (c): potential applied 1.25 V (vs Ag/AgCl 3 M), acquisition time: 4 sec (EM-CCD mode, gain 5, sensitivity 100, 20x obj).

The photoluminescence and ECL emission profiles of a single MCF10A cell adhered on CNTs electrode have been reported in figure 4.7 b and 4.7 c, respectively. The emission profile obtained from the photochemical excitation results very different compared with the profile of the electrochemical excitation. In fact, while the photoluminescence emission is homogeneous overall the cell, the ECL emission is localized only in the proximity of the cell border, in close proximity of the electrode surface. In addition, the ECL emission is totally absent towards the center of the cell. This difference is due to the different method of excitation. As previously discussed, the rate determining step in the ECL signal generation strongly depends on the diffusion rate of the electrogenerated radicals from the electrode surface to the top of the cell. Thus, since the medium size of a MCF10A cell is several tens of µm, the ECL emission occurs only in the peripheral zones of the cell.

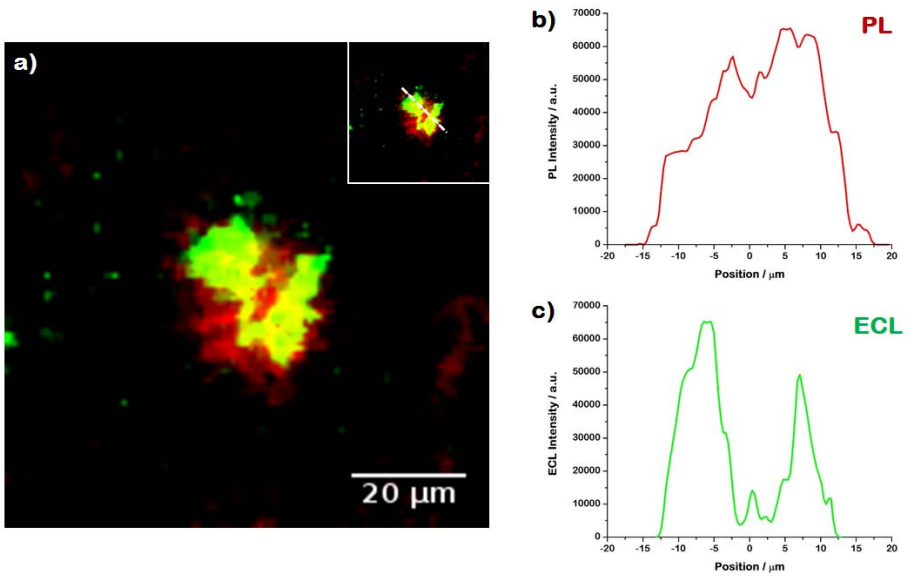

Figure 4.7: a) ECL and photoluminescence merged image, b) photoluminescence emission intensity profile and c) ECL emission intensity profile of a single MCF10A cell, labelled with Ab@Ru and adhered on the CNTs electrode, in phosphate buffer solution 0.2 M (pH=6.8) in presence of 200 mM TPrA. The experimental conditions are the same reported in figure 4.6.

Lastly, in order to prove the integrity of the analyzed cell, the nucleus has been marked with DAPI (4',6-diamidino-2-phenylindole) dye and its image has been recorded in photoluminescence mode (reported in figure 4.8).

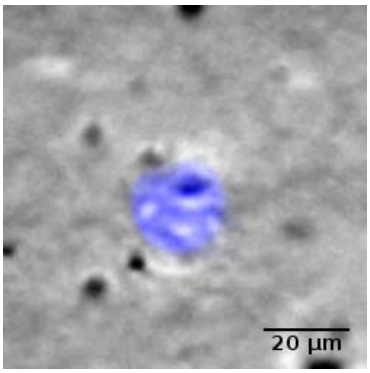

Figure 4.8: Photoluminescence image of a single MCF10A cell adhered on CNTs electrode and marked with DAPI dye. Acquisition time: 800 msec (CCD mode, gain 3, 20x obj, filter excitation: 330-380 nm, emission > 400 nm).

According to this strategy, the ECL image of a single cell results not homogeneous and differs considerably from the same image obtained in photoluminescence. In order to obtain homogeneous ECL images of cells, CNTs can also be employed for the development of carbon-based structures for the detection of cells in solution.

4.7 CNTs-based architectures for cell targeting and cancer therapy

Targeting of cancer cells using CNTs structures has already reported in literature. For example, it was reported that CNTs with magnetic properties, due to iron particles content inside the carbon-based structure, were successfully used for magnetic cell sorting and magnetic fluid hyperthermia[24]. The authors demonstrated that these hybrids allow in few minutes a very selective catching of a population of cancer cells over healthy ones.

In another work was reported a multifunctional platform based on the modification of mesoporous silica coated single walled carbon nanotubes (SWCNTs). This platform could be used simultaneously as a drug loading carrier, a NIR photothermal heater and a multimodal imaging probe useful for imaging and combination therapy of cancer[25].

Furthermore, CNTs have emerged also as an alternative and efficient tool for transporting and translocating therapeutic molecules thanks to their low toxicity[26].

Among the numerous examples reported in literature, in the second part of this chapter, it has been proposed a protocol for the recognition of cells, combining ECL technology with the selective cells catching properties of expressly designed CNTs. In fact, the cells recognition has performed taking advantage of the double functionalization of Multiwalled Carbon Nanotubes (MWCNTs).

The carbon materials used in this work present two different chemical modifications: *i)* with an antibody, specific for the selective recognition of the EGFR protein in cancer cells, and *ii)* equipped with a ferromagnetic core for cells separation (Fe@MWCNTs). The CNTs structures have been synthesized in the laboratories of Prof. Davide Bonifazi, at the University of Namur[23] (Belgium). The cells used for

this study have been cultivated in the laboratory of Dr. Stefania Rapino, at University of Bologna. As already mentioned in the first part of this chapter, MCF10A cells have been chosen since they present the membrane protein EGFR over-expressed, a peculiarity also presents in cancer cells. Hence, MCF10A cells have studied as a model system for Circulating Tumor Cells (CTC). CTC are epithelial cells detached from the primary tumor and transported in blood vessels triggering metastasis process[27]. The evaluation of CTC concentration in blood samples can give information about tumor proliferation and diagnosis.

4.8 ECL detection of cells using Fe@MWCNTs

A protocol for cells recognition and separation in solution has been developed and optimized. This protocol combines the capturing properties of CNTs structures with the sensitive ECL detection (figure 4.9).

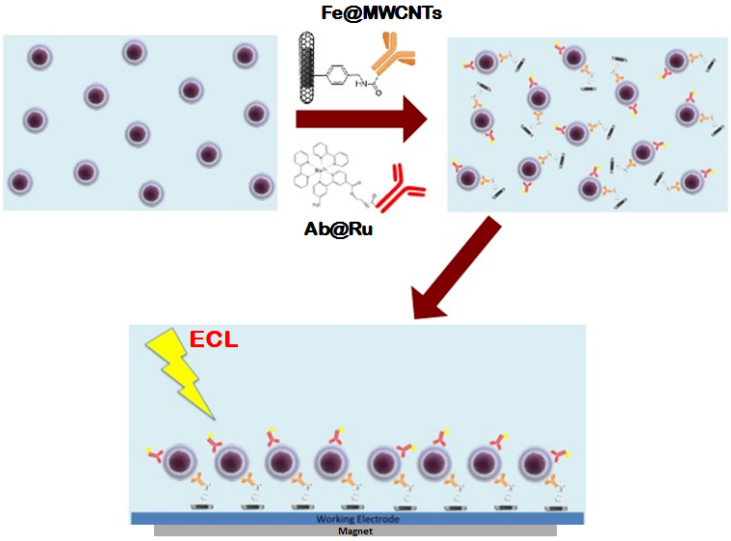

Figure 4.9: Schematic representation of the phases of the protocol for MCF10A cells separation and detection.

The magnetically-active Fe@MWCNTs represent a multifunctional scaffold for the anchoring of a monoclonal antibody, Cetuximab, specific for the EGFR present of the surface of MCF10A cells. This architecture represents the so-called "cell fishing system". In the recognition step MCF10A cells have been incubated with Fe@MWCNTs and with Cetuximab antibody labelled with a $[Ru(bpy)_3]^{2+}$ complex (Ab@Ru), which acts as ECL transduction probe. After the recognition step, the entire system composed of CNTs, cells and labelled antibody (Fe@MWCNTs/MCF10A/Ab@Ru) has attracted on the surface of an electrode using magnetic forces (experimental details reported in appendix A.2.4). This awkward step permits the separation of the cells from the solution of potential interferents. Lastly, the ECL detection of the cells has performed adding a solution of phosphate buffer 0.2 M (pH=6.8) containing 200 mM TPrA and applying the potential (1.4 V vs Ag/AgCl 3 M). The ECL image of a MCF10A cell separated and detected with the above-described protocol is reported in figure 4.10 a.

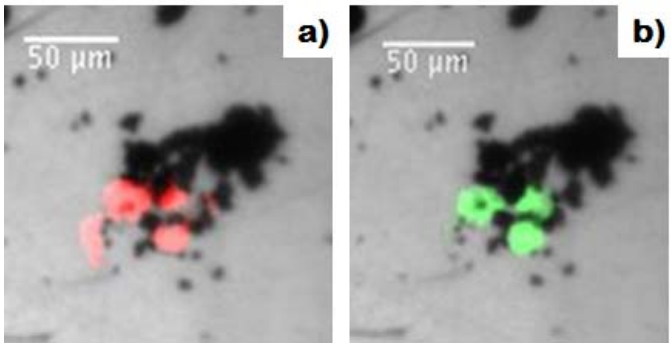

Figure 4.10: ECL (a) and photoluminescence (b) images of a single MCF10A cell separated with the proposed protocol in phosphate buffer solution 0.2 M, pH=6.8, with 200 mM TPrA. The black spots represent aggregations of Fe@MWCNTs in solution. ECL (a): potential applied 1.4 V (vs Ag/AgCl 3 M), acquisition time: 10 sec (EM-CCD mode, gain 5, sensitivity 100, 20x obj). PL (b): acquisition time: 800 msec (CCD mode, gain 3, 20x obj, filter excitation: 330-380 nm, emission > 400 nm).

The MCF10A cells can be effectively separated using the proposed analytical protocol. It is noteworthy that the ECL and photoluminescence emission intensities on the cell surface are very

similar. In particular, the ECL emission intensity results homogeneous as obtained in photoluminescence. This result can be explained considering the catalytic properties of carbon-based materials towards the oxidation of the coreactant[20]. In fact, their catalytic effect might extend the oxidation of TPrA until the top of the cell, enabling the excitation of the chromophores placed far away from the electrode surface.

4.9 Conclusion

The image of a single cell using ECL as transduction technique has been reported for the first time. This imaging approach has been tested on a disposable and transparent electrode material made of CNTs, which it has demonstrated biocompatibility for cell culture and far superiority in the transduction capability compared with the conventional materials. Immunochemistry has used for labeling of cells and mapping the distribution of important membrane receptor, such as EGFR, over-expressed in several kinds of cancers. The approach used in this work, which requires an electrochemical stimulus for the signal generation, guarantees low background signal, since auto-fluorescence typical in biological samples is avoided. Furthermore, the capability of the protocol developed for the detection of cells has been assessed. The results obtained have showed that the protocol is effective in cell recognition and detection and, even more important, the ECL emission from a single cell results intense and homogeneous on the entire cell surface. This interesting result is attributed to the capability of the CNTs structure to catalyze the oxidation of the coreactant also on the top of the cell. The reported results may contribute to the development of new and ultrasensitive technique in the future.

Appendix

A.1 ECL IMAGING

A.1.1 Chemicals and materials

Tri-n-propylamine (TPrA), Paraformaldehyde (PFA), 4',6-diamidino-2-phenylindole dihydrochloride (DAPI), N-(3-dimethylaminopropyl)-N'-ethylcarbodiimide hydrochloride (EDC), N,N'-dicyclohexylcarbodiimide (DCC), N-hydroxysuccinimide (NHS), phosphate buffer saline (PBS) pH 7.4 and Tris(2,2'-bipyridyl)dichlororuthenium(II) hexahydrate ($[Ru(bpy)_3]Cl_2*6H_2O$) were from Sigma-Aldrich and used without any further purification. Bis(2,2'-bipyridine)-[4-(4'-methyl-2,2'-bipyridin-4-yl)butanoic acid] ruthenium bis(hexafluorophosphate) ($Ru(bpy)_3^{2+}$-COOH) and biotin-cadaverine-TFAc were purchased from Cyanagen (Bologna, Italy). PB 0.2 M, pH 6.8, was obtained mixing 0.2 M of sodium phosphate monobasic dihydrate ($NaH_2PO_4*2H_2O$) and 0.2 M of sodium phosphate dibasic (Na_2HPO_4), both from Sigma-Aldrich and used as received. Cetuximab antibody was obtained from the Erbitux© formulation by discontinuous diafiltration in centrifugal concentrators (Vivaspin 6 10,000 g/mol molecular weight cut-off) and isolated through lyophylization. Ruthenium-butanic acid-ester ($Ru(bpy)_2$-bpy-CO-OSu) was purchased from Roche Diagnostics GmbH (Mannheim, Germany) and used as received. Amicon® centrifugal filters were obtained from Millipore (Vimodrone, Italy) and dialysis membranes (12000-14000 Da cut-off, in regenerated cellulose) were obtained from Spectrum Lab (Rancho Dominguez, CA, USA). The polystyrene streptavidin-coated magnetic microbeads (diameter 1 and 2.8 μm) were purchased from Thermo Fisher Scientific (Massachusetts, USA).

A.1.2 Labeling of Cetuximab antibody with ruthenium complex (Ab@Ru)

At 1 mg/mL of Cetuximab antibody in PBS solution, pH 7.8, 85 molar equivalents of EDC, NHS and $Ru(bpy)_2$-bpy-CO-OSu were added. The solution was shaken gently for 90 minutes at room temperature and then exchanged to pH 7.4 by dialysis using a 12000-14000 Da cut-off membrane and maintained overnight at 4°C. In order to remove the unreacted dye complex, the solution was centrifuged with Millipore Amicon® Ultra 0.5 μm centrifugal filter devices, with 50000 cut-off membrane and refilled with fresh PBS.

A.1.3 Cells culture on CNTs electrode and labeling with Ab@Ru

MCF10A cells (ATCC® crl-10317™) were cultured in (1:1) Dulbecco's Modified Eagle's Medium (DMEM)/Nutrient Mixture F-12Ham (that do not contain glutathione) (Gibco-Life Technologies Corporation) supplemented with 5% horse serum, 20 ng/mL epidermal growth factor (EGF), 50 ng/mL cholera toxin, 500 ng/mL hydrocortisone and 0.01 mg/mL insulin (Gibco-Life Technologies Corporation) using CNTs electrode surface as support (presented in Chapter 3).
After cells growth, the medium was removed washing with PBS solution for two times. Successively, 60 µL of solution containing Ab@Ru 0.15 nM in PBS were added to cells and maintained for 7 minutes at room temperature. The unreacted Ab@Ru was removed washing with PBS for two times. Cells/Ab@Ru were than fixed adding 1 mL PFA 0.5% for 20 minutes. After two washing steps using PBS, CNTs substrate with adherent Cells/Ab@Ru cells was suitable for ECL detection.

A.1.4 Labelling of magnetic microbeads with $[Ru(bpy)_3]^{2+}$ complex

The labelling procedure of the magnetic microbeads was carried out according to the procedure reported in[20].
A volume of 70 µL of Ru(bpy)32+-COOH (7.1x10-3 M in DMF) was added to 1.5 equivalents of N,N'-dicyclohexylcarbodiimide (DDC) and the reaction solution was mixed gently for 4 hours at room temperature (RT 25°). A streptavidin solution (630 µL of 2.0x10-5 M) in 0.1 M borate buffer (pH 9.4) was then added to conjugate streptavidin to the activated [Ru(bpy)3]2+-COOH. The solution was incubated overnight and the labelled protein was subsequently purified with dialysis against 5 L of PBS. Beads were then conjugated to the amino derivative of biotin. The suspension of beads (200 µL) was washed three times in 0.1 mol/L borate buffer (pH 9.6) and two times in 0.1 mol/L in 2-(N-morpholino)ethanesulfonic acid buffer (MES pH 5.5). Upon resuspension of the beads in 250 µL of MES buffer, N-(3-dimethylaminopropyl)-N'-ethyl-carbodiimide hydrochloride (EDC) and NHS were added to a final concentration of 50 mM and 2 mM, respectively. The reaction mixture was mixed for 1 hour at RT. After one washing cycle (as described above), 500 µL of 9 mM biotin cadaverine in 0.1 mol/L borate buffer (pH 8.6) was added. The mixture was incubated overnight at 4°C and the solution was finally washed three times in PBS. Beads conjugated to biotin were then coupled with the streptavidin-$[Ru(bpy)_3]^{2+}$ using the following procedure. A suspension of 50 µL of beads was centrifuged and after buffer

removal, 50 µL of labelled streptavidin was added. The mixture was mixed gently for 2 hours at RT and then three washing steps were performed by centrifugation and resuspension with PBS.

A.1.5 ECL detection

ECL measurements were carried out with PGSTAT302 (AUTOLAB Instrument) in a three electrodes arrangement using CNTs with Cells/Ab@Ru cells as working electrode, a Pt wire as counter electrode and Ag/AgCl 3 M as homemade reference electrode. The ECL measurements were conducted in phosphate buffer solution (PB 0.2 M, pH 6.8) using 200 mM TPrA as coreactant. The ECL signal generated by performing the potential step program was measured with a photomultiplier tube (PMT, Hamamatsu R4220p) placed at a constant distance above the cell and inside a dark box. The voltage supplied to the PMT was in the range 550-750 V. The light/current/voltage curves were recorded by collecting the preamplified PMT output signal (by an ultralow-noise Acton research model 181) with the second input channel of the ADC module of the AUTOLAB instrument. Chronoamperometry technique was used for ECL detection: E_1 = 0 V, t_1 = 2 sec ; E_2 = 1.2 V, t_2 = 6 sec.

A.1.6 ECL imaging instrumentation

The ECL/optical/photoluminescence imaging was performed in a PTFE (Teflon) homemade electrochemical cell in a three electrodes configuration: CNTs (20 mm^2) as working electrode, Ag/AgCl 3 M as reference electrode and a Pt wire as counter electrode. ECL images were performed using 200 mM TPrA in phosphate buffer solution (PB 0.2 M, pH 6.8, Tween 0.1%).
For microscopy imaging, an epifluorescence microscope from Nikon (Chiyoda, Tokyo, Japan) equipped with ultrasensitive Electron-Multiplying CCD camera (EM-CCD 9100-13 from Hamamatsu, Hamamatsu Japan) was used with a resolution of 512 pixel x 512 pixel with a size of 16 x 16 µm. The microscope was enclosed in a homemade dark box to avoid interferences from external light. It was equipped with a motorized microscope stage (Corvus, Marzhauser, Wetzlar, Germany) for sample positioning and with long distance objectives from Nikon (10x/0.30 DL17, 5mm, 20x/0.40 DL13mm). The system was connected to the AUTOLAB potentiostat to provide the needed potential for the ECL reaction.

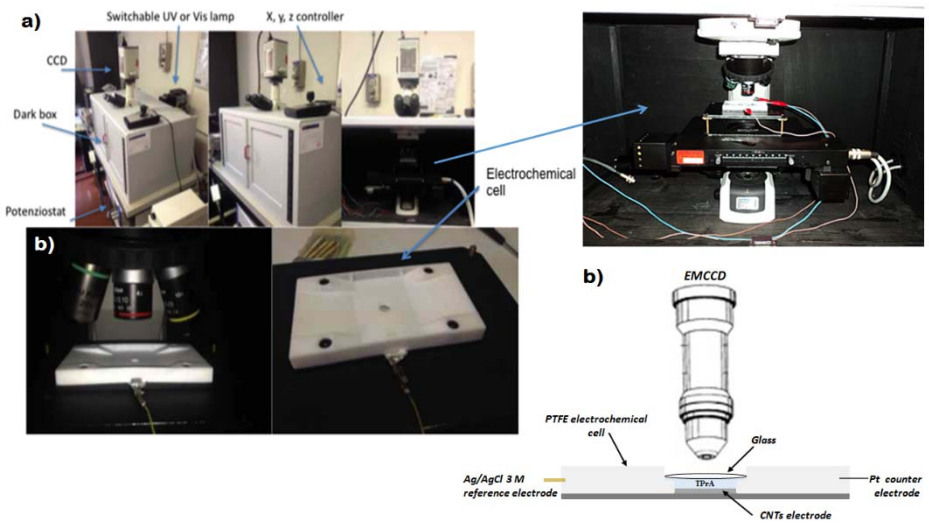

Figure 4.11: a) ECL imaging instrumentation set-up currently in use at the electrochemistry group; b) particular of the electrochemical cell disposition on the motorized stage of the microscope.

A.2 CELL DETECTION

A.2.1 Chemicals and materials

Tri-n-propylamine (TPrA), Paraformaldehyde (PFA), 4',6-diamidino-2-phenylindole dihydrochloride (DAPI), N-(3-dimethylaminopropyl)-N'-ethylcarbodiimide hydrochloride (EDC), N,N'-dicyclohexylcarbodiimide (DCC), N-hydroxysuccinimide (NHS), phosphate buffer saline (PBS) pH 7.4 and 2-(N-morpholino)ethanesulfonic acid hydrate (MES) were from Sigma-Aldrich and used without any further purification. Ruthenium-butanic acid-ester ($Ru(bpy)_2$-bpy-CO-OSu) was purchased from Roche Diagnostics GmbH (Mannheim, Germany) and used as received. PB 0.2 M, pH 6.8, was obtained mixing 0.2 M of sodium phosphate monobasic dihydrate ($NaH_2PO_4*2H_2O$) and 0.2 M of sodium phosphate dibasic (Na_2HPO_4), both from Sigma-Aldrich and used as received. Cetuximab antibody was obtained from the Erbitux© formulation by discontinuous diafiltration in centrifugal concentrators (Vivaspin 6 10,000 g/mol molecular weight cut-off) and isolated through lyophylization. Amicon® centrifugal filters were obtained from Millipore (Vimodrone, Italy) and dialysis membranes (12000-14000 Da cut-off, in

regenerated cellulose) were obtained from Spectrum Lab (Rancho Dominguez, CA, USA).

A.2.2 Labeling of Cetuximab antibody with ruthenium complex (Ab@Ru)

At 1 mg/mL of Cetuximab antibody in PBS solution, pH 7.8, 85 molar equivalents of EDC, NHS and $Ru(bpy)_2$-bpy-CO-OSu were added. The solution was shaken gently for 90 minutes at room temperature and then exchanged to pH 7.4 by dialysis using a 12000-14000 Da cut-off membrane and maintained overnight at 4°C. In order to remove the unreacted dye complex, the solution was centrifuged with Millipore Amicon® Ultra 0.5 μm centrifugal filter devices, with 50000 cut-off membrane and refilled with fresh PBS.

A.2.3 MCF10A cells culture

MCF10A cells (ATCC® crl-10317™) were cultured in (1:1) Dulbecco's Modified Eagle's Medium (DMEM)/Nutrient Mixture F-12Ham (that do not contain glutathione) (Gibco-Life Technologies Corporation) supplemented with 5% horse serum, 20 ng/mL epidermal growth factor (EGF), 50 ng/mL cholera toxin, 500 ng/mL hydrocortisone and 0.01 mg/mL insulin (Gibco-Life Technologies Corporation). After cells growth, the medium was removed washing with PBS solution for two times. Before the detection, the cells were dispersed in 3 mL PBS solution at the concentration of 200·000 cells/mL.

A.2.4 Analytical protocol for cell detection with ECL

At 2.2 mL solution of MCF10A cells 200·000 cells/mL in PBS, 700 μL of a dispersion of Fe@MWCNTs 0.2 mg/mL in PBS were added and the solution was gently shaken for 7 minutes at room temperature. Successively, 100 μL of a solution of Ab@Ru 4.5 nM in PBS were added (total volume 3 mL) and the solution was gently shaken for 7 minutes at room temperature. In order to remove the unreacted species, the solution was centrifuged at 1200 rpm for 5 minutes, the supernatant was removed and then refilled with 3 mL of fresh PBS. This step was repeated twice. After the second washing step, the supernatant was removed and 1 mL of PFA 0.5 % was added. After 20 minutes, the solution was centrifuged again (1200 rpm, 5'), the supernatant was removed and other two washing step with PBS were performed. The final solution was resuspended in PBS (3 mL).
The cells detection was performed in a conventional three electrodes arrangement (working electrode: flat Pt, counter electrode: Pt, reference electrode: Ag/AgCl 3 M) combined with a fluidic system. A magnet was placed

under the working electrode during the injection of the solution to analyze and then removed after the detection. After injection of the solution to analyze, a solution containing 200 mM TPrA in phosphate buffer solution (PB 0.2 M, pH 6.8, Tween 0.1%) was added. Chronoamperometry technique was used for ECL detection: E_1 = 0 V, t_1 = 1 sec ; E_2 = 1.4 V, t_2 = 10 sec.

For microscopy imaging, an epifluorescence microscope from Nikon (Chiyoda, Tokyo, Japan) equipped with ultrasensitive Electron-Multiplying CCD camera (EM-CCD 9100-13 from Hamamatsu, Hamamatsu Japan) was used with a resolution of 512 pixel x 512 pixel with a size of 16 x 16 µm. The microscope was enclosed in a homemade dark box to avoid interferences from external light. It was equipped with a motorized microscope stage (Corvus, Marzhauser, Wetzlar, Germany) for sample positioning and with long distance objectives from Nikon (10x/0.30 DL17, 5mm, 20x/0.40 DL13mm). The system was connected to the AUTOLAB potentiostat to provide the needed potential for the ECL reaction.

Bibliography

[1]. Miao, W. *Chem Rev.* 2506–2553 (2008)
[2]. Amatore, C. *et al.*, *ChemPhysChem* **7,** 1322–1327 (2006)
[3]. Hvastkovs, E. G. *et al.*, *Anal. Chem.* **79,** 1897–1906 (2007)
[4]. Krishnan, S. *et al.*, *Anal. Chem.* **80,** 5279–5285 (2008)
[5]. Chen, X. *et al.*, *Anal. Chem.* **81,** 830–833 (2009)
[6]. Chow, K. F., Mavré, F. and Crooks, R. M., *J. Am. Chem. Soc.* **130,** 7544–7545 (2008)
[7]. Sardesai, N. P., Barron, J. C. and Rusling, J. F., *Anal. Chem.* **83,** 6698–6703 (2011)
[8]. Venkatanarayanan, A. *et al.*, *Biosens. Bioelectron.* **31,** 233–239 (2012)
[9]. Wilson, A. J., Marchuk, K. and Willets, K. A., *Nano Lett.* **15,** 6110–6115 (2015)
[10]. Cristarella, T. C., Chinderle, A. J., Hui, J. and Rodríguez-López, J., *Langmuir* **31,** 3999–4007 (2015)
[11]. Xu, L., Li, Y., Wu, S., Liu, X. and Su, B., *Angew. Chem. Int. Ed.* **51,** 8068–8072 (2012)
[12]. Fan, F.-R. F., Park, S., Zhu, Y., Ruoff, R. S. and Bard, A. J., *J. Am. Chem. Soc.* **131,** 937–939 (2009)
[13]. Fan, F.-R. F. and Bard, A. J., *Nano Lett.* **8,** 1746–1749 (2008)
[14]. Dick, J. E., Renault, C., Kim, B. K. and Bard, A. J. *Angew. Chem. Int. Ed.* **53,** 11859–11862 (2014)
[15]. Imai, K. *et al.*, *J. Phys. Chem. C* **119,** 26111–26118 (2015)
[16]. Daviddi, E. *et al.*, *ChemElectroChem* **4,** 1–13 (2017)
[17]. Sentic, M. *et al.*, *Chem. Sci.* **5,** 2568 (2014)
[18]. Xu, L., Zhou, Z., Zhang, C., He, Y. and Su, B., *Chem. Commun.* **50,** 9097–9100 (2014)
[19]. Zhou, J. *et al.*, *Anal. Chem.* **87,** 8138–8143 (2015)
[20]. Valenti, G. *et al.*, *Chem. Eur. J.* **21,** 12640–12645 (2015)
[21]. Baselga, J. and Albanell, J., *Curr Oncol Rep* **4,** 317–324 (2002)
[22]. Dassonville, O., Bozec, A., Fischel, J. L. and Milano, G., *Crit. Rev. Oncol. Hematol.* **62,** 53–61 (2007)
[23]. Marega, R. *et al.*, *Adv. Funct. Mater.* **23,** 3173–3184 (2013)
[24]. Pineux, F. *et al.*, *Nanoscale* **7,** 20474–20488 (2015)
[25]. Liu, J. *et al.*, *Adv. Funct. Mater.* **25,** 384–392 (2015)
[26]. Bianco, A., Kostarelos, K. and Prato, M. *Curr. Opin. Chem. Biol.*

9, 674–679 (2005)
[27]. V. Plaks, C. D. Koopman, Z. W., *Science,* **341,** 1186–1188 (2013)

Chapter 5

General conclusion

Cover picture: logo of the International Meeting on Electrogenerated Chemiluminescence.

In this doctoral thesis, new functional materials have been studied for sensing and imaging applications, using ECL as transduction technique.

ECL is the generation of light at the electrode surface following an electrochemical stimulus and, among the electrochemical techniques is the most suitable method for the development of sensing applications. In particular, thanks to the electrochemical nature of the signal generation, an external light source is not necessary. In this case, low background signal, high range of sensitivity and extremely low detection limits can be achieved. At the same time, drawbacks such as light scattering, photobleaching and sample auto-fluorescence can be avoided. These characteristics of the ECL foster its application to the design and development of innovative sensors. In particular, the development of such sensors can be performed choosing and designing the proper electrode material. This reason has motivated the investigation of the electrochemical properties of very different electrode materials.

In the first part of this thesis, the development of a sensor for the early diagnosis of prostate cancer has been developed combining a supramolecular receptor and ECL methodology. The target analyte is sarcosine, recently indicated as a biomarker for the diagnosis of prostate cancer that can be detected non-invasively in urine. The approach used is based on magnetic microbeads technology. Magnetic microbeads have been functionalized on the surface with a supramolecular cavitand that exerts high selective recognition of sarcosine molecule. The magnetic properties of the functionalized microbeads can be exploited both for the separation of sarcosine in solution and for its concentration on the electrode surface, enabling its quantification using ECL. This architecture results in a disposable

and easy to use device with low detection limits and fast and economic detection. This sensor has tested successfully in real urine samples derived from patients with verified prostate cancer, proving both the capability of the device to detect sarcosine and the role of this molecule as a biomarker for the early diagnosis of prostate cancer. Nevertheless, the limits of detection using this sensor are considerably higher than the limits of detection obtained with the chromatography technique that is, even now, the standard method for sarcosine quantification. However, this standard methodology requires sarcosine derivatization, difficult sample manipulation and long times analysis; all these drawbacks are completely avoided using the proposed ECL sensor.

Another sensor has been developed for the detection of cells in solution using carbon nanotubes as multifunctional scaffold. In this case, carbon nanotubes possess a double chemical modification. The first one has made with a monoclonal antibody specific for the recognition of a membrane protein over-expressed in the cells of several tumors; the second one has obtained with a ferromagnetic loading in the carbon structure, which confers to the system magnetic properties. This carbon-based architecture performs cells recognition and capturing in solution and it has used to concentrate the cells on the electrode surface through the application of a magnetic field. Moreover, an immunochemistry procedure has used for cells labelling in order to perform the ECL detection. The results obtained have demonstrated both the capturing capability of the carbon nanotubes architecture and the effective labelling procedure of the cells. However, the most important result is the intense and homogeneous ECL emission obtained from the cells. This effect is attributed to the catalytic properties of the carbon-based structure, which enables the generation of the radicals necessary in ECL on the entire surface of the cell.

Carbon nanotubes materials have also been used for the design of transparent electrodes for the ECL imaging of cells. This kind of electrode presents good electrochemical properties, such as conductivity, reproducibility and fast kinetics of electron transfer reactions. Transparency is an important property for the study of biological samples, since the visualization of the object can be achieved in transmitted light. This material have been used, for the first time,

for the ECL imaging of a single cell. The ECL imaging approach permits the spatial visualization of the emission, since the light is generated in situ, avoiding photobleaching and sample auto-fluorescence. Although the ECL emission profile of a single cell results surprisingly intense, thanks to the catalytic effect of the carbon nanotubes material, the signal is not homogeneously distributed, showing a significant decrease towards the center of the cell. This effect is attributed to the short distance diffusion of the radicals from the electrode surface, where they are generated, towards the solution. For this reason, only the peripheral zones of the cell can be illuminated.

Transparent electrodes are also interesting materials for surface functionalization with ECL chromophores. Indium-tin oxide electrode has been functionalized on the surface with a spirobifluorene dye, which has been demonstrated to produce very intense blue ECL emission with high quantum yield. The resulting pattern can be used for the study of the ECL on solid state. ECL imaging studies on this surface have been performed using two different coreactants. Unfortunately, both approaches have failed and no ECL imaging of the spirobifluorene pattern could be recorded. This inconvenient has hampered further studies of solid state ECL.

Lastly, nanoporous gold electrodes have been studied for surface enhancement ECL. This approach exploits the stabilization effect of a gold surface plasmon towards the excited state of the chromophore, increasing the overall ECL emission. The gold materials investigated present different porosity thanks to the method of preparation. The use of tripropylamine as coreactant has revealed an instable behaviour of the materials. Surface analysis have demonstrated the degradation effect of the amine towards the porous surface of gold. It is hypothesized that the amine chemisorption on metallic surface might provoke surface dissolution, leading to organometallic complex formation. Further investigations using persulfate as coreactant have showed that the ECL emission increases linearly increasing the porosity of the material. This ECL enhancement is attributed to the increased surface area and not to surface enhancement ECL.

List of publications

Scientific articles

1. Giovanni Valenti, Enrico Rampazzo, Elisa Biavardi, Elena Villani, Giulio Fracasso, Massimo Marcaccio, Federico Bertani, Dunia Ramarli, Enrico Dalcanale, Francesco Paolucci and Luca Prodi, *"An electrochemiluminescence - supramolecular approach to sarcosine detection for early diagnosis of prostate cancer"*, **Faraday Discussions**, 2015, 185, 299-309.

2. Kenta Imai, Giovanni Valenti, Elena Villani, Stefania Rapino, Enrico Rampazzo, Massimo Marcaccio, Luca Prodi and Francesco Paolucci, *"Numerical simulation of doped silica nanoparticle electrochemiluminescence"*, **Journal of Physical Chemistry C**, 2015, 119, 26111-26118.

Contribution to a book chapter

Andrea Fiorani, Giovanni Valenti, Elena Villani, Massimo Marcaccio, Enrico Rampazzo, Luca Prodi and Francesco Paolucci, *"Electrochemically driven luminescence in organometallic and inorganic systems"* in **"Luminescence in electrochemistry – Applications in analytical chemistry, physics and biology"**, Miomandre Fabien and Audebert Pierre Editors, pp. 293-326, **Springer**, 2017.

Invited research

PhD visiting student at Roche Diagnostics GmbH – System Integration Technology and Product Care Department, Penzberg (Germany). Supervisor: Dr. Stefan Quint. Period: March-May 2015.

PhD visiting student at Hitachi High-Technologies Corporation – Medical System Design Second Department, Hitachinaka (Japan). Supervisors: Mr. Shigeki Matsubara and Ms. Kyoko Imai. Period: October-December 2015.

Scientific contributions to international congresses

March 30 - April 3, 2014: *ChemOnTubes 2014 - International Meeting on the Chemistry of Graphene and Carbon Nanotubes*, Riva del Garda, Italy. Poster contribution: **"Catalysis of oxygen reduction by adenine functionalized MWCNTs"**.

September 7-10, 2014: *ECL 2014 – First International Meeting on Electrogenerated Chemiluminescence*, Bertinoro, Italy. Poster contribution: **"Sarcosine as prostate cancer marker detected by Electrogenerated Chemiluminescence"**.

August 21-26, 2016: *67th ISE 2016 - 67th Annual Meeting of the International Society of Electrochemistry*, The Hague, The Netherlands. Poster contribution: **"Sarcosine as prostate cancer marker detected by Electrogenerated Chemiluminescence"**.

August 29-31, 2016: *ECL 2016 – Second International Meeting on Electrogenerated Chemiluminescence*, Bordeaux, France. Poster contribution: **"Porous gold electrodes for Electrogenerated Chemiluminescence"**.

Scientific contributions to national congresses

October 27-29, 2014: *SAYCS – Sigma-Aldrich Young Chemists Symposium*, Riccione, Italy. Flash and poster contributions: **"Sarcosine as prostate cancer marker detected by Electrogenerated Chemiluminescence"**.

September 20-24, 2015: *GEI 2015 - Giornate dell'Elettrochimica Italiana,* Bertinoro, Italy. Poster contribution: **"Sarcosine as prostate cancer marker detected by Electrogenerated Chemiluminescence"**.

September 11-14, 2016: *GEI 2016 - Giornate dell'Elettrochimica Italiana*, Gargnano (Bs), Italy. Oral contribution: **"Sarcosine as prostate cancer marker detected by Electrogenerated Chemiluminescence"**.

December 19th, 2016: *XVI Giornata della Chimica dell'Emilia-Romagna*, Ferrara, Italy. Flash communication: **"Sarcosine as prostate cancer marker detected by Electrogenerated Chemiluminescence"**.

Awards

Best Poster Prize at the 67th Annual Meeting of the International Society of Electrochemistry (ISE 2016), The Hague, The Netherlands, August 21-26, 2016.

Best Flash Communication at the XVI Giornata della Chimica dell'Emilia-Romagna, Ferrara, Italy, 19th December 2016.

Prof. Gian Piero Spada Medal Award for the best paper in Physical Chemistry published in the XXIX cycle of the PhD in Chemistry, Department of Chemistry "Giacomo Ciamician", Alma Mater Studiorum University of Bologna, 20th February 2017.

Acknowledgements

I wish to thank firstly my PhD supervisors, Prof. Francesco Paolucci and Dr. Giovanni Valenti, for their constant support, friendship and careful supervision during the four years that I have spent in their laboratories of the *Electrochemistry of Molecular and Functional Materials (EMFM)* trying to make ECL and electrochemistry related studies. I wish to thank Prof. Massimo Marcaccio for the AFM analysis, for scientific discussions and advices and, in particular, for having host me in his office during the writing of this thesis work. I also would like to thank Dr. Andrea Fiorani for the patient guidance and for some effective inspirations to improve the composition of this thesis. Furthermore, I would like to thank sincerely former and present members of the EMFM group for the pleasant years spent together at the department of Chemistry "Giacomo Ciamician": Mr. Luca Bartolini, Dr. Alessandro Boni, Mr. Kenta Imai, Dr. Matteo Iurlo, Dr. Stefania Rapino, Dr. Alice Soldà and Dr. Eleonora Ussano.

I wish to thank all the collaborators who I had the pleasure to work with:

Prof. Enrico Dalcanale and Dr. Elisa Biavardi from the University of Parma (Italy)

Prof. Luca Prodi, Dr. Enrico Rampazzo and Dr. Stefania Rapino from the Department of Chemistry "Giacomo Ciamician", University of Bologna (Italy)

Mr. Giulio Fracasso from the University of Verona (Italy)

Dr. Sandro Cattarin and Mr. Luca Mattarozzi from ICMATE-CNR of Padua (Italy)

Dr. Fabio Rizzo from Istituto di Scienze e Tecnologie Molecolari (ISTM) of Milan (Italy)

Dr. Andreas Lesch from the École Polytechnique Fédérale de Lausanne (EPFL) (Switzerland)

Prof. Davide Bonifazi and Dr. Riccardo Marega from the University of Namur (Belgium)

I also would like to thank the students who worked with me making ECL: Gianluca Capucci, Jacopo Fadanni and Ruggero Poiana.

Last, but not least, I would like to thank my Family for the incomparable support.

Lastly, I am very proud for having attended the very FIRST edition of the International Meeting on ECL and for having given my contribution in the organizing committee. I think it is worthy to conclude this thesis on ECL with the pictures of the first and second editions of the International Meeting on Electrogenerated Chemiluminescence:

First International Meeting on ECL held in Bertinoro (Italy) in September 2014

Second International Meeting on ECL held in Bordeaux (France) in August 2016